

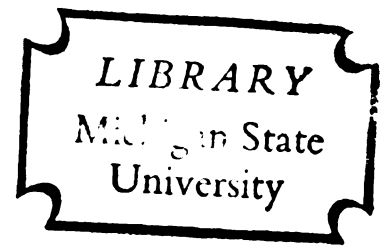
EXPERIMENTAL INVESTIGATION OF THE MODIFICATION
OF THE BACKSCATTERING CROSS SECTIONS OF
METALLIC OBJECTS

Thesis for the Degree of Ph. D.

MICHIGAN STATE UNIVERSITY

MERVIN C. VINCENT

1967



This is to certify that the
thesis entitled
EXPERIMENTAL INVESTIGATION OF THE
MODIFICATION OF THE BACKSCATTERING
CROSS SECTIONS OF METALLIC OBJECTS
presented by

Mervin C. Vincent

has been accepted towards fulfillment
of the requirements for
Electrical Engineering
Ph. D. degree in ~~Philosophy~~

Kim-Mu Chien
Major professor

Date 11-16-67

EXPERIMENT

OF

EXPERIMENTAL INVESTIGATION OF THE MODIFICATION
OF THE BACKSCATTERING CROSS SECTIONS
OF METALLIC OBJECTS

By

Mervin C. Vincent

AN ABSTRACT OF A THESIS

Submitted to
Michigan State University
in partial fulfillment of the requirements
for the degree of

DOCTOR OF PHILOSOPHY

Department of Electrical Engineering

1967

6-31-58
7-2-58

EXPERI
OF

An ex
sections of th
The metallic
electromagne
the backscatt
employing the
method. The
on the object
attaching son

The b
by the addit
impedances.
in good agree
either circula
with a pair of
sides of the
placing an imp
the scattered
loaded cylinde
(or cavity) has

ABSTRACT

EXPERIMENTAL INVESTIGATION OF THE MODIFICATION OF THE BACKSCATTERING CROSS SECTIONS OF METALLIC OBJECTS

by Mervin C. Vincent

An experimental investigation on the backscattering cross sections of the metallic objects of various shapes are presented. The metallic scatterers are assumed to be illuminated by a plane electromagnetic wave at normal incidence. The modification of the backscattered fields of these targets are accomplished by employing the impedance loading method or the compensation method. The impedance loading method is to add some impedances on the object surface and the compensation method consists of attaching some impedance loaded wires to the target object.

The backscattering cross section of a sphere is modified by the addition of two vertical cylinders loaded with appropriate impedances. Both theory and experiment yield results which are in good agreement. The backscattering cross sections of loops, either circular or rectangular, are modified by loading the loop with a pair of impedances positioned symmetrically on opposite sides of the loop. The backscattering of a plate is modified by placing an impedance loaded loop in front of the plate. Similarly, the scattered field of a thick cylinder is modified by placing a thin loaded cylinder adjacent to it. In all these schemes, a coaxial line (or cavity) has been used as the loading impedance in the experiment.

The
methods en
are improv
characteris
impedance

The bandwidths of the impedance loading and the compensation methods employed for modifying the backscatters of the above objects are improved by either using a coaxial line (or cavity) with a high characteristic impedance or adding a resistive component to the impedance loading.

EXPERIM

OF

EXPERIMENTAL INVESTIGATION OF THE MODIFICATION
OF THE BACKSCATTERING CROSS SECTIONS
OF METALLIC OBJECTS

By

Mervin C. Vincent

A THESIS

Submitted to
Michigan State University
in partial fulfillment of the requirements
for the degree of

DOCTOR OF PHILOSOPHY

Department of Electrical Engineering

1967

The a
professor Dr
the course of
of his guidan
and Dr. P. E
Nyquist for c
Appreciation
Hoffman of th
reported in th
Research Lab

ACKNOWLEDGMENTS

The author wishes to express his indebtedness to his major professor Dr. K. M. Chen for his guidance and encouragement in the course of this research. He also wishes to thank the members of his guidance committee, Dr. L. W. Von Tersch, Dr. B. Ho, and Dr. P. K. Wong for reading the thesis and Dr. Dennis P. Nyquist for correcting the manuscript and valuable suggestions. Appreciation is also expressed for the help extended by Mr. J. W. Hoffman of the Division of Engineering Research. The research reported in this thesis was supported by the Air Force Cambridge Research Laboratories under contract AF 19(628)-5732.

ACKNOWLEDGMENTS

LIST OF FIGURES

I. INTRODUCTION

- 1.1. Motivation
- 1.2. Definitions
- 1.3. Background
- 1.4. Outline

II. EXPERIMENTAL

- 2.1. Measurements
- 2.2. Experimental Results
 - 2.2.1. Results
 - 2.2.2. Discussion

III. MODIFICATION OF
A SPHERE

- 3.1. Theory
- 3.2. Experimental
- 3.3. Comparison

IV. MODIFICATION OF
METALLIC

- 4.1. Circular
- 4.2. Rectangular

V. MODIFICATION OF
A CONDUCTOR

- 5.1. Round Plates
- 5.2. Rectangular

VI. MODIFICATION OF
CYLINDERS

- 6.1. Solid and Hollow
 - 6.1.1. Solid
 - 6.1.2. Hollow
- 6.2. Thick Cylinders
Loaded

VII. TECHNIQUE

- 7.1. Resistive
- 7.2. Reactive
High Character

REFERENCES . . .

TABLE OF CONTENTS

	Page
ACKNOWLEDGMENTS	ii
LIST OF FIGURES	iv
I. INTRODUCTION	1
1.1. Motivation and History of Radar Back- scattering Measurements	1
1.2. Definition of Radar Backscattering Cross Section . .	3
1.3. Backscatter Measurement Techniques	5
1.4. Outline of Research Objectives	6
II. EXPERIMENTAL ARRANGEMENT	10
2.1. Measurement Apparatus	10
2.2. Experimental Techniques	20
2.2.1. SWR Method	21
2.2.2. The Cancellation Method	27
III. MODIFICATION OF BACKSCATTERING FROM A SPHERE	32
3.1. Theory	32
3.2. Experiment	40
3.3. Comparison of Theory and Experiment	44
IV. MODIFICATION OF BACKSCATTERING FROM METALLIC LOOPS	53
4.1. Circular Loop	53
4.2. Rectangular Loop	56
V. MODIFICATION OF BACKSCATTERING FROM A CONDUCTING PLATE	73
5.1. Round Plate and Loop	73
5.2. Rectangular Plate and Loop	96
VI. MODIFICATION OF BACKSCATTERING FROM CYLINDERS	106
6.1. Solid and Loaded Cylinders	106
6.1.1. Solid or Unloaded Cylinder	106
6.1.2. Impedance Loaded Cylinder	108
6.2. Thick Cylinder With a Parallel, Impedance Loaded Thin Cylinder	110
VII. TECHNIQUES FOR BANDWIDTH IMPROVEMENT . . .	124
7.1. Resistive Loading	124
7.2. Reactive Loading Using a Coaxial Cavity with High Characteristic Impedance	128
REFERENCES	132

Figure

- 1.1. Ge
- 1.2. Ge
- 1.3. Ci
- 1.4. Th
- 2.1. Ar
- 2.2. Ar
an
- 2.3. La
- 2.4. De
- 2.5. Str
- 2.6. Ph
- 2.7. Ex
- 2.8. SW
of
ho
- 2.9. Ex
me
- 3.1. Ge
- 3.2. Ge
lea
- 3.3. Op
ba
fur
- 3.4. A
- 3.5. Ba
lea
of

LIST OF FIGURES

Figure		Page
1.1.	Geometry of problem of sphere	7
1.2.	Geometry of problem of a loop	7
1.3.	Circular plate with a loaded loop	8
1.4.	Thick cylinder with loaded thin cylinder	8
2.1.	Anechoic chamber showing access from rear	12
2.2.	Anechoic chamber with a scattering target and the transmitting horn	13
2.3.	Layout of ground plane	15
2.4.	Description of detector probe mount	18
2.5.	Structure of the probe carriage	19
2.6.	Physical description of the SWR method	23
2.7.	Experimental arrangement of the SWR method	24
2.8.	SWR of the empty anechoic chamber as a function of the distance of probe from the transmitting horn ($f = 2.0$ GHz)	26
2.9.	Experimental arrangement of the cancellation method	29
3.1.	Geometry of problem of sphere with loaded wires	33
3.2.	Geometry of reduced problem of sphere with loaded wires	33
3.3.	Optimum loading impedance for zero broadside backscatter from sphere with loaded wires as a function of electrical length of wires	39
3.4.	A sphere with loaded wires	41
3.5.	Backscattering cross section of a sphere with loaded wires as a function of loading impedance of loaded wires ($a = 5.71$ cm, $h = 3.5$ cm)	45

Figure

- 3.6. Ba
lea
of
- 3.7. Ba
lea
of
- 3.8. Ba
lea
of
- 3.9. Ba
lea
of
- 3.10. Ma
sph
elec
- 3.11. Opti
fren
of e
- 3.12. Opti
a sp
elec
- 4.1. Lea
- 4.2. Lea
- 4.3. Back
as a
- 4.4. Back
a fun
- 4.5. Back
a fun
- 4.6. Back
a fun
- 4.7. Back
a fun

LIST OF FIGURES (continued)

Figure		Page
3.6.	Backscattering cross section of a sphere with loaded wires as a function of loading impedance of loaded wires ($a = 5.71$ cm, $h = 6.1$ cm)	46
3.7.	Backscattering cross section of a sphere with loaded wires as a function of loading impedance of loaded wires ($a = 5.71$ cm, $h = 6.7$ cm)	47
3.8.	Backscattering cross section of a sphere with loaded wires as a function of loading impedance of loaded wires ($a = 5.71$ cm, $h = 8.4$ cm)	48
3.9.	Backscattering cross section of a sphere with loaded wires as a function of loading impedance of loaded wires ($a = 5.71$ cm, $h = 10.5$ cm)	49
3.10.	Maximum and minimum backscatters from a sphere with loaded wires as a function of electrical length of wires	50
3.11.	Optimum reactance for minimum backscatter from a sphere with loaded wires as a function of electrical length of wires	51
3.12.	Optimum reactance for maximum backscatter from a sphere with loaded wires as a function of electrical length of wires	52
4.1.	Loaded, circular wire loop	54
4.2.	Loaded square wire loop	57
4.3.	Backscattering cross section of a loaded loop as a function of loading impedance ($f = 1.61$ GHz)	60
4.4.	Backscattering cross section of a loaded loop as a function of loading impedance ($f = 1.7$ GHz)	61
4.5.	Backscattering cross section of a loaded loop as a function of loading impedance ($f = 1.75$ GHz)	62
4.6.	Backscattering cross section of a loaded loop as a function of loading impedance ($f = 1.8$ GHz)	63
4.7.	Backscattering cross section of a loaded loop as a function of loading impedance ($f = 1.9$ GHz)	64

Figure

4.8. Ba
a f

4.9. Ba
a f

4.10. Ba
a f

4.11. Ba
a f

4.12. Ba
a f

4.13. Ba
a f

4.14. Op
bac
by

4.15. Op
bac
by

5.1. Cir

5.2. Ba
lca
(f =

5.3. Ba
lca
(f =

5.4. Ba
lca
(f =

5.5. Ba
lca
(f =

5.6. Ba
lca
(f =

LIST OF FIGURES (continued)

Figure	Page
4.8. Backscattering cross section of a loaded loop as a function of loading impedance ($f = 2.0$ GHz)	65
4.9. Backscattering cross section of a loaded loop as a function of loading impedance ($f = 2.1$ GHz)	66
4.10. Backscattering cross section of a loaded loop as a function of loading impedance ($f = 2.2$ GHz)	67
4.11. Backscattering cross section of a loaded loop as a function of loading impedance ($f = 2.3$ GHz)	68
4.12. Backscattering cross section of a loaded loop as a function of loading impedance ($f = 2.4$ GHz)	69
4.13. Backscattering cross section of a loaded loop as a function of loading impedance ($f = 2.5$ GHz)	70
4.14. Optimum reactive impedance for minimum backscattering from a loaded loop illuminated by a plane wave at normal incidence	71
4.15. Optimum reactive impedance for maximum backscattering from a loaded loop illuminated by a plane wave at normal incidence	72
5.1. Circular plate and loaded loop	74
5.2. Backscatter of the small circular plate with a loaded loop as a function of loop loading ($f = 1.9$ GHz)	76
5.3. Backscatter of the small circular plate with a loaded loop as a function of loop loading ($f = 1.97$ GHz)	77
5.4. Backscatter of the small circular plate with a loaded loop as a function of loop loading ($f = 2.1$ GHz)	78
5.5. Backscatter of the small circular plate with a loaded loop as a function of loop loading ($f = 2.2$ GHz)	79
5.6. Backscatter of the small circular plate with a loaded loop as a function of loop loading ($f = 2.78$ GHz)	80

Figure

5.7.

5.8.

5.9.

5.10.

5.11.

5.12.

5.13.

5.14.

5.15.

5.16.

5.17.

5.18.

LIST OF FIGURES (continued)

Figure		Page
5.7.	Backscatter of the medium circular plate with a loaded loop as a function of loop loading (f = 2.1 GHz)	81
5.8.	Backscatter of the medium circular plate with a loaded loop as a function of loop loading (f = 2.2 GHz)	82
5.9.	Backscatter of the medium circular plate with a loaded loop as a function of loop loading (f = 2.3 GHz)	83
5.10.	Backscatter of the medium circular plate with a loaded loop as a function of loop loading (f = 2.4 GHz)	84
5.11.	Backscatter of the medium circular plate with a loaded loop as a function of loop loading (f = 2.5 GHz)	85
5.12.	Backscatter of the medium circular plate with a loaded loop as a function of loop loading (f = 2.7 GHz)	86
5.13.	Backscatter of the medium circular plate with a loaded loop as a function of loop loading (f = 2.9 GHz)	87
5.14.	Backscatter of the medium circular plate with a loaded loop as a function of loop loading (f = 3.04 GHz)	88
5.15.	Backscatter of a large circular plate with a loaded loop as a function of loop loading (f = 1.9 GHz)	89
5.16.	Backscatter of a large circular plate with a loaded loop as a function of loop loading (f = 1.97 GHz)	90
5.17.	Backscatter of a large circular plate with a loaded loop as a function of loop loading (f = 2.1 GHz)	91
5.18.	Backscatter of a large circular plate with a loaded loop as a function of loop loading (f = 2.3 GHz)	92

Figure

- 5.19. Back
load
($f = 2$)
- 5.20. Back
load
($f = 2$)
- 5.21. Optin
from
- 5.22. Recta
- 5.23. Back
a loa
($f = 1$)
- 5.24. Back
a loa
($f = 1$)
- 5.25. Back
a loa
($f = 1$)
- 5.26. Back
a loa
($f = 1$)
- 5.27. Back
a loa
($f =$)
- 5.28. Back
a loa
($f =$)
- 6.1. Bac
as a
- 6.2. Phys
- 6.3. Thic
- 6.4. Bac
load
impe
 $h_2 =$

LIST OF FIGURES (continued)

Figure	Page
5.19. Backscatter of a large circular plate with a loaded loop as a function of loop loading (f = 2.5 GHz)	93
5.20. Backscatter of a large circular plate with a loaded loop as a function of loop loading (f = 2.78 GHz)	94
5.21. Optimum impedance for minimum backscattering from a circular plate with a loaded circular loop. .	95
5.22. Rectangular plate and loaded loop	98
5.23. Backscatter of the small rectangular plate with a loaded loop as a function of loop loading (f = 1.72 GHz)	100
5.24. Backscatter of the small rectangular plate with a loaded loop as a function of loop loading (f = 1.8 GHz)	101
5.25. Backscatter of the small rectangular plate with a loaded loop as a function of loop loading (f = 1.97 GHz)	102
5.26. Backscatter from a large rectangular plate with a loaded loop as a function of loop loading (f = 1.72 GHz)	103
5.27. Backscatter from a large rectangular plate with a loaded loop as a function of loop loading (f = 1.8 GHz)	104
5.28. Backscatter from a large rectangular plate with a loaded loop as a function of loop loading (f = 1.97 GHz)	105
6.1. Backscattering cross sections of solid cylinders as a function of cylinder half-length h	107
6.2. Physical description of cylinders	109
6.3. Thick cylinder with a loaded thin cylinder	112
6.4. Backscattering cross section of a thick with a loaded thin cylinder as a function of loading impedance of thin cylinder ($h_1 = 2.5$ cm, $h_2 = 2.7$ cm)	114

LIST OF FIGURES (continued)

Figure		Page
6.5.	Backscattering cross section of a thick with a loaded thin cylinder as a function of loading impedance of thin cylinder ($h_1 = 3.8$ cm, $h_2 = 12.9$ cm)	115
6.6.	Backscattering cross section of a thick with a loaded thin cylinder as a function of loading impedance of thin cylinder ($h_1 = 12.8$ cm, $h_2 = 15.2$ cm)	116
6.7.	Maximum and minimum backscatters from a thick with a loaded thin cylinder as a function of thin cylinder half-length h_2 ($h_1 = 2.5$ cm)	117
6.8.	Maximum and minimum backscatters from a thick with a loaded thin cylinder as a function of thin cylinder half-length h_2 ($h_1 = 3.8$ cm)	118
6.9.	Maximum and minimum backscatters from a thick with a loaded thin cylinder as a function of thin cylinder half-length h_2 ($h_1 = 5.0$ cm)	119
6.10.	Maximum and minimum backscatters from a thick with a loaded thin cylinder as a function of thin cylinder half-length h_2 ($h_1 = 10.1$ cm)	120
6.11.	Maximum and minimum backscatters from a thick with a loaded thin cylinder as a function of thin cylinder half-length h_2 ($h_1 = 11.6$ cm)	121
6.12.	Maximum and minimum backscatters from a thick with a loaded thin cylinder as a function of thin cylinder half-length h_2 ($h_1 = 12.8$ cm)	122
6.13.	Maximum and minimum backscatters from a thick with a loaded thin cylinder as a function of thin cylinder half-length h_2 ($h_1 = 15.0$ cm)	123
7.1.	Backscattering cross section of a cylinder loaded with reactive and resistive elements as a function of reactive loading impedance ($h = 2.7$ cm)	125
7.2.	Backscattering cross sections of solid and loaded cylinders as a function of frequency ($h = 3.5$ cm)	127

Figure

7.3. Bac
cyl

7.4. Bac
with
(a =

LIST OF FIGURES (continued)

Figure		Page
7.3.	Backscattering cross sections of solid and loaded cylinders as a function of frequency ($h = 3.5$ cm) . . .	129
7.4.	Backscattering cross sections of sphere and sphere with loaded wires as a function of frequency ($a = 5.71$ cm, $h = 3.4$ cm)	130

Since
has been qua
and reflecte
was in modifi
towers of bro
the interest
since the inve
has been use
conventional a
measurement
and consequen
camouflage as

1.1. Motivat

A grea
the area assoc
metallic bodie
value of exper
however, when
exact solutions
of course, exc
simple shapes.
in theoretical b

CHAPTER I

INTRODUCTION

Since the first experiments with radio waves by Hertz, there has been qualitative observations that radio waves are scattered and reflected by almost everything. The only interest at that time was in modifying these reflections and scatterings from the supporting towers of broadcast antennas and surrounding structures. However, the interest in scattering of radio waves has increased exponentially since the invention of radar in World War II. In recent years, radar has been used to detect the space vehicles in addition to many conventional aircrafts. As the result, intensive research on radar measurements has improved its detecting efficiency tremendously and consequently has generated great interest in methods of radar camouflage as a counter measure to this advance.

1.1. Motivation and History of Radar Backscattering Measurements

A great number of the investigations performed thus far in the area associated with the radar backscattering cross sections of metallic bodies have been concerned with theoretical problems. The value of experimental investigations of scattered fields is quite obvious, however, when one realizes that there are very few bodies for which exact solutions for the scattering is possible, although there are, of course, excellent approximate solutions for a small number of simple shapes. Much dependence is placed upon approximate solutions in theoretical backscattering studies, and experimental results have

been v

justify

to allo

fields.

trucks

exper:

for ser

pattern

made i

technic

cross s

at Chic

to obtai

the des

many a

scatter

by King

of meta

Liepa,

either o

symmet

the bac

a circu

been very important in helping to develop such solutions and in justifying their validities.

There are many metallic bodies which are far too complex to allow either exact or approximate solutions for the scattered fields. The backscattering cross sections of most space vehicles, trucks, ships, and similar objects must always be determined experimentally, although approximate formulas have been developed for some which permit fairly accurate calculations of the scattering patterns. It is the comparison with experimental data which has made it possible to prove the reliability of these theoretical techniques.

It is believed that the first comprehensive backscattering cross section measurements, using models, were those performed at Ohio State University around 1945. The principle objective was to obtain the backscattering cross sections of aircrafts for use in the design of decoys as radar-confusing devices. Since that time, many advancements have been made in the techniques for measuring scattering cross sections. Several of these methods are described by King and Wu,¹ and Blacksmith, Hiatt, and Mack.²

In recent years, the modification of the backscattered fields of metallic cylinders has been studied with success by Chen and Liepa,³⁻⁵ where the scattering cross sections were controlled by either central loading of the cylinder or double loading at two symmetric points along its axis. Liepa and Senior⁶ have reduced the backscattering cross section of a metallic sphere by installing a circumferential slot backed by an impedance on the spheric surface.

An inve

cross s

slots or

there ha

modifica

This wa

two sym

most ca

exact, w

of the p

1.2. De

I

of incide

given di

is usual

where R

object fi

of a plan

and S_r^s

corresp

distance

of the in

in any c

An investigation was also made on the modification of the backscattering cross section of a conducting plate by the techniques of cutting resonant slots or installing a cavity-backed aperture on the plate.⁷ Recently, there has been some successful theoretical work performed on the modification of the scattering cross section of a conducting wire loop. This was also accomplished by the technique of loading the loop at two symmetrical points with a pair of identical impedances.⁸ In most cases, however, the theoretical work is neither extensive nor exact, which again stimulates an interest in the experimental aspect of the problem.

1.2. Definition of Radar Backscattering Cross Section

In the study of the backscattering problem, where the fraction of incident energy which is scattered or reflected by an object in a given direction is desired, a scattering cross section for the object is usually defined. This scattering cross section σ is defined as

$$\sigma(\theta, \phi, \theta_i, \phi_i) = \lim_{R \rightarrow \infty} 4\pi R^2 \frac{|S_r^s(\theta, \phi)|}{|S^i(\theta_i, \phi_i)|} \quad (1.1)$$

where R, θ, ϕ , are spherical coordinates with the scattering object fixed at their origin, S^i is the time-average Poynting vector of a plane wave incident upon the object from the direction θ_i, ϕ_i , and S_r^s is the time-average radial component of the Poynting vector, corresponding to the scattering in a direction θ, ϕ at a far-field distance R from the object. When σ is evaluated in the direction of the incident wave, it is called the backscattering cross section; in any other direction it is referred to as the bistatic cross section.

It

ou

wa

an

av

E^s

is a

fel

the

and

wh

Poy

The

ma

the

st

in

It is the backscattering cross section which will be of interest throughout this research.

In the radiation zone or far-zone of the object the scattered wave is spherical, the radiation field components are transverse, and the Poynting vector has only a radial component with a time-average value given by

$$S_r^s(\theta, \phi) = \frac{1}{2} \operatorname{Re} \hat{r} \cdot (\vec{E}^s \times \vec{H}^{s*}) \quad (1.2)$$

E^s and H^s are the scattered electric and magnetic fields, and \hat{r} is a unit vector in the radial direction. Additionally, the illuminating field at the scatterer is nearly a plane wave. Since it is known that the electric and magnetic fields are mutually orthogonal to one another in the far-zone and are related by

$$\vec{H}^s = \frac{\hat{r} \times \vec{E}^s}{\zeta} \quad (1.3)$$

where ζ is the characteristic wave impedance of the media, the Poynting vector for the scattered field can be written as

$$S_r^s(\theta, \phi) = \frac{1}{2} \frac{|\vec{E}^s(\theta, \phi)|^2}{\zeta} \quad (1.4)$$

The Poynting vector for the incident field can be found in a similar manner. The backscattering or radar cross section of an object then becomes

$$\sigma(\theta, \phi) = \lim_{R \rightarrow \infty} 4\pi R^2 \frac{|\vec{E}^s(\theta, \phi)|^2}{|\vec{E}^i(\theta, \phi)|^2} \quad (1.5)$$

where $\vec{E}^s(\theta, \phi)$ is the component of the scattered field at the receiver, in the direction (θ, ϕ) , which is polarized parallel to the incident



p
s
m
u
w
i:
s
s
s
s
s
s
s
s
l
c
s
c
t:
S
te
s:
o:
m
r:
a:

plane wave field $\vec{E}^i(\theta, \phi)$ which illuminates the object from the same direction (θ, ϕ) as that in which the scattered field is measured.

In this research a ground plane measuring range has been used. The incident and scattered fields are vertically polarized with reference to the ground plane, and the illuminating field is incident broadside ($\theta = 0^\circ$) to all the scattering models which are studied. Off-broadside angles were not considered in this research since the image-type scattering range utilized is not suitable for such measurements.

Dimensionally, σ is an area which is usually specified in square meters, but can be expressed in decibels referred to some standard backscattering cross section σ_0 .

1.3. Backscatter Measurement Techniques

Procedures or methods for measuring σ are quite easily deduced from the definition of σ in terms of the incident and scattered fields. Although many measurement methods have been developed, only two of these are utilized in this research; they are the SWR (standing wave ratio) and the cancellation methods. The SWR method is analogous to transmission line measurement techniques, in that the absolute value of σ can be determined from measurements of the standing waves caused by interference of the incident field and the scattered field due to the scattering model. The cancellation method provides a way of measuring the relative value of σ by cancelling out the detected incident signal at the measuring probe and measuring only the reflected signal.

Of the
fast
altho
for a
used

1. 4.

back

rese

a pla

minin

of the

exten

attach

in Fig

and c

loads

of the

imped

be con

is don

a tech

a plate

schem

the pla

backsc

Of these two techniques for measuring σ , the latter has a much faster data rate and provides adequate information in most cases, although a standard reference model, usually a sphere, is needed for absolute measurements of σ . The cancellation method is used almost exclusively for the models studied in this research.

1.4. Outline of Research Objectives

Both experimental and theoretical investigations of the backscattering cross section of a sphere are carried out in this research, as well as experimental studies of backscattering from a plate, round and square loops, and cylinders. Further, both minimization and enhancement of the backscattering cross sections of these objects are studied, although minimization is studied more extensively. The radar cross section of a sphere is modified by attaching two thin, loaded cylinders symmetrically to it as shown in Figure 1.1. The total backscattering of the composite of sphere and cylinder can be controlled by adjusting the impedance which loads the cylinder. To modify the backscattering cross section of the loop, it is loaded symmetrically with a pair of identical impedances as shown in Figure 1.2. Again the backscattering can be controlled by adjusting the impedance loading on the loop. This is done successfully for both the square and the round loops. By a technique similar to that for the sphere, the backscattering from a plate can be modified by means of a composite structure. The scheme of this method is to place a loaded loop directly in front of the plate and parallel to it as shown in Figure 1.3 so that the total backscatter of the plate and loop can be controlled by adjusting the

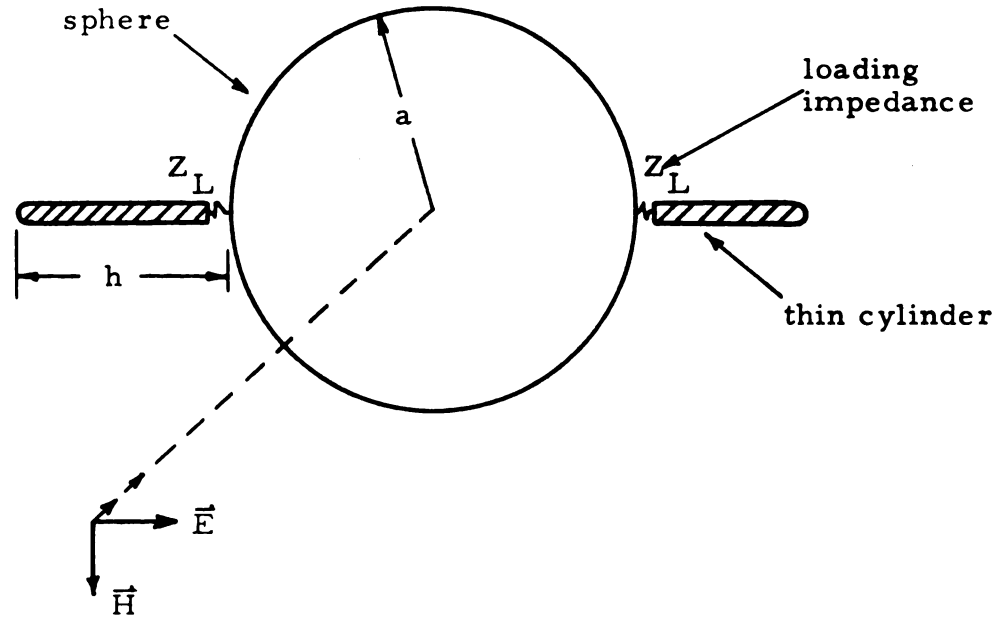


Figure 1.1. Geometry of problem of sphere.

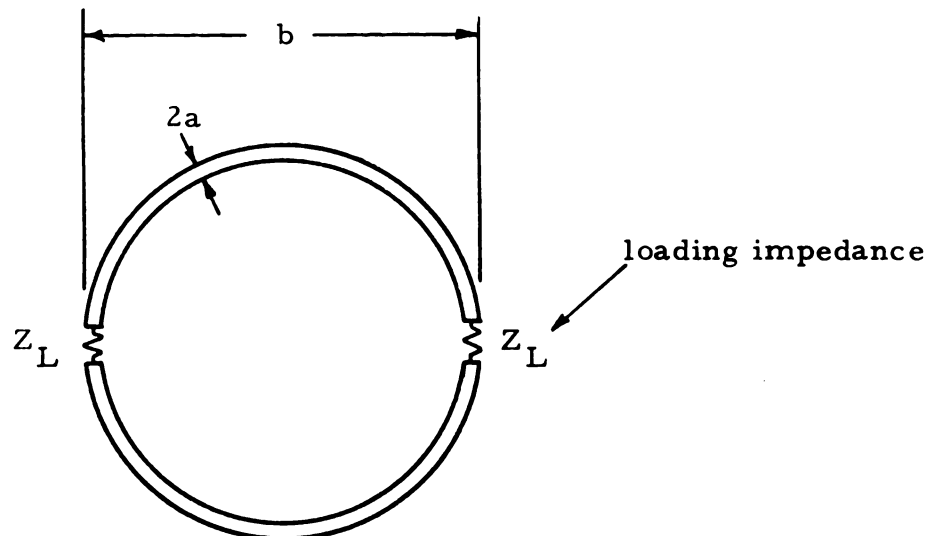


Figure 1.2. Geometry of problem of a loop.

large plate $d = 12.7$ cm
 medium plate $d = 10.2$ cm
 small plate $d = 7.6$ cm

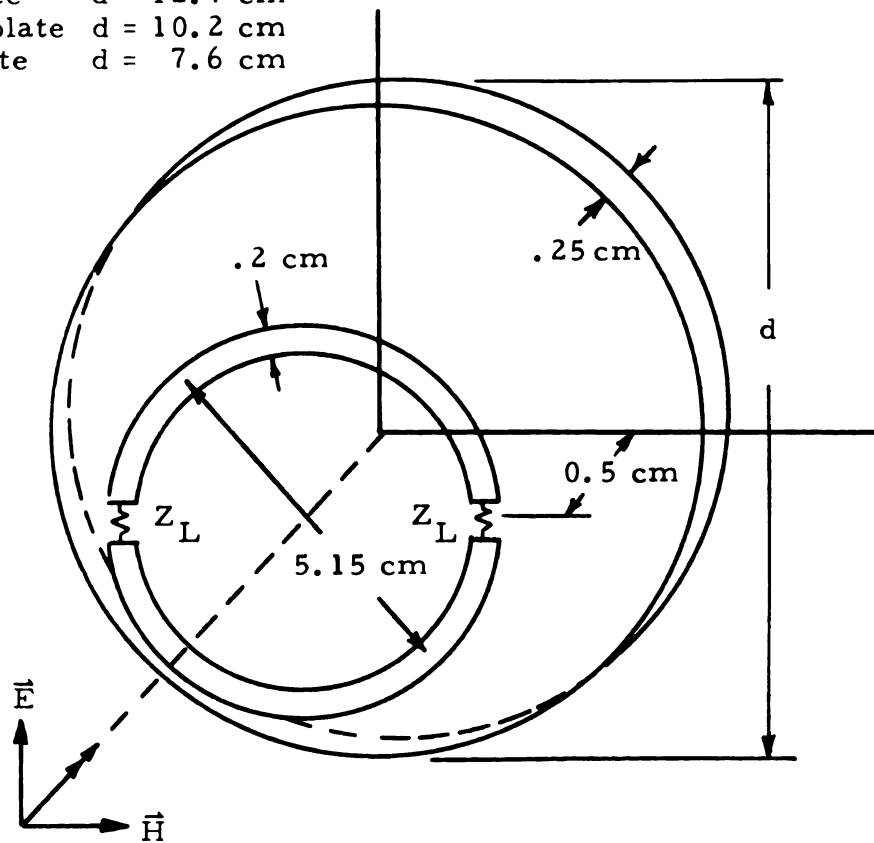


Figure 1.3. Circular plate with a loaded loop.

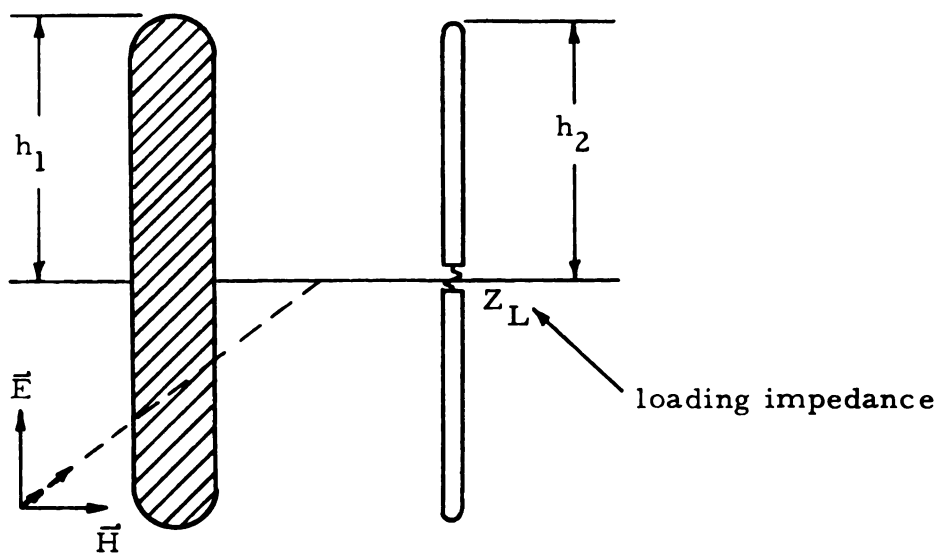


Figure 1.4. Thick cylinder with loaded thin cylinder.

loading impedance. The backscatter from a thick cylinder can be modified in a similar way as that for the plate. A thin loaded cylinder is placed in the plane containing the large cylinder and transverse to the incident field as shown in Figure 1.4. The thin cylinder can be placed a small distance on either side of the thick cylinder since the cylinder has azimuthal symmetry. By adjusting the impedance, the total backscatter of the two cylinders can be controlled.

As a further investigation on the modification of the backscattering cross sections of these objects, the bandwidth characteristics are studied. In all of the above models, only reactive loading was considered, which in most cases was sufficient to minimize the backscattering of these models. Addition of resistive components and careful design of a reactive loading have been tried and have been found to improve the bandwidth.



CHAPTER II

EXPERIMENTAL ARRANGEMENT

Backscattering measurements logically would be performed out-of-doors since the ultimate purpose of these measurements is its use on full-scale objects such as space vehicles. In most cases these full-scale measurements are both too expensive and inconvenient. This readily suggests scaled model measurements which can be done indoors. Since free space conditions can easily be simulated indoors, measurement variables involved may be scaled without loss of generality.

2.1. Measurement Apparatus

The experimental arrangement consists basically of an anechoic chamber constructed on an aluminum image or ground plane. It is in this anechoic chamber that all the experimental measurements are made. The purpose of this chamber is to simulate a free space environment, which is the usual electromagnetic medium upon which actual radar systems depend for their operation. Furthermore, the measurements can be performed above the ground plane with only a detecting probe placed inside the chamber. This reduces the possibility of extraneous reflections from monitoring devices. The dimensions of the anechoic chamber are adjusted so that the measuring devices are in the radiation zone of both the source antenna and the scattering body. A simultaneous requirement is that the scatterer be in the radiation field of the transmitting antenna such that the incident wave approximates a

plane wave field. These conditions require that the distances of concern be of the order of 10 wavelengths. At a frequency of 2 GHz, the distance requirement for the radiation zone is therefore approximately 150 cm or about 60 inches.

The anechoic chamber is constructed as shown in Figures 2.1 and 2.2. It consists of a tapered wooden structure with the dimensions of 3.65 meters (12 feet) in length, 3.05 meters (10 feet) and .915 meters (3 feet) respectively in width at the two ends, and 1.22 meters (4 feet) in height. The narrow end of the chamber is left open. This chamber structure then is located above a rectangular aluminum ground plane erected 1.02 meters (40 inches) above the floor. The dimensions of the ground plane are 3.65 meters in length, 3.05 meters in width, and .635 cm thick. The wooden table supporting the ground plane has dimensions of 3.65 meters in length, 3.05 meters in width, and 1.02 meters in height. No metallic parts are used in the construction of the anechoic chamber. All measurement and monitoring apparatus are located beneath the conducting image plane. The shielding effect of the ground plane thus eliminates the possibility of spurious reflections from the equipment or its operator. The walls of the chamber are secured with glue and wooden dowels to avoid any possibility of unnecessary stray reflections. The three wooden walls and top are covered with B. F. Goodrich type VHP-8 microwave absorbers. This R.F. absorber is effective, over the range of frequencies used (1.7 - 4.1 GHz), in reducing the reflected power by at least 20 dB. It is felt that any interaction of the reflected fields with the



Figure 2.1. Anechoic chamber showing access from rear.

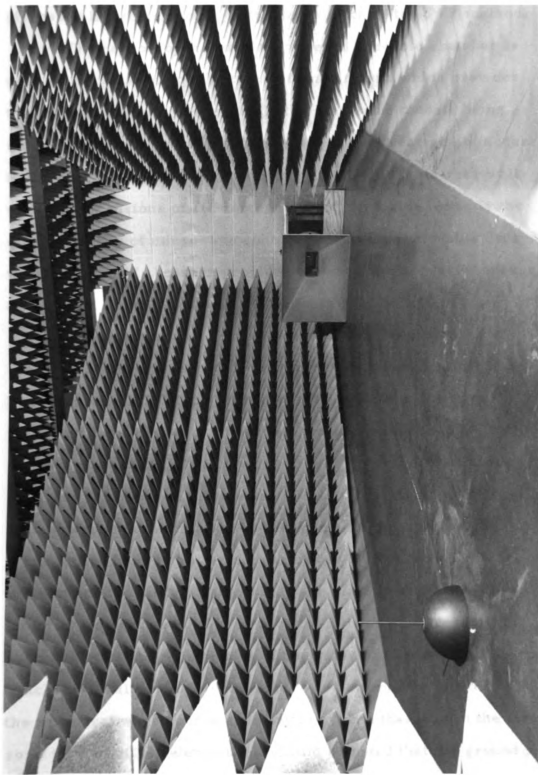


Figure 2.2. Anechoic chamber with a scattering target and the transmitting horn.

incident and scatter fields is entirely negligible. This topic is discussed in greater detail in the description of the SWR method.

The narrow open end of the tapered anechoic chamber is used as the location for the transmitting antenna which provides the incident traveling wave, while the scattering models being studied are positioned at its wide end. For convenience of access to the rear of the chamber, a square hole is cut in its rear wall with the dimensions of .61 meters (2 feet) on a side, exactly the size of a piece of microwave absorber. Thus a removable door with a section of absorber provides the required access whenever a change of scattering models is necessary.

The construction of the ground plane is as indicated in Figure 2.3. Field measurements in the chamber are facilitated by a .318 cm (0.125 inch) wide slot which is cut in the ground plane and through which a detecting probe protrudes. The slot starts approximately 1.52 meters (5 feet) from the front of the plate and terminates .915 meters (3 feet) from the opposite end. It is centered in the transverse dimension of the image plane. A transmitting horn is placed approximately 80 cm from the front of the slot and the models under study are placed essentially 23 cm from its terminal end. The separation between the transmitting horn and scattering element is of the order of 15 wavelengths, which easily allows a detecting probe to be properly located between the spherical wave source and scatterer such that it is in the far zone field of either element. It should be noted that the ground plane has dimensions of the order of 20 wavelengths by 24 wavelengths

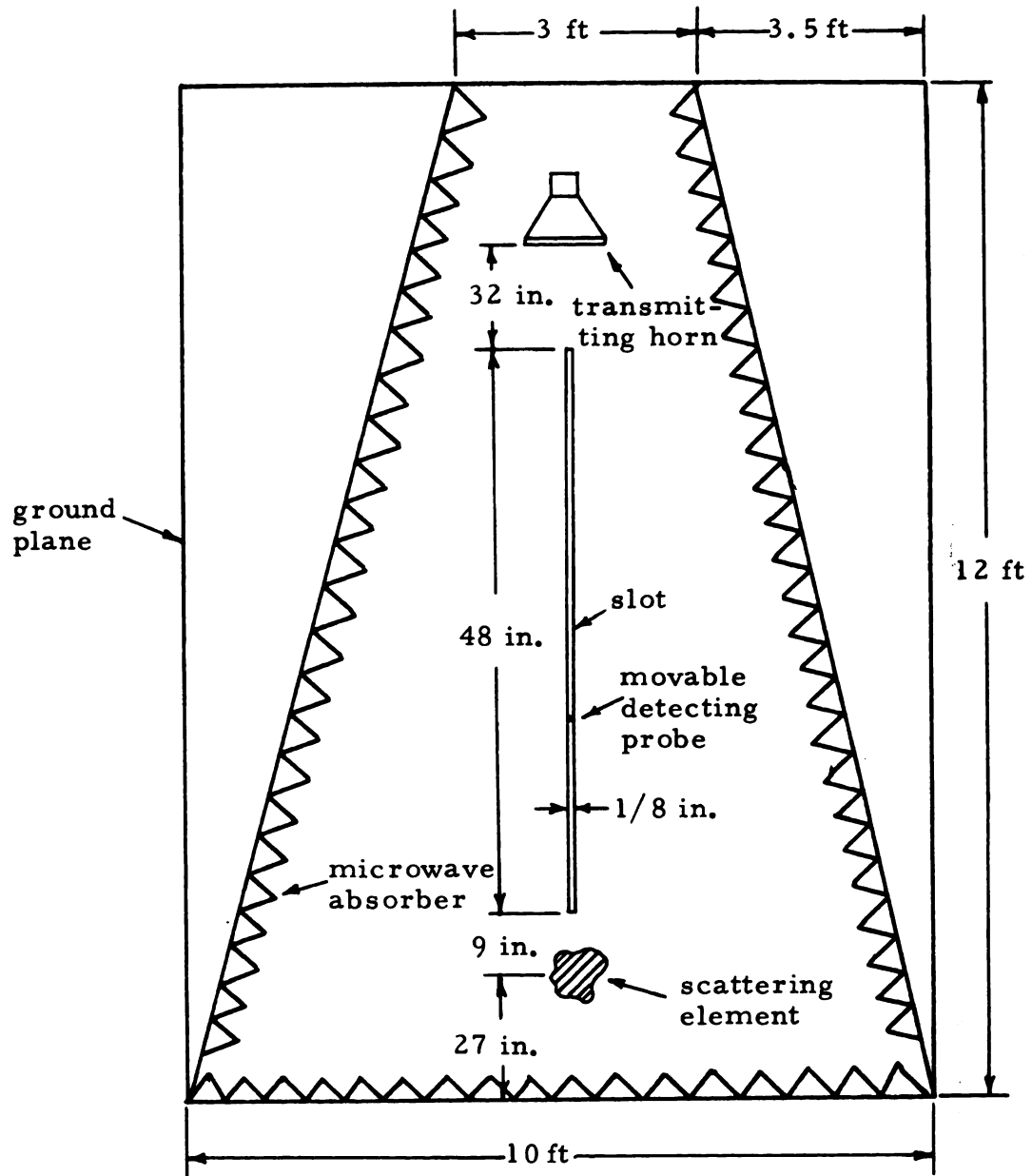


Figure 2.3. Layout of ground plane.

which surrounded by absorbers will essentially eliminate the edge effects, characteristic of a non-infinite image plane. Further, since the microwave absorber terminates against the ground plane along most of the chamber extremities, particularly along the side walls where they rest on the ground plane, the surface wave fields at the plate edges (and hence the reflections) are negligible.

A pyramidal transmitting horn (Scientific Atlantic Standard gain horn, model 12-1.7) is utilized with a lower cutoff frequency of 1.7 GHz. The horn is driven by a General Radio microwave oscillator (GR 1360B) having a frequency range from 1.7 to 4.1 GHz. A 50 ohm coaxial (RG58) transmission line is used to couple the microwave energy from the generator to the transmitting horn. The horn is placed directly upon the ground plane such that the radiated field is imaged continuously to form the total transmitted wave. Since the radial distance between the horn and scattering element is of the order of 15 wavelengths, then the wave incident upon the scatterer may be assumed to consist of a plane wave field provided its height is small compared with the above radial separation. Furthermore, since the horn is assumed to radiate a spherical traveling wave, the amplitude of the electric and magnetic fields must decay as $1/R$ where R denotes the distance from the horn. It is indicated in a later description (section 2.2.1) of the SWR method that this assumption is approximately valid. The signal amplitude therefore becomes quite small at large radial distances, and limits the allowable separations between horn, scatterer, and detecting probe.



i
:
P
i
T
r
s
r
is
th
b
h
c
is
w
t
P
:
:
P
:
ep

The movable detecting probe structure and carriage is indicated in Figures 2.4 and 2.5 respectively. This probe has the freedom to traverse the full length of the four foot longitudinal slot in the ground plane. The thin-wire probe structure (Central Res.Lab. MX-1019/u) illustrated in Figure 2.4 is mounted in the carriage of Figure 2.5. This probe carriage is supported by two 1.22 meters (4 feet) steel rods .127 cm (0.50 inch) diameter which are secured to the under side of the ground plane. The carriage configuration makes use of roller bearings which ride on the steel supporting rods. The probe is centered in the longitudinal seat to prevent electric contact with the conducting image plane, which would short the signal detected by the monopole probe. Additionally the probe maintains a constant height while traversing the length of the slot. To provide a means of moving the probe when in front of the ground plane, a pulley system is constructed with a large pulley secured at the front of the table which can be rotated manually to locate the probe at any point along the slot. For convenience in measuring relative positions of the probe, a steel measuring tape, scaled in centimeters, is used in place of string or wire in the pulley system. By measuring the physical distance between probe and scatterer or horn and noting the centimeter reading on the tape for a given position of the probe, these physical distances are known for all other probe locations.

The detecting probe utilizes a self-contained stub tuner to provide optimum tuning of the receiving monopole or detecting probe to the coaxial line (RG58-50 ohm line) which couples it to the measuring apparatus. For all frequencies utilized, it is easily tuned to provide an

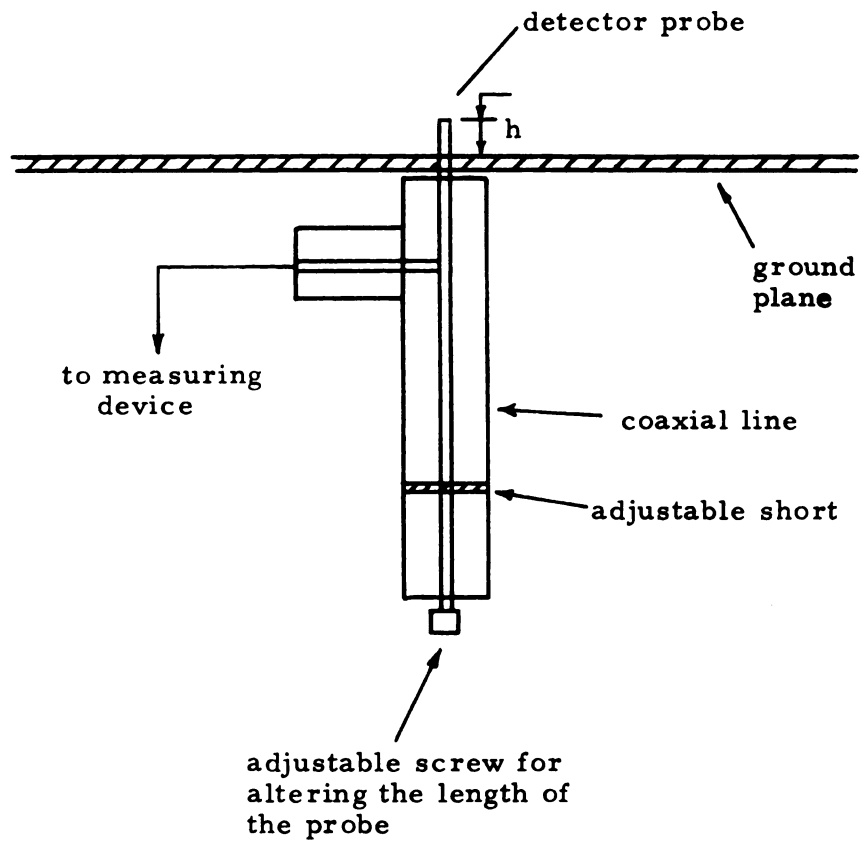


Figure 2.4. Description of detector probe mount.

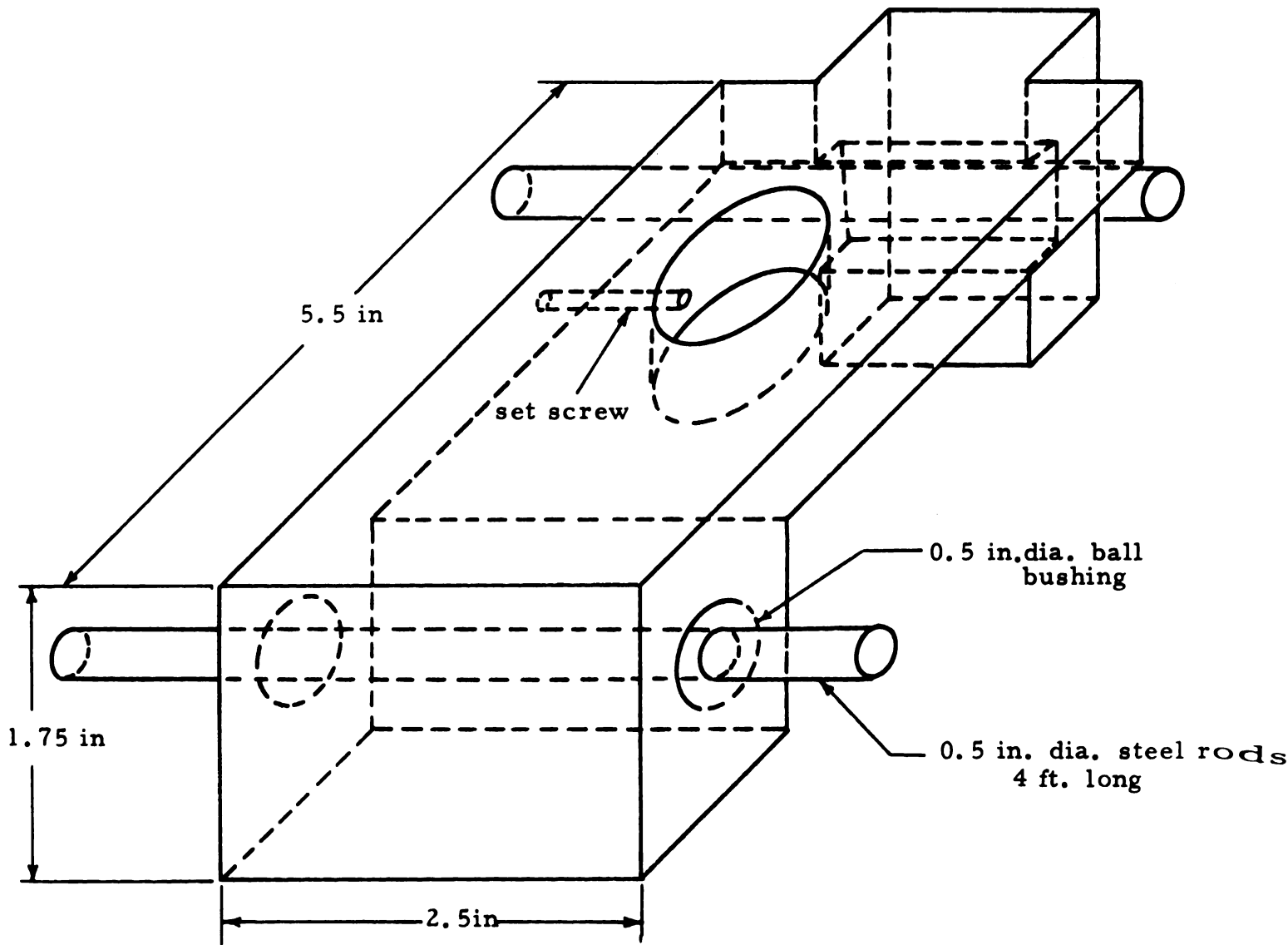


Figure 2.5. Structure of the probe carriage.

adequate maximum signal. At the base of the probe structure is an adjustment screw which varies the height of the probe above the ground plane. The probe height can be adjusted from 1.7 cm to 3.8 cm. An optimum height is that which provides a signal of satisfactorily large amplitude with minimum protrusion above the ground plane. A probe of minimum length is necessary to avoid reradiation from the probe which might subsequently interact with the transmitted signal or, more importantly, with the scattered field from the metallic object being investigated. It is felt that the power reradiated from the probe is negligible over the range of frequencies used.

2.2. Experimental Techniques

The experimental techniques used for the investigation of backscattering cross sections of metallic objects are the SWR and cancellation methods. These are the only methods applicable with the experimental setup of section 2.1 since the anechoic chamber is based upon a ground plane. Due to the presence of the detecting probe above the ground plane, only the broadside backscatter ($\theta=0^\circ$) can be measured. It is felt that the broadside backscatter is of sufficiently greater importance than the oblique or off-broadside backscatter that the experimental results presented here contribute significantly to the state of the art knowledge in this area of study. The induced current due to oblique incidence upon a scatterer is significantly smaller in amplitude than that for normal incidence (the case being investigated in this research). Consequently, the off broadside scatter field is smaller and in many cases can be neglected completely.

2.2.1. SWR Method

The first of the techniques utilized for measuring the backscatter fields of metallic objects is designated as the SWR method. In accordance with the above discussion of normal incidence of the illuminating plane wave upon the scatterer, it is observed that the probe is excited by both the incident \vec{E} -field from the horn and the scattered electric field from the metallic object. These incident and scatter fields interfere to produce a spacially distributed standing wave between horn and scatterer which is analogous to the one produced by incident and reflected waves on a transmission line.

The backscattering cross section of a metallic object can be determined uniquely from measurements of the standing wave it sets up in space, just as the terminal impedance of a transmission line can be determined from probe measurements of the standing wave pattern on the line. Since the total field which excites the probe is measured in the radiation zones of the transmitting horn and scattering obstacle, the incident and reflected fields are both spherically diverging waves; consequently the $1/R$ variation in amplitude must be considered. The usual definition of standing-wave ratio (SWR) in terms of incident and scatter fields is

$$\text{SWR} = \frac{E_{\max}(W_1)}{E_{\min}(W_2)} = \frac{E^i(W_1) + E^s(W_1)}{E^i(W_2) - E^s(W_2)} \quad (2.1)$$

where W_1 is the distance from the model to a maximum and W_2 the distance to an adjacent minimum of the standing wave.

obsta

the o

at a

and t

defin

to th

field

By s

the

Fin

cro

techn

descr

sectio

Let the separation between the transmitter and the scattering obstacle be designated as L and E_o as the incident field strength at the obstacle. Suppose that the movable detecting probe is located at a distance W from the scatterer along a line joining the scatterer and transmitter. An electric field reflection coefficient Γ may be defined as the ratio of the scattered field $E^s(L)$ at the transmitter to the incident field E_o at the scatterer as $\Gamma = E^s(L)/E_o$. The fields at the probe are then (see Figure 2.6)

$$E^i(W) = \frac{E_o L}{L-W}, \quad E^s(W) = \frac{E_o |\Gamma| L}{W} \quad (2.2)$$

By substitution of equation 2.2 into equation 2.1, the amplitude of the reflection coefficient can be found as

$$|\Gamma| = \frac{W_2}{L-W_2} \left[\frac{\text{SWR} - \frac{1}{1 + \frac{W_2 - W_1}{L - W_2}}}{\text{SWR} + \frac{1}{1 - \frac{W_2 - W_1}{W_2}}} \right] \quad (2.3)$$

Finally, from the definition of Γ and σ , the broadside backscattering cross section of the reflecting obstacle is obtained as

$$\sigma = \lim_{L \rightarrow \infty} 4\pi L^2 |\Gamma|^2 \quad (2.4)$$

The experimental arrangement for the SWR measurement technique is indicated in Figure 2.7. The microwave oscillator described previously in conjunction with the arrangement of section 2.1 is utilized with amplitude modulation provided by an

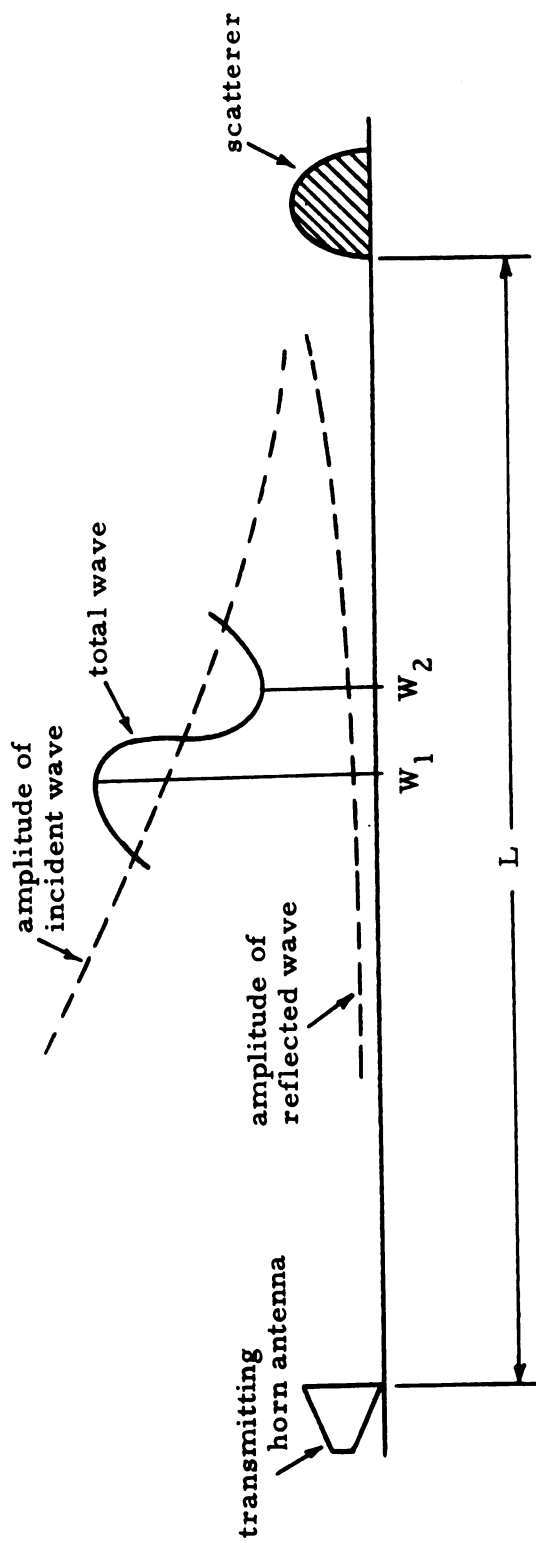


Figure 2.6. Physical description of the SWR method.

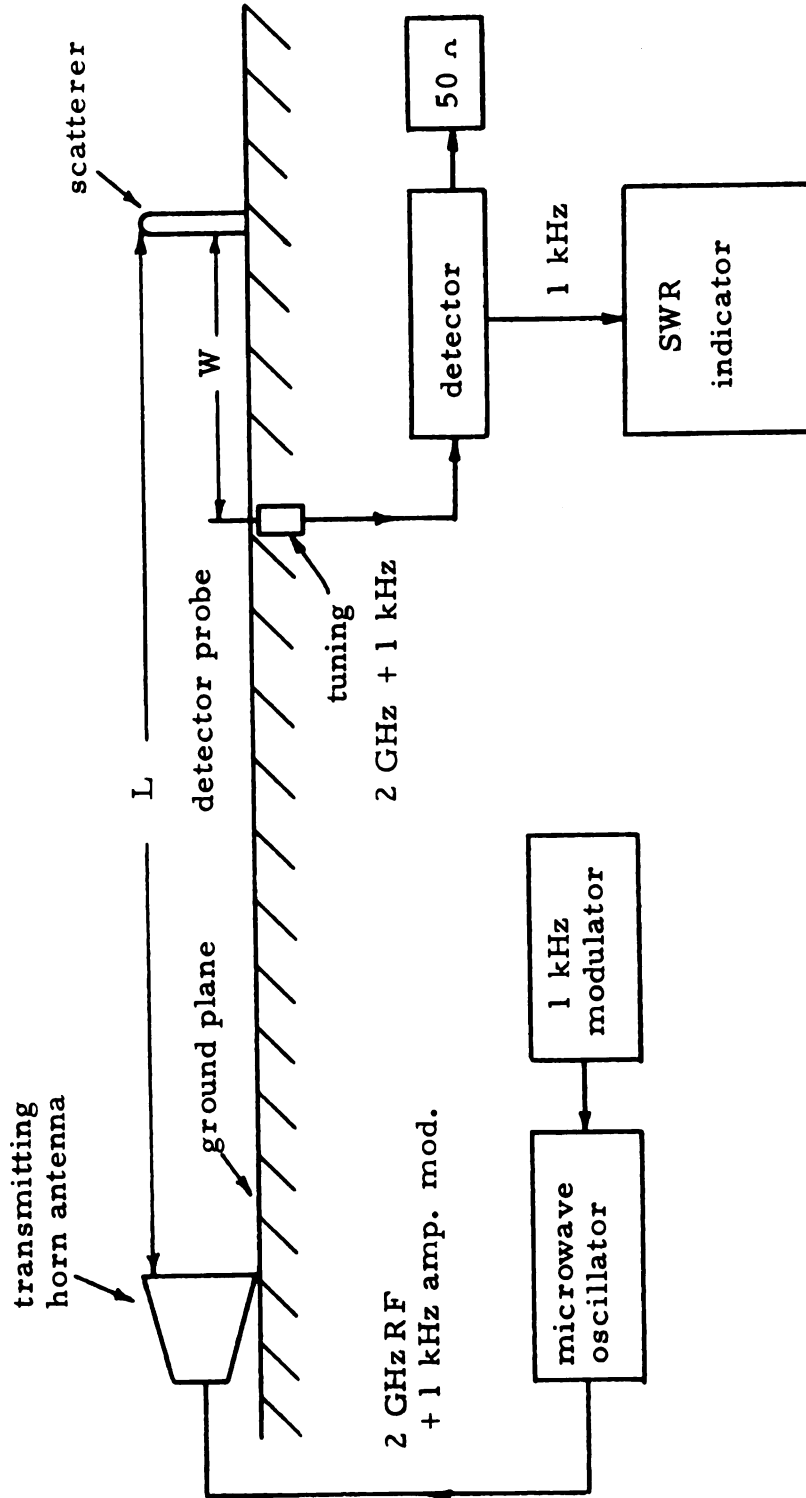


Figure 2.7. Experimental arrangement of the SWR method.



exter
as the
to ex
wave
excit
scatt
proce
874-
(Sylv
pass
1 RE
prob
be e

is s
for
com
inse
inci
sinc
mod
adap

anech
meas
empty

external 1 kHz modulator built in for convenience, which was used as the external 1 kHz source. The modulated R. F. signal is used to excite the transmitting horn, which provides a spherical traveling wave in its radiation or far-zone. The incident and scattered fields excite the monopole probe located between the transmitter and scatterer. An amplitude modulated received R. F. signal is processed through a detector or demodulator (General Radio 874-VQL detecting tee), which utilizes a microwave crystal diode (Sylvania IN23B) as a square law detecting device. A 1 kHz band-pass standing-wave-ratio indicator (HP415B) is used to monitor the 1 kHz detected signal. By adjusting the position of the receiving probe along the longitudinally slotted ground plane, the SWR can be experimentally determined from the indicator readings.

The principle advantages of this technique are that: (i) it is self-normalizing, thus requiring no standard scattering model for comparison; (ii) the equipment is very simple; (iii) no special components are required; (iv) and the measurements are relatively insensitive to small changes in frequency or amplitude of the incident wave. Its principle disadvantage is the slow data rate, since the standing wave pattern must be measured at each scattering model aspect for which σ is desired. This method is particularly adaptable to use with a ground plane boxed anechoic chamber.

With use of the SWR technique, the effectiveness of the anechoic chamber in suppressing spurious reflections can be measured. Figure 2.8 displays the standing wave pattern of the empty chamber in the absence of a scattering model. By direct

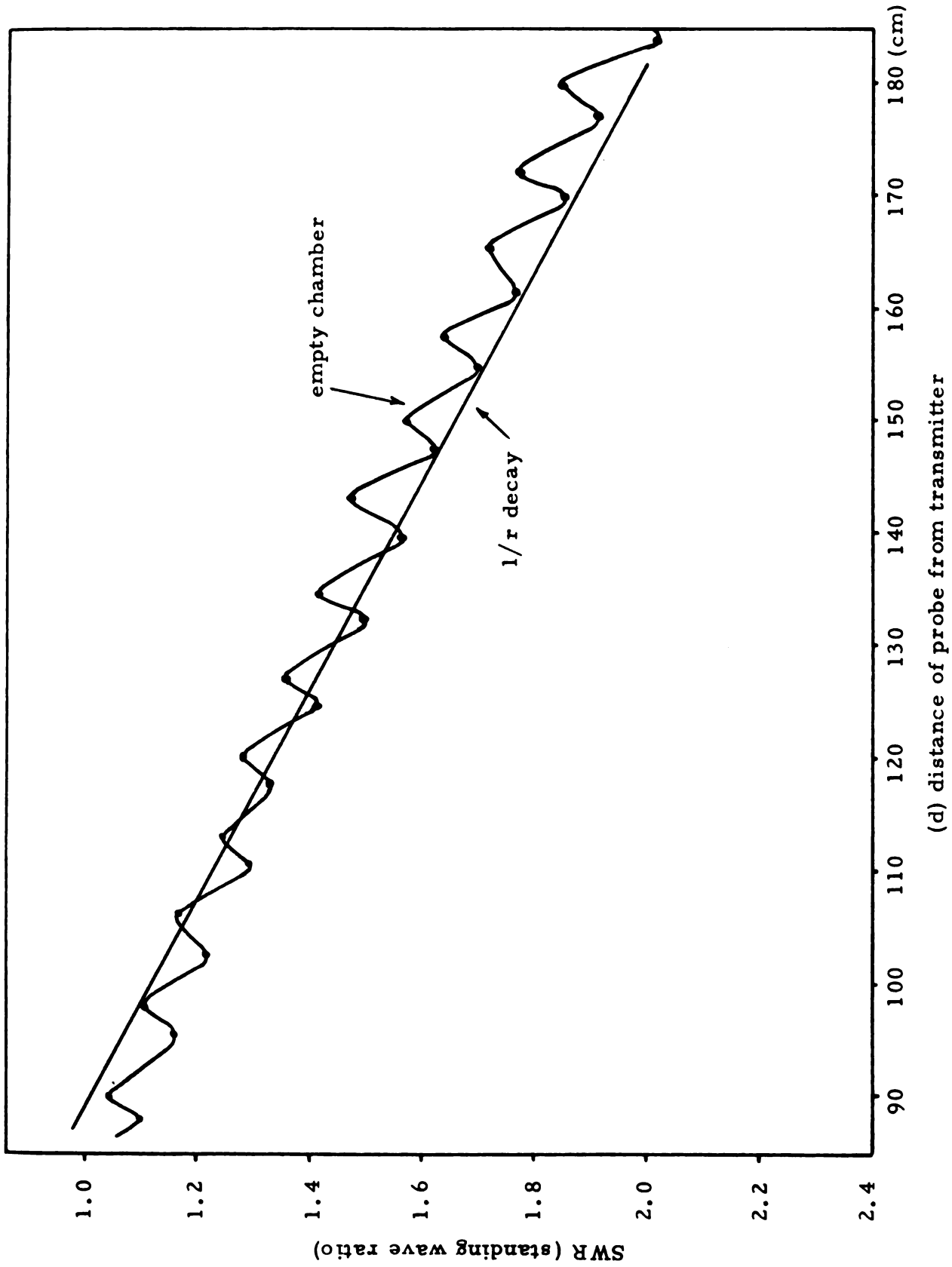


Figure 2.8. SWR of the empty anechoic chamber as a function of the distance of probe from the transmitting horn ($f = 2.0$ GHz).

observation it is noted that the SWR is less than 1.1 for all positions of the probe. Furthermore, the rate of decay is nearly the desired $1/R$ rate mentioned previously. According to comparison with measurements by King¹ and Sletten,⁹ it is felt that this SWR is sufficiently small for an empty anechoic chamber. The non-zero SWR can be attributed to reflections from the edges of the ground plane, the chamber walls, and objects outside of the chamber.

2.2.2. The Cancellation Method

A second technique for experimentally determining the back-scattering cross sections of metallic objects is known as the cancellation method. For this technique, a stationary detecting probe is placed at a position d between the transmitter and the scattering object in the far-field of each and on a line joining the transmitter and scattering object. Just as for the SWR method, it is noted that both incident and scatter fields excite the probe. Correspondingly, the total signal from the probe can be written as

$$V_{\text{total}} = V_i + V_s = V_1 e^{-j(\theta_1 - \omega t)} + V_2 e^{j(\theta_2 + \omega t)} \quad (2.4)$$

where V_1 and V_2 are the magnitudes of voltages due to the incident and scattered fields. The essential mechanism of this method is to cancel the probe signal excited by the incident wave, obtained with the scattering object absent from the anechoic chamber, by mixing it with a reference signal from the microwave oscillator which has the same amplitude but is exactly 180° out of phase with the probe signal. Mathematically, this reference signal is



V
i
V
i
t
d
t
r
s
p
c
b
a
s
h

(
d
m
b
c
t
ca

$$V_{\text{ref}} = V_1 e^{-j(\theta_1 - \omega t + \pi)} = -V_1 e^{-j(\theta_1 - \omega t)}$$

When the scattering object is replaced, the probe signal measured is directly proportional to only the reflected field since

$$V_{\text{total}} + V_{\text{ref}} = V_s \cdot$$

The experimental arrangement for the cancellation method is indicated in Figure 2.9. A reference signal is obtained from the same oscillator which drives the transmitting horn. The detected and reference signals are then mixed by processing them through a directional coupler. This also serves to isolate the reference signal from the detecting probe, which in turn avoids spurious radiation of the reference signal from the probe. The phase of the reference signal is varied by means of a line section of adjustable length (GR874-LK20L), while its amplitude is adjusted by means of a variable 20dB attenuator (ARRA 2414-20). Phase and amplitude of the reference voltage are then adjusted until the mixed signal is zero. All R.F. connections are with RG58 coaxial lines having a characteristic resistance of 50 ohms.

The mixed signal can be monitored by either of two procedures:

(i) 1 kHz modulation and amplitude detection, or (ii) hetrodyne detection. The first technique is identical to that used for the SWR method (section 2.2.1) where the R.F. signal is amplitude-modulated by a 1 kHz square-wave source and subsequently demodulated by a crystal detector. A 1 kHz bandpass SWR indication may then be used to monitor the mixed and processed signal. The meter scale is calibrated in both a linear scale of volts, which is proportional to



transmitting
horn antenna



detector probe

scatterer

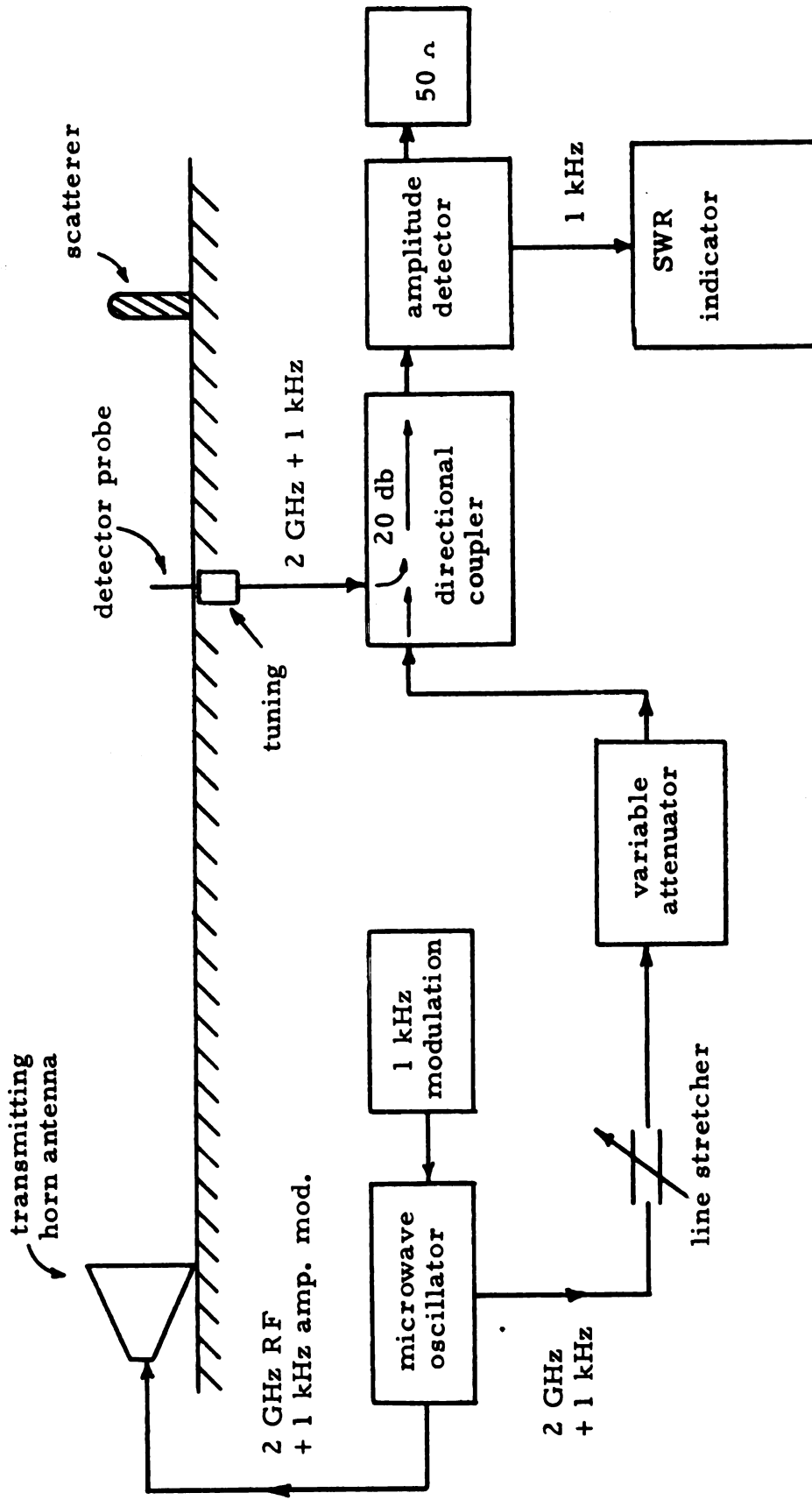


Figure 2.9. Experimental arrangement of the cancellation method.

the electric
is a relative
desired rel

A se

at the output
signal with
than the me
signal of di
I. F. or inte
used in this
requires the
the desired
calibrated e
measurement
technique as

The p

method is the
cancellation m
in the frequen
may be minim
to be short. I
in the present
rate.

An adv
level, althoug
sufficiently sr

the electric field, and decibels. Since the dB or decibel reading is a relative measurement of power, it produces directly the desired relative measurements for σ in decibels.

A second technique for measuring the mixed R.F. signals at the output of the directional coupler involves heterodyning this signal with another having a frequency slightly higher or lower than the measurement frequency in such a way as to produce a signal of difference frequency low enough to amplify easily. The I. F. or intermediate frequency amplifier (General Radio 1216A) used in this research has a passband centered at 30 MHz, which requires the heterodyning frequency to be $f_s \pm 30$ MHz to produce the desired I. F. frequency of 30 MHz. Again, the meter scale is calibrated either linearly in volts or in decibels. The same measurements may therefore be made with this heterodyning technique as with the 1 kHz amplitude modulation method.

The principle advantage of the cancellation over the SWR method is the rapid data rate. A decided disadvantage of the cancellation method is its extreme sensitivity to small changes in the frequency or amplitude of the incident wave. This problem may be minimized by requiring the time period of data-taking to be short. It is this method which has proved to be most valuable in the present investigation, primarily because of the rapid data rate.

An advantage of the heterodyning method is its low noise level, although that of the 1 kHz modulation method is generally sufficiently small. The heterodyning method is felt to be too sensitive

to extrane
persons in
there are t
even great
modulation
consequent

to extraneous reflections, particularly when there is movement of persons in the vicinity of the anechoic chamber. Further, since there are two mixing signals involved in this method, there is even greater sensitivity to small changes in frequency. The 1 kHz modulation method, applied to the cancellation technique, is consequently utilized almost exclusively throughout this research.

MODIF

Sinc

of the back

bodies are

configurati

radar cross

and theoret

wires symm

3.1. When

electromagn

wires. The

can be contr

that the total

reduced (or e

of simplicity,

3.1. Theory

Let th

wave at a dis

Figure 3.1.

cylinders is t

where E_0 is

CHAPTER III

MODIFICATION OF BACKSCATTERING FROM A SPHERE

Since the object of this research is to study the modification of the backscatters of metallic objects, several shapes of conducting bodies are considered; the solid conducting sphere being the first configuration to be investigated. A new technique for modifying the radar cross section of a metallic sphere is investigated experimentally and theoretically. This method consists of attaching two thin, loaded wires symmetrically to the sphere in the manner indicated in Figure 3.1. When the sphere and the loaded wires are illuminated by an electromagnetic wave, currents are induced on the sphere and the wires. The amplitude and phase of the induced current on the wire can be controlled by adjusting the loading impedance in such a way that the total scattered field from the sphere and wires can be reduced (or enhanced). This method has the practical advantage of simplicity, and should prove valuable in radar camouflage.

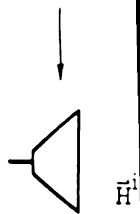
3.1. Theory

Let the sphere with loaded wires be illuminated by a plane wave at a distance R from the transmitting horn as indicated in Figure 3.1. The incident field at the center of the sphere and cylinders is then

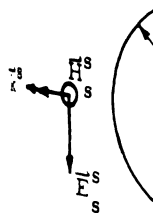
$$E^i = E_o e^{-j\beta_o R} \quad (3.1)$$

where E_o is a constant electric field amplitude, and β_o is the

transmission
horn



Figure



Figure

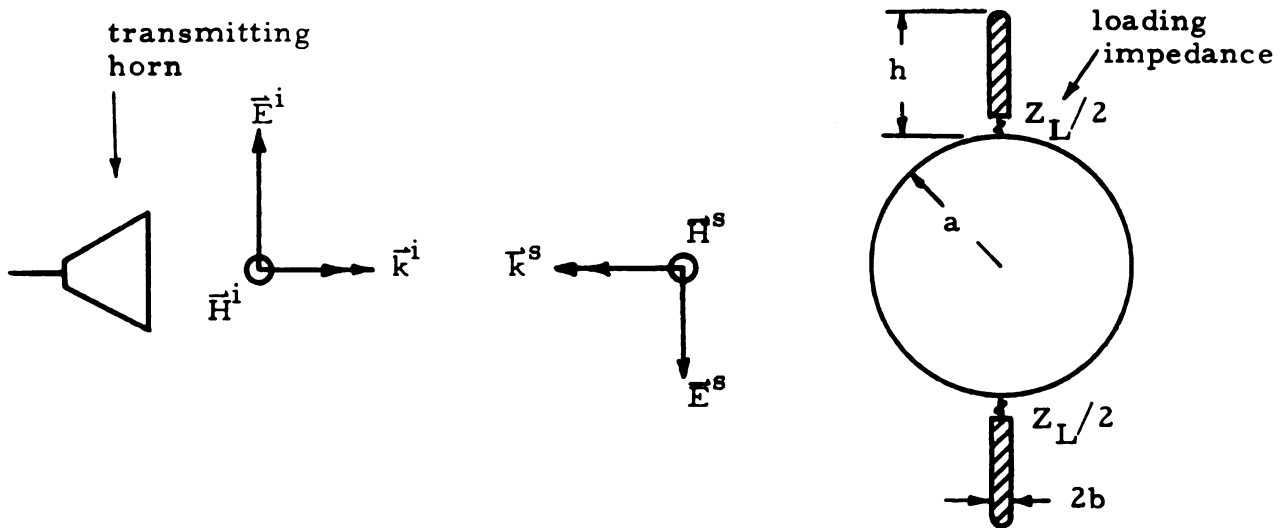


Figure 3.1. Geometry of problem of sphere with loaded wires.

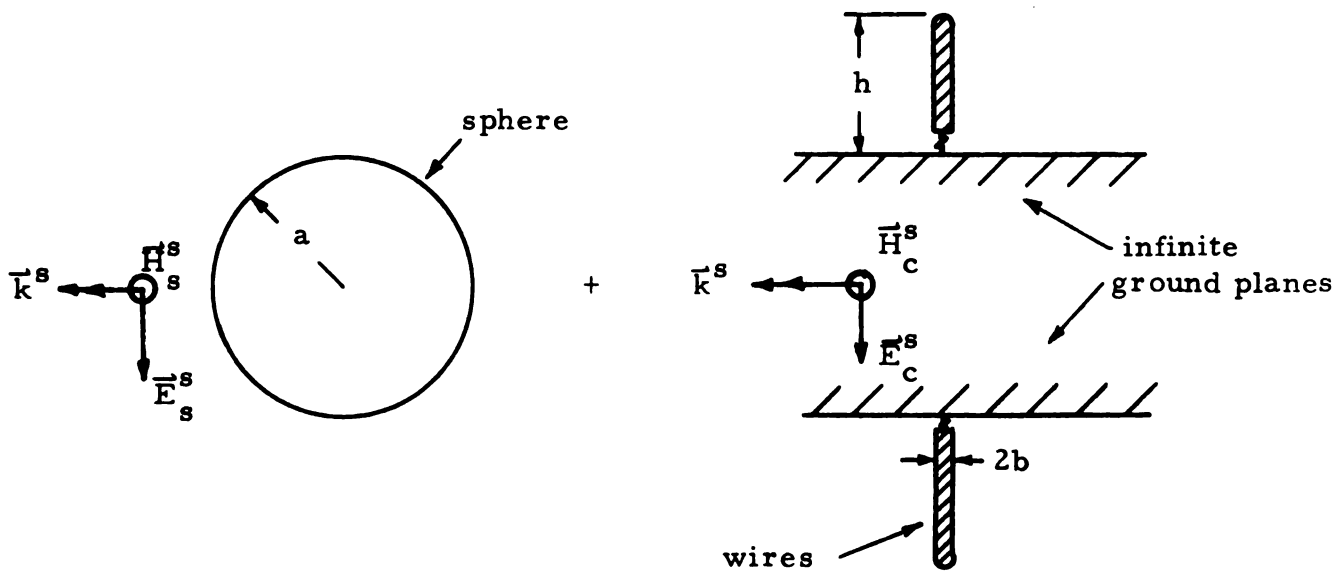


Figure 3.2. Geometry of reduced problem of sphere with loaded wires.

free space

Since

to obtain, b

wires is di

employed fo

wires can b

conducting s

pair of infin

(see Figure

of the source

compared to

This

the backscatt

monopole, cy

($\theta = 0^\circ$) is co

form a two el

the two cylind

fields of the s

to yield an exp

The so

is well known,

M. E. Bechtel

scatter field of

free space wave number.

Since an exact solution to this problem is far too complicated to obtain, because the coupling between the sphere and the loaded wires is difficult to account for, the superposition principle is employed for this complex structure. The sphere with the loaded wires can be approximated by two separate structures, the solid conducting sphere and two loaded wires which are attached to a pair of infinite ground planes separated by the sphere diameter $2a$ (see Figure 3.2). It is assumed that the scatterer is in the far field of the source (i. e., $R \gg h, \lambda, a$) and that the wire radius is small compared to the wavelength such that $\beta_0 b \ll 1$.

This reduced problem may now be solved easily by considering the backscattered fields from the sphere and from the two imaged, monopole, cylindrical scatterers. Since only the backscatter field ($\theta = 0^\circ$) is considered in this research, the two imaged cylinders form a two element colinear array and the total scattered field by the two cylinders is twice that of a single cylinder. The backscattered fields of the sphere and the loaded cylinders can then be superposed to yield an expression for the total backscattered field.

The solution for the backscatter from a solid conducting sphere is well known, and detailed numerical results have been tabulated by M. E. Bechtel.¹⁰ Given the incident field described above, the backscatter field of the sphere is,

$$E_s^s = E_o \frac{a}{2R} e^{-j2\beta_0(R-a)} G \quad (3.2)$$

where

$G =$

and $J_n(\beta_0)$ a

the Hankel

space wave

indicates the

Hankel funct

function. It

approximate

As in

field of the 1

Liepa.³ With

far-zone back

where

and

where

$$G = \frac{-je^{-j2\beta_0 a}}{\beta_0 a} \sum_{n=1}^{\infty} (-1)^n (2n+1) \left[\frac{J_n(\beta_0 a)}{H_n^{(2)}(\beta_0 a)} - \frac{[\beta_0 a J_n(\beta_0 a)]'}{[\beta_0 a H_n^{(2)}(\beta_0 a)]'} \right] \quad (3.3)$$

and $J_n(\beta_0 a)$ is the Bessel function of order n while $H_n^{(2)}(\beta_0 a)$ is the Hankel function of the second kind and order n . β_0 is the free-space wave number and a is the radius of the sphere. The prime indicates the first derivative of the quantity containing the Bessel or Hankel function, in either case, with respect to the argument of that function. It is of interest to note here that G is a complex number approximately equal to one for all arguments $\beta_0 a$.

As in the case for the sphere, the solution for the backscattered field of the loaded cylinder has been obtained theoretically by Chen and Liepa.³ With the assumption of a plane wave illuminating field, the far-zone backscatter field from the central loaded cylinder is

$$E_c^s = \left(\frac{-4}{\beta_0 R} \right) e^{-j2\beta_0 R} g \quad (3.4)$$

where

$$g = \frac{M(\sin \beta_0 h - \beta_0 h \cos \beta_0 h) + N(1 - \cos \beta_0 h)}{\cos \beta_0 h - M T_{ca} - N T_{sa}} \quad (3.5)$$

and

$$M = \frac{1}{T_{cd}} (1 - \cos \beta_0 h) \quad (3.6)$$

$$N = \frac{-Z_L \sin \beta_0 h (1 - \cos \beta_0 h)^2}{T_{cd} Z_L \sin^2 \beta_0 h - j60 T_{cd} T_{sd} \cos \beta_0 h} \quad (3.7)$$

T_{cd}, T_{sd}
numerically

where the k

and

The radius of
the cylinder w
the cylinder.

Since t
by expressions
field of the sp

T_{cd} , T_{sd} , T_{ca} , and T_{sa} are integrals which must be computed numerically and are given as follows

$$T_{cd} = \int_{-h}^h (\cos \beta_o z' - \cos \beta_o h) K_d(0, z') dz' \quad (3.8)$$

$$T_{sd} = \int_{-h}^h \sin \beta_o (h - |z'|) K_d(0, z') dz' \quad (3.9)$$

$$T_{ca} = \int_{-h}^h (\cos \beta_o z' - \cos \beta_o h) K_a(h, z') dz' \quad (3.10)$$

$$T_{sa} = \int_{-h}^h \sin \beta_o (h - |z'|) K_a(h, z') dz' \quad (3.11)$$

where the kernels are,

$$K_d(z, z') = K_a(z, z') - K_a(h, z') \quad (3.12)$$

and

$$K_a(z, z') = \frac{e^{-j\beta_o \sqrt{(z-z')^2 + b^2}}}{\sqrt{(z-z')^2 + b^2}} \quad (3.13)$$

The radius of the cylinder is taken as b , z denotes position along the cylinder with origin at its center, and $2h$ is the total length of the cylinder.

Since the backscattering of the sphere and cylinders are given by expressions (3.2) and (3.4), respectively, then the total backscatter field of the sphere with loaded wires must be,

$$\begin{aligned}
E^s &= E_s^s + E_c^s \\
&= E_o e^{-j2\beta_o R} \left[\frac{a}{2R} e^{j2\beta_o a} G - \frac{4g}{\beta_o R} \right] \\
&= 4 E_o \frac{e^{-j2\beta_o R}}{\beta_o R} \left[\frac{\beta_o a}{8} e^{j2\beta_o a} G - g \right] \quad (3.14)
\end{aligned}$$

It is the objective here to find the optimum impedance $[Z_L]_o$ which will result in zero broadside backscattering from the composite structure. The backscattered field E^s is therefore equated to zero to yield

$$\begin{aligned}
M(\sin \beta_o h - \beta_o h \cos \beta_o h) + N(1 - \cos \beta_o h) \\
= G_1(\cos \beta_o h - M T_{ca} - N T_{sa}) \quad (3.15)
\end{aligned}$$

where G_1 is defined by

$$G_1 = \frac{\beta_o a}{8} e^{j2\beta_o a} G \quad (3.16)$$

It is observed from equations (3.6) and (3.7) that only N is dependent upon Z_L , so expression (3.15) may therefore be solved for $N = N_o$ (at zero backscatter) and later equated to the right hand side of equation (3.7) as

$$N_o = \frac{G_1 \cos \beta_o h - M(\sin \beta_o h - \beta_o h \cos \beta_o h + G_1 T_{ca})}{1 - \cos \beta_o h + G_1 T_{sa}} \quad (3.17)$$

By solving for Z_L from (3.7) in terms of $N = N_o$, the optimum loading impedance for zero broadside backscatter is obtained as

$$[Z_L]_o = \frac{j N_o 60 T_{cd} T_{sd} \cos \beta_o h}{N_o T_{cd} \sin^2 \beta_o h + \sin \beta_o h (1 - \cos \beta_o h)^2} \quad (3.18)$$

where N_o has been defined in (3.17).

Figure 3.3 indicates the optimum loading impedance $[Z_L]_o$ as a function of electrical length of the wires. The real part of the optimum impedance R_2 is represented by a solid curve, while the imaginary part X_2 is represented by a dashed line curve. For this research, $\beta_o a$ is chosen to be approximately 2.0, since this is near the first resonant peak of the backscatter from a sphere.

It is noted that a negative resistance is required to produce zero broadside backscatter from the composite structure for nearly all lengths of h , which is very difficult to achieve in practice. Consequently, to simplify this problem, a purely reactive loading is investigated as a means for modifying the backscatter from a sphere with loaded wires. By substituting $Z_L = jX_L$ into (3.14) and finding an optimum reactance $[X_L]_o$ to minimize this expression, the backscattered field is effectively minimized. Likewise, the optimum reactance for enhancement of the backscatter from this structure can be obtained.

It is therefore desired to minimize the right hand side of (3.14), which subsequently implies that

$$A = G_1 - g \quad (3.19)$$

be minimized, where G_1 and g are defined by (3.16) and (3.5) with Z_L replaced by jX_L . Substituting G_1 and g and then

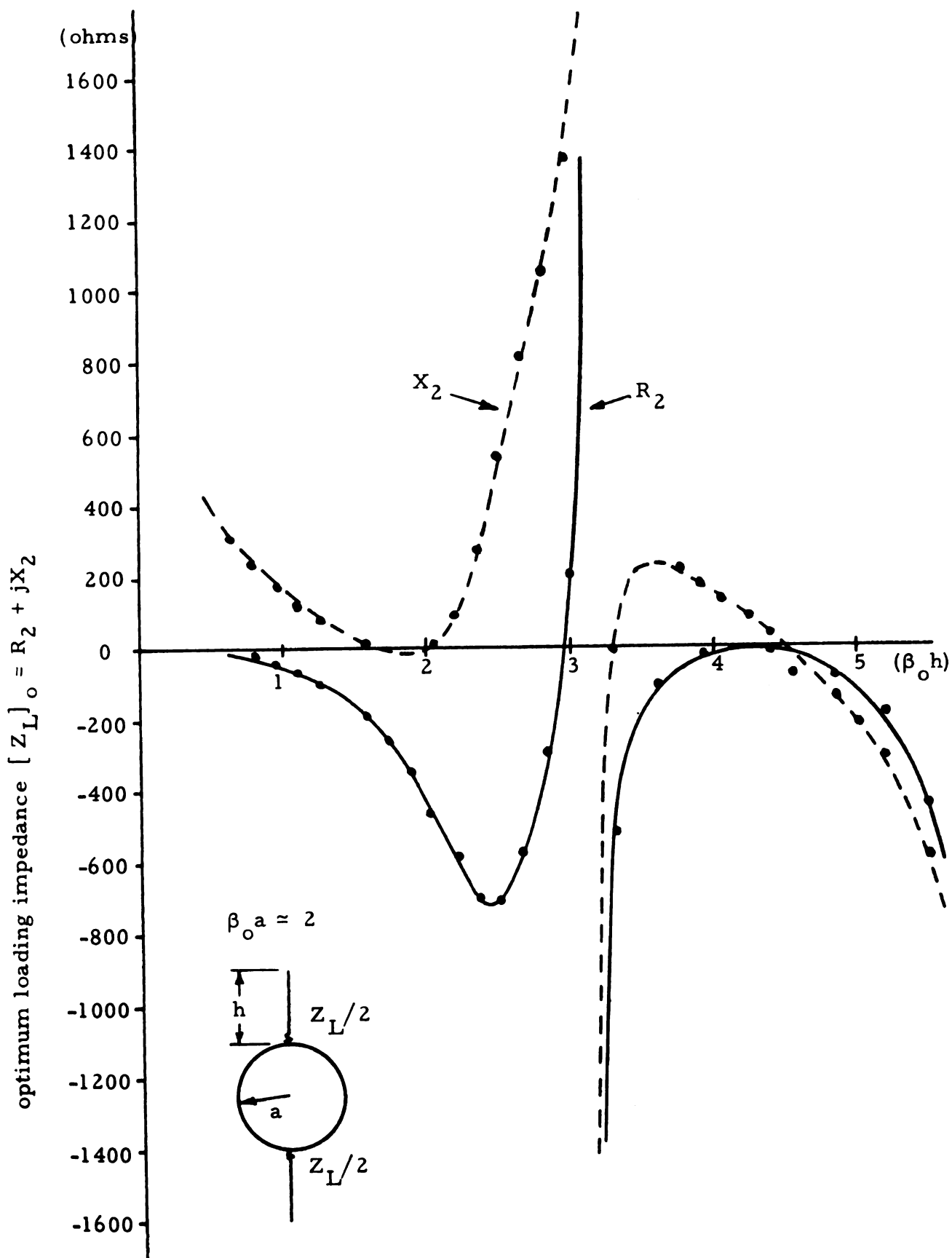


Figure 3.3. Optimum loading impedance for zero broadside backscatter from sphere with loaded wires as a

simplifying, (3.19) can then be written as

$$A(X_L) = \frac{G_1(\cos\beta_o h - MT_{ca}) - M(\sin\beta_o h - \beta_o h \cos\beta_o h) + \frac{(1 - \cos\beta_o h + G_1 T_{sa})X_L \sin\beta_o h(1 - \cos\beta_o h)^2}{T_{cd}(X_L \sin^2\beta_o h - 60 T_{sd} \cos\beta_o h)}}{(\cos\beta_o h - MT_{ca}) + \frac{X_L T_{sa} \sin\beta_o h(1 - \cos\beta_o h)^2}{T_{cd}(X_L \sin^2\beta_o h - 60 T_{sd} \cos\beta_o h)}} \quad (3.20)$$

where M is defined in (3.6) and the integrals T_{cd} , T_{sd} , T_{ca} , and T_{sa} are defined in (3.9) to (3.11). The optimum reactances $[X_L]_o$ for minimum or maximum backscatters are obtained directly from the plots of $A(X_L)$ as a function of load reactance X_L . Figures 3.5 to 3.9 indicate these plots and will be discussed in section 3.3, which is concerned with the comparison of theory with experiment. In these Figures, the theoretical results are represented by circular data points.

3.2. Experiment

The compensation technique for modifying the backscattering cross section of a conducting sphere is studied experimentally in this research and excellent results are obtained. Part of these research results have already been published.¹¹ Experimentally, it is observed that the radar backscattering cross section of a conducting sphere ($\beta_o a \sim 2$ where β_o is the free-space wave number and a the sphere's radius) can be practically eliminated by attaching two reactively loaded wires ($h = \frac{\lambda_o}{6}$ to $\frac{3\lambda_o}{4}$ where h is the wire length and β_o the free-space wavenumber) as shown in Figure 3.4. The

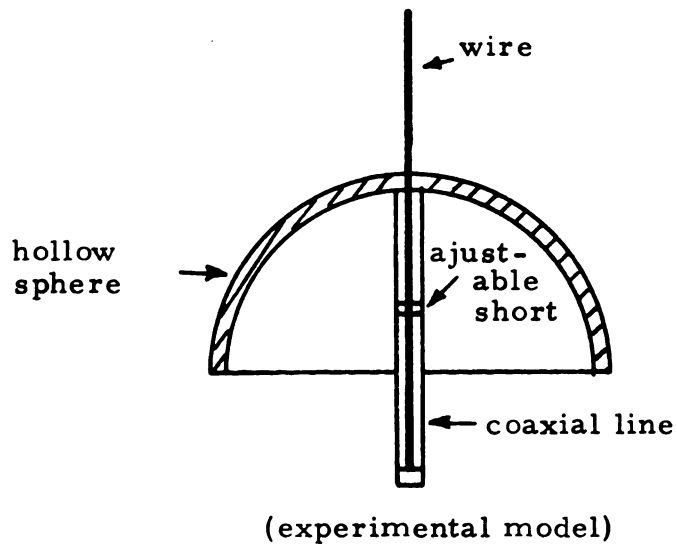
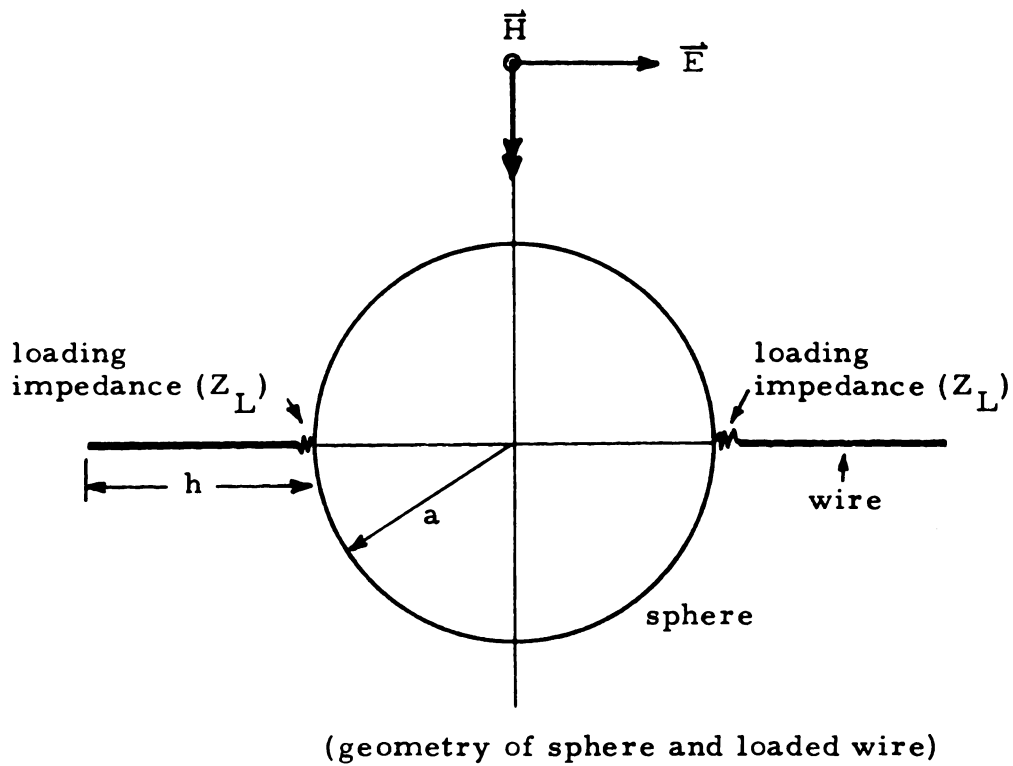


Figure 3.4. A sphere with loaded wires.

wires are loaded at the surface of the sphere by purely reactive impedances which are realized in practice by adjusting coaxial cavities. Measurement of the backscattered field is accomplished as described in section 2.2.2. A frequency of 1.72 GHz is utilized in the experiment.

Results of this experiment are indicated in Figures 3.5 to 3.12. In Figures 3.5 to 3.10, the backscattering cross section of a sphere ($a = 5.71 \text{ cm} = 0.328 \lambda_0$) is represented by a solid straight line and that of a sphere with solid wires (zero loading) by straight dashed lines. In Figure 3.5 the cross section of the combination of the sphere ($a = 5.71 \text{ cm}$) with the loaded wires ($h = 3.5 \text{ cm}$) is plotted as a function of the reactive loading of the wires, and is represented by a solid curve. It is observed in Figure 3.5 that if the length of the coaxial cavity (or the value of the loading reactance) is properly chosen, the total backscatter produced by the sphere and the loaded wires can be reduced by 8 dB. It is also observed in Figure 3.5 that, by varying the loading reactance, the backscatter of the sphere can be enhanced. Figure 3.6 demonstrates the case of a sphere ($a = 5.71 \text{ cm}$) with loaded wires of greater length ($h = 6.1 \text{ cm}$). In this case, the backscattering of the sphere can be minimized to the system noise level. At this condition, the sphere becomes invisible to a radar detecting system. For the same wire length, by adjusting the loading reactance, the backscatter of the sphere can also be enhanced by approximately 7 dB. Thus, by simple adjustment of the loading of the wires, the backscatter of a sphere can be varied

over a 14 dB range. Figures 3.7 and 3.8 indicate the cases of a sphere ($a = 5.71$ cm) with loaded wires of still greater length ($h = 6.7$ cm and $h = 8.4$ cm).

Using longer loaded wires, the radar cross section of a sphere can be similarly minimized to the system noise level. The minimum peak, however, is very sharp compared with the cases of Figures 3.5 to 3.8. This implies that the bandwidth associated with this minimization technique is optimized by using shorter loaded wires, as is discussed in greater detail in Chapter VII. Figure 3.9 indicates a similar case of the same sphere ($a = 5.71$ cm) with longer loaded wires ($h = 10.5$ cm). Similar phenomena are again observed. The backscattering cross section of the sphere may be minimized to the system noise level, but the minimum peak is quite sharp. It is also observed that the maximum peak is less sharp for longer wires while the backscatter is nearly constant for a wide range of loading impedances.

Various other excitation frequencies are used with similar success. At a frequency of 1.72 GHz, various lengths of wires are utilized and the maximum and minimum backscatters of the composite structure are plotted as a function of the electrical length of the wires (see Figure 3.10). The maximum backscatter of the sphere with loaded wires is represented by a dashed line curve and the minimum backscattering cross section is represented by a solid curve. It is observed that minimization is very successful for $\beta_0 h = 0.16$ to 0.5. The optimum reactances for minimum and maximum backscatters from a sphere with loaded wires are indicated

in Figures 3.11 and 3.12, which are also plotted as a function of the electrical length of the loaded wires. Stray capacitance which exists at the terminal end of the coaxial cavity is taken into account when calculating the effective load reactance X_L .

3.3. Comparison of Theory and Experiment

For the case where $f = 1.72$ GHz and the sphere radius is $a = 5.71$ cm, the comparison of experiment with theory is quite favorable. It is observed in Figures 3.5 to 3.9 that the maximum peaks of the theoretical results are much sharper than the experimental results. This is most likely due to the finite conductivity of the sphere and wires, which attenuates the induced currents on the sphere and wires in the resonant cases. The minimum peaks however, compare quite well.

The comparison of theory with experiment of the optimum impedances for minimum and maximum backscatters of the composite sphere-loaded wire structure is presented in Figures 3.11 and 3.12. There is an additional discontinuity in the optimum theoretical minimizing reactance at $\beta_0 h = \pi$ which the experiment does disclose. Excluding this point, the comparison for both the optimum minimizing and maximizing reactances is excellent.

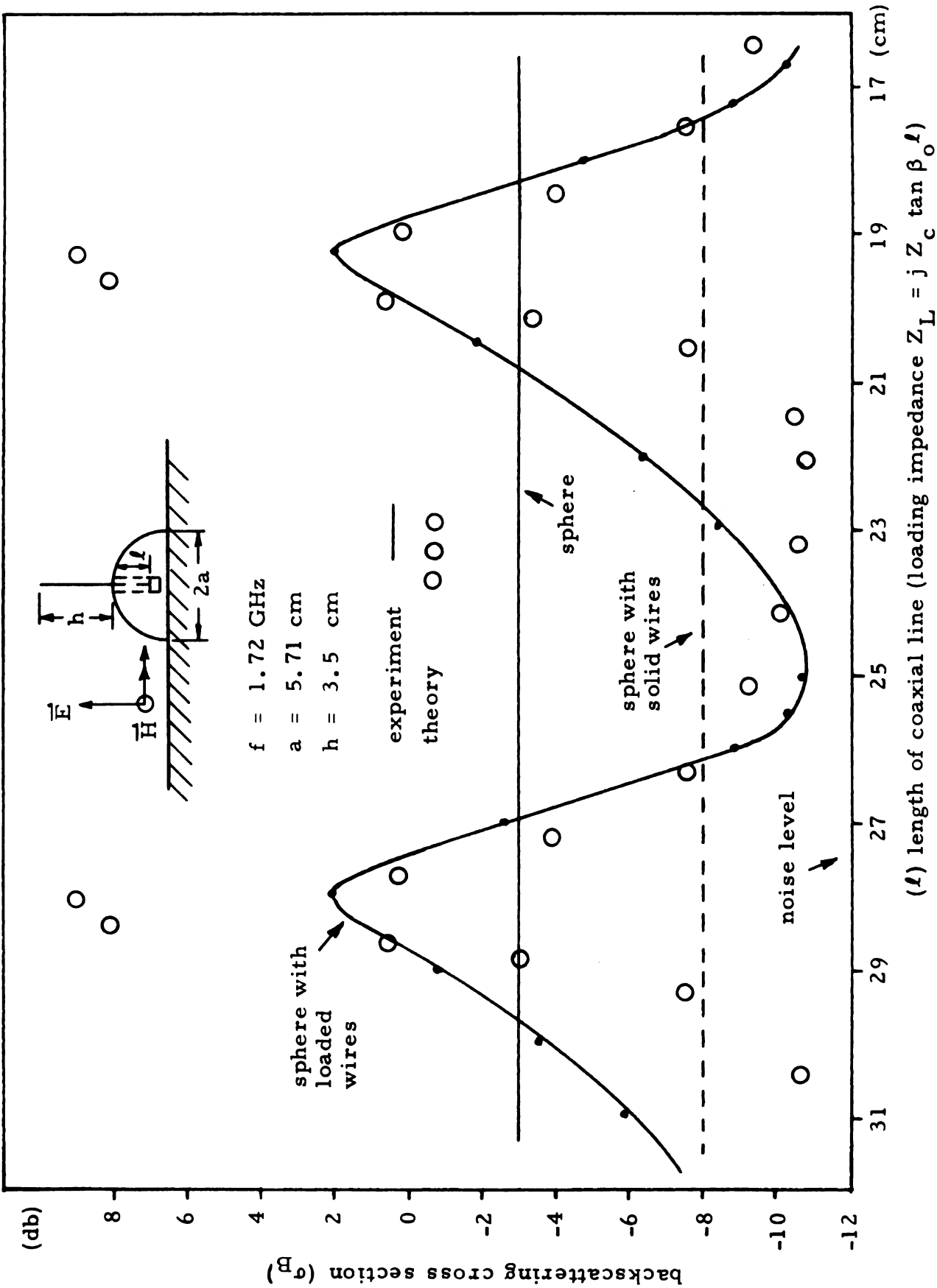


Figure 3.5. Backscattering cross section of a sphere with loaded wires as a function of loading impedance of loaded wires ($a = 5.71$ cm, $h = 3.5$ cm).

(b)

$\frac{1}{h}$

1.72 GHz

0 0

0.00000000

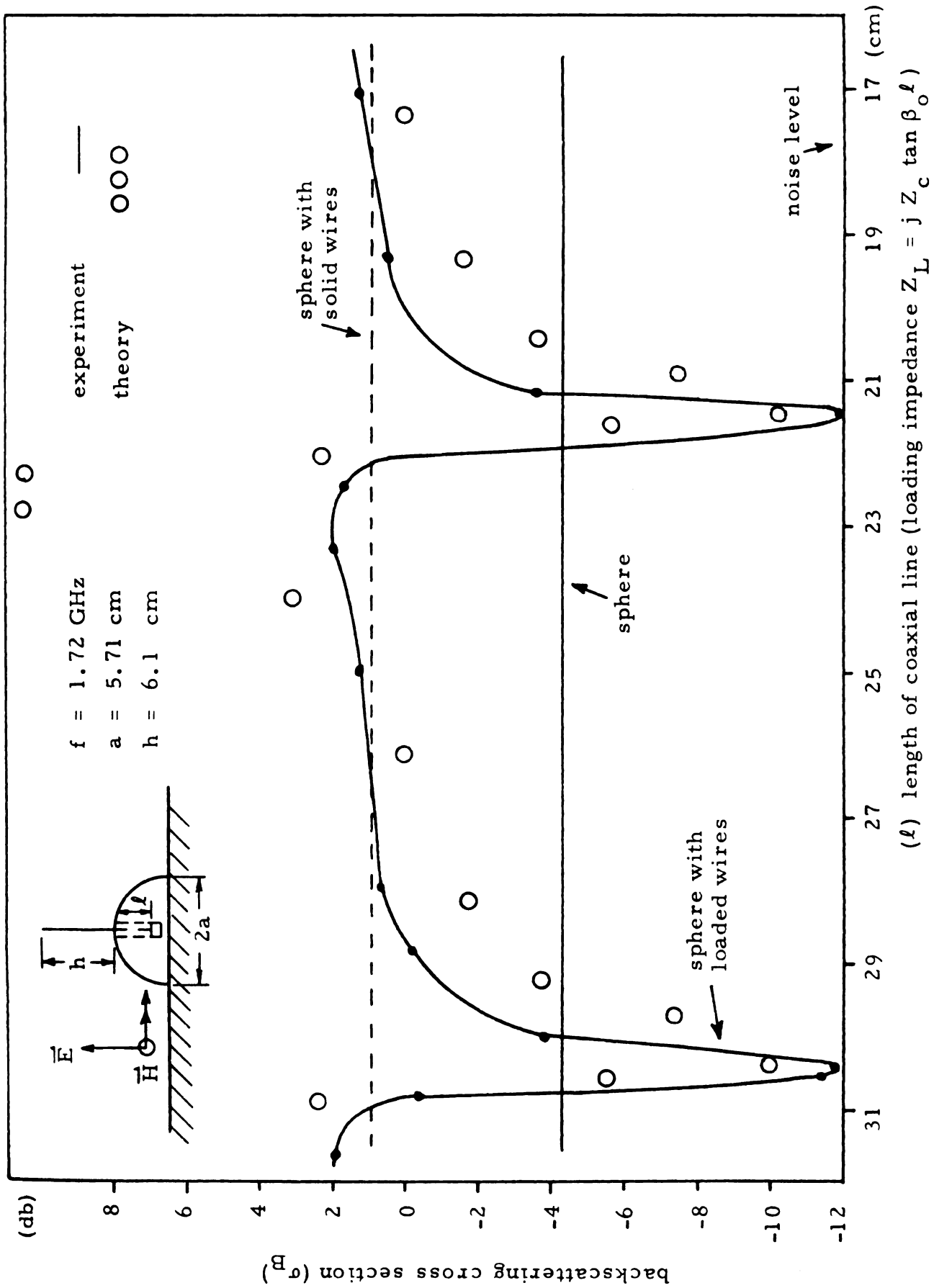


Figure 3.6. Backscattering cross section of a sphere with loaded wires as a function of loading impedance $Z_L = j Z_c \tan \beta_o l$ of loading impedance of loaded wires ($a = 5.71 \text{ cm}$, $h = 6.1 \text{ cm}$).

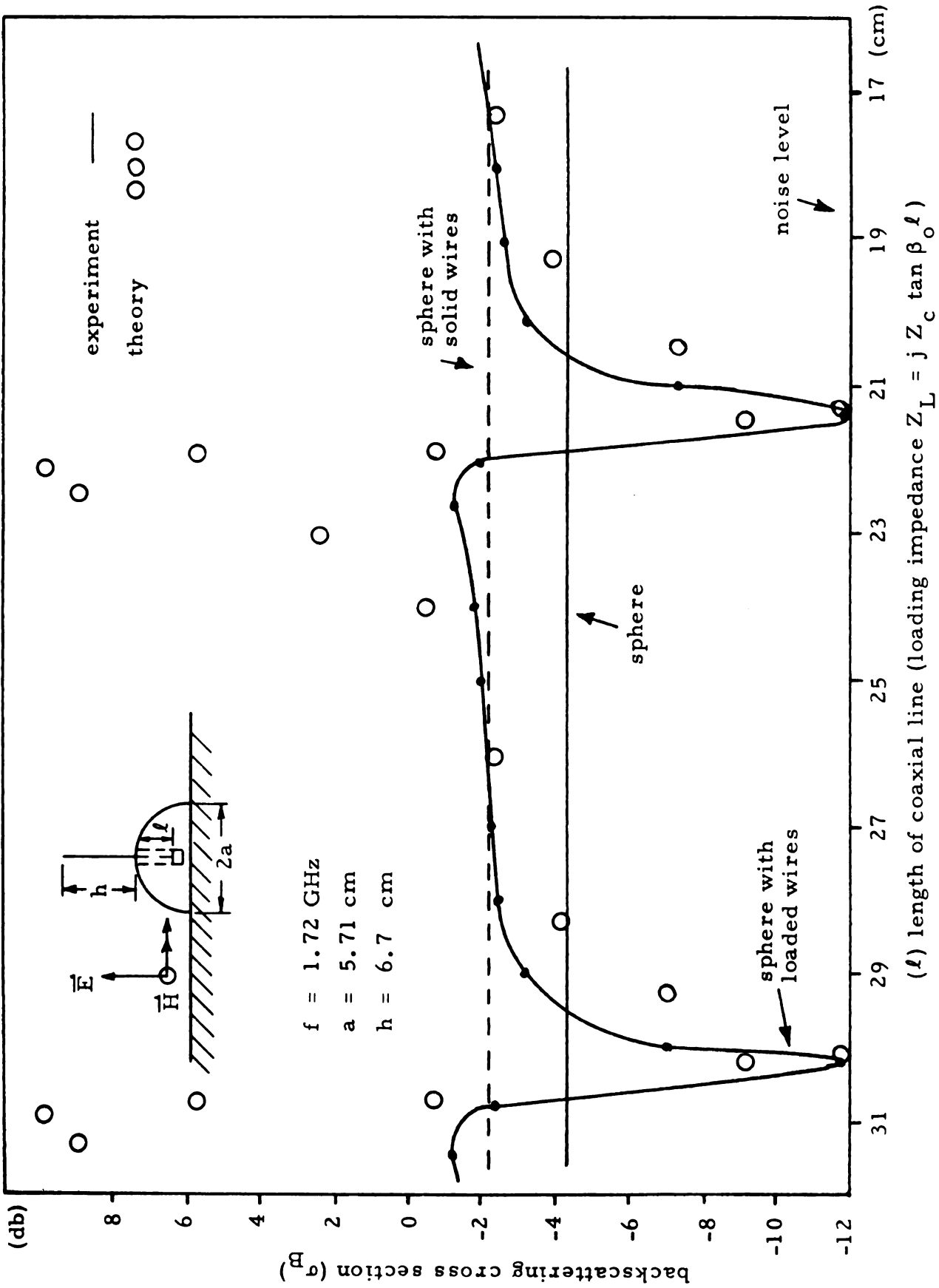


Figure 3.7. Backscattering cross section of a sphere with loaded wires as a function of loading impedance $Z_L = j Z_C \tan \beta_0 l$ (l length of coaxial line (loading impedance $Z_L = j Z_C \tan \beta_0 l$)).

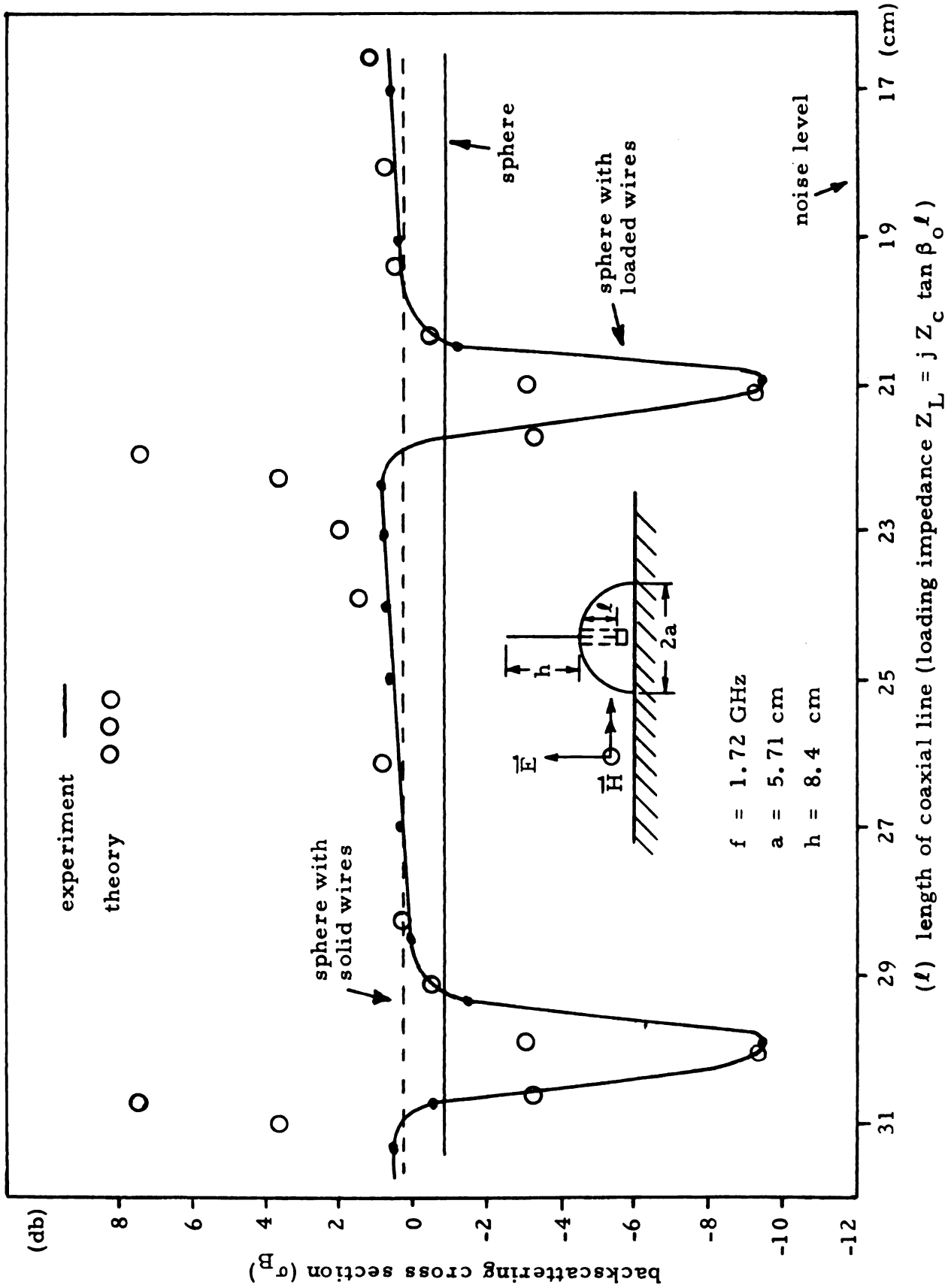


Figure 3.8. Backscattering cross section of a sphere with loaded wires as a function of loading impedance of loaded wires ($a = 5.71 \text{ cm}$, $h = 8.4 \text{ cm}$).

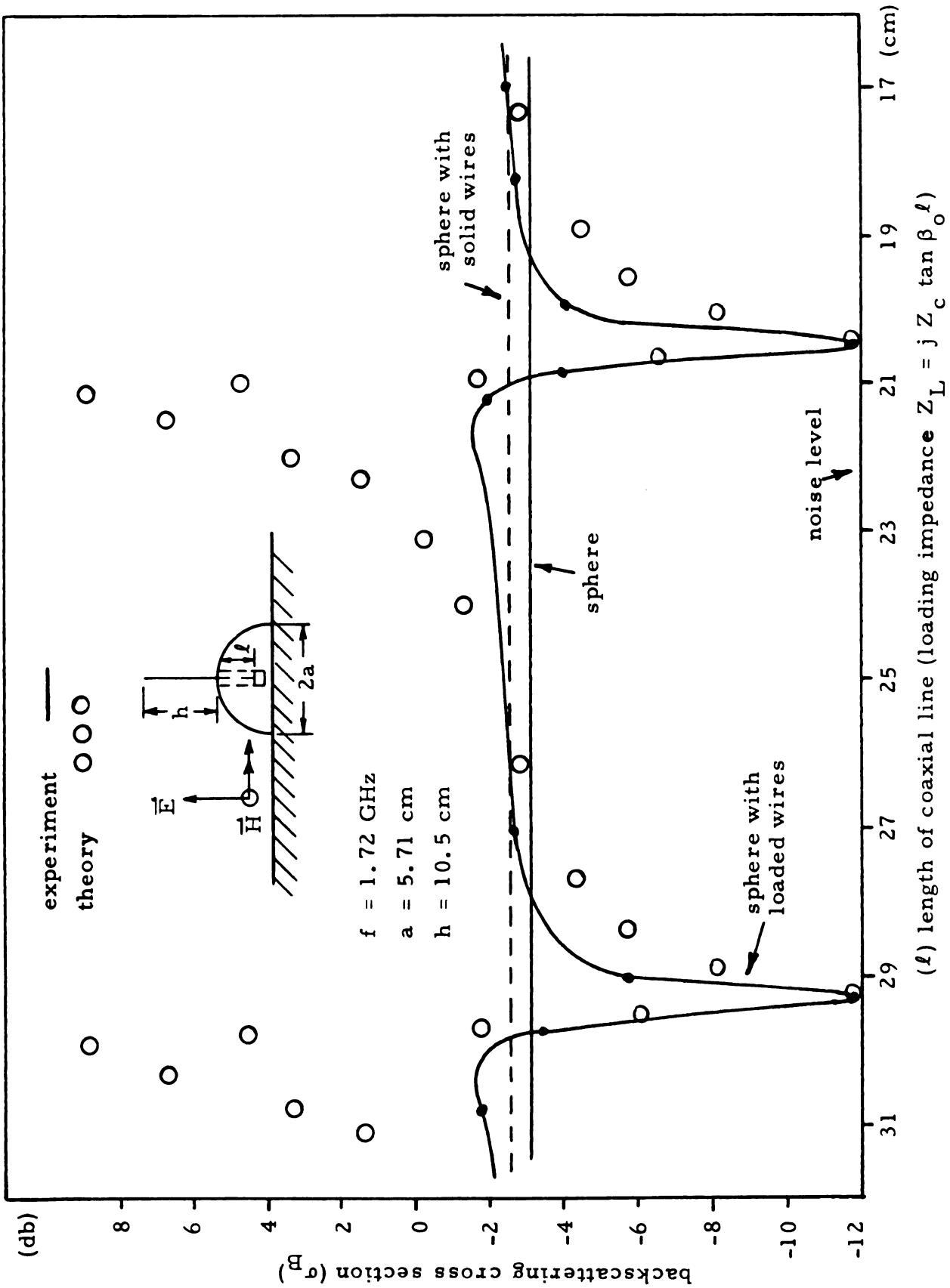


Figure 3.9. Backscattering cross section of a sphere with loaded wires as a function of loading impedance of loaded wires ($a = 5.71 \text{ cm}$, $h = 10.5 \text{ cm}$).



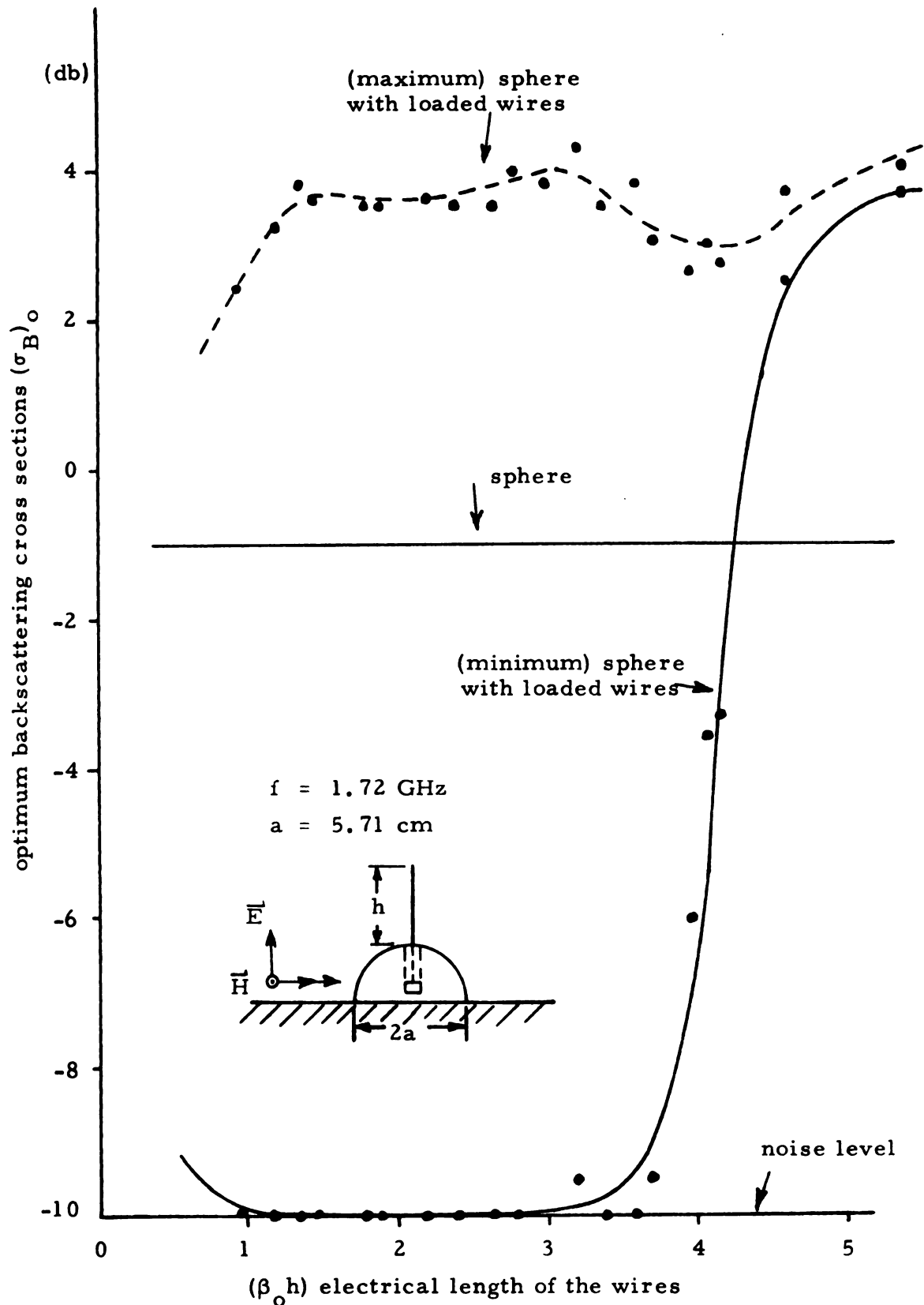


Figure 3.10. Maximum and minimum backscatters from a sphere with loaded wires as a function of

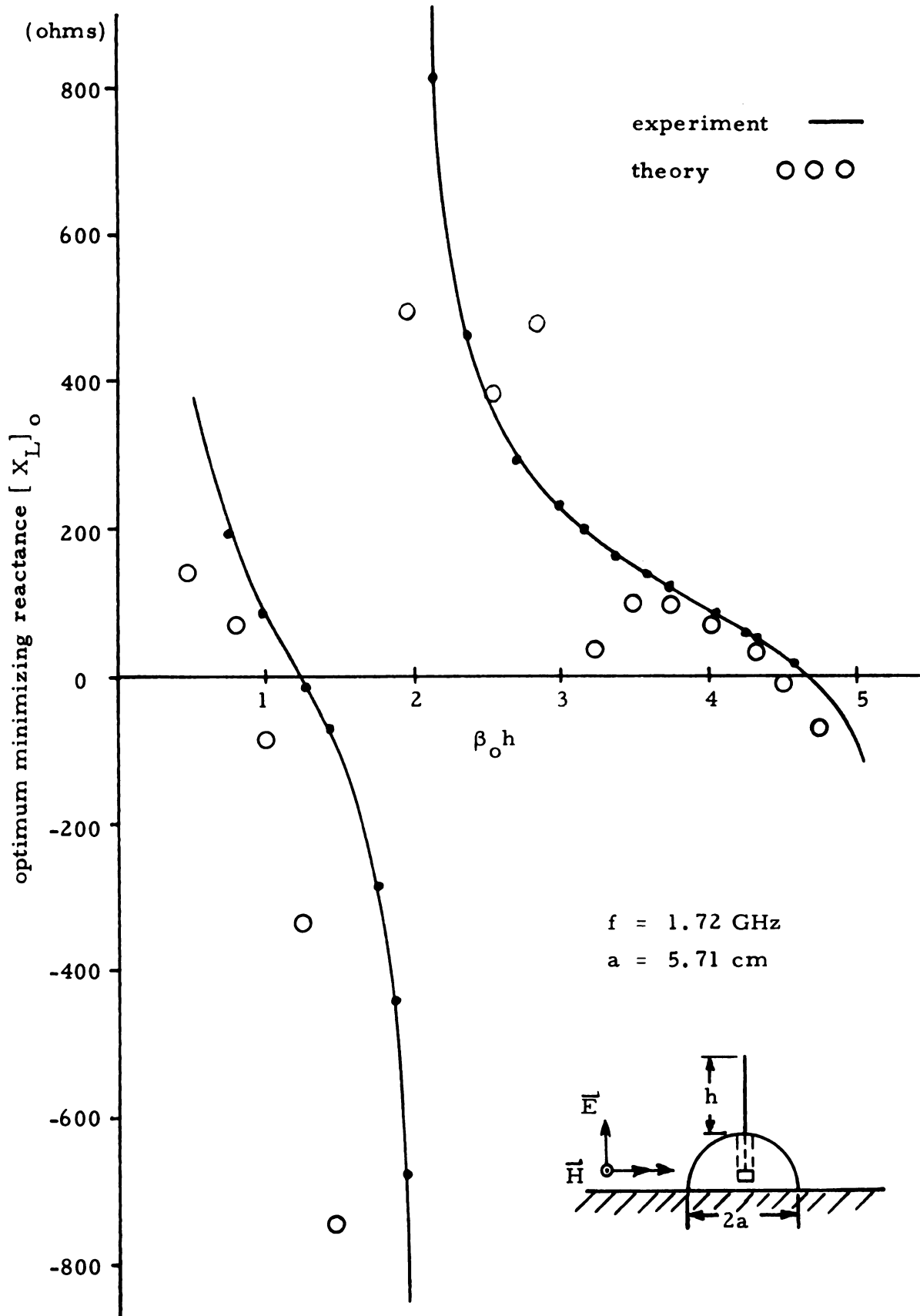


Figure 3.11. Optimum reactance for minimum backscatter from a sphere with loaded wires as a function of electrical length of wires.



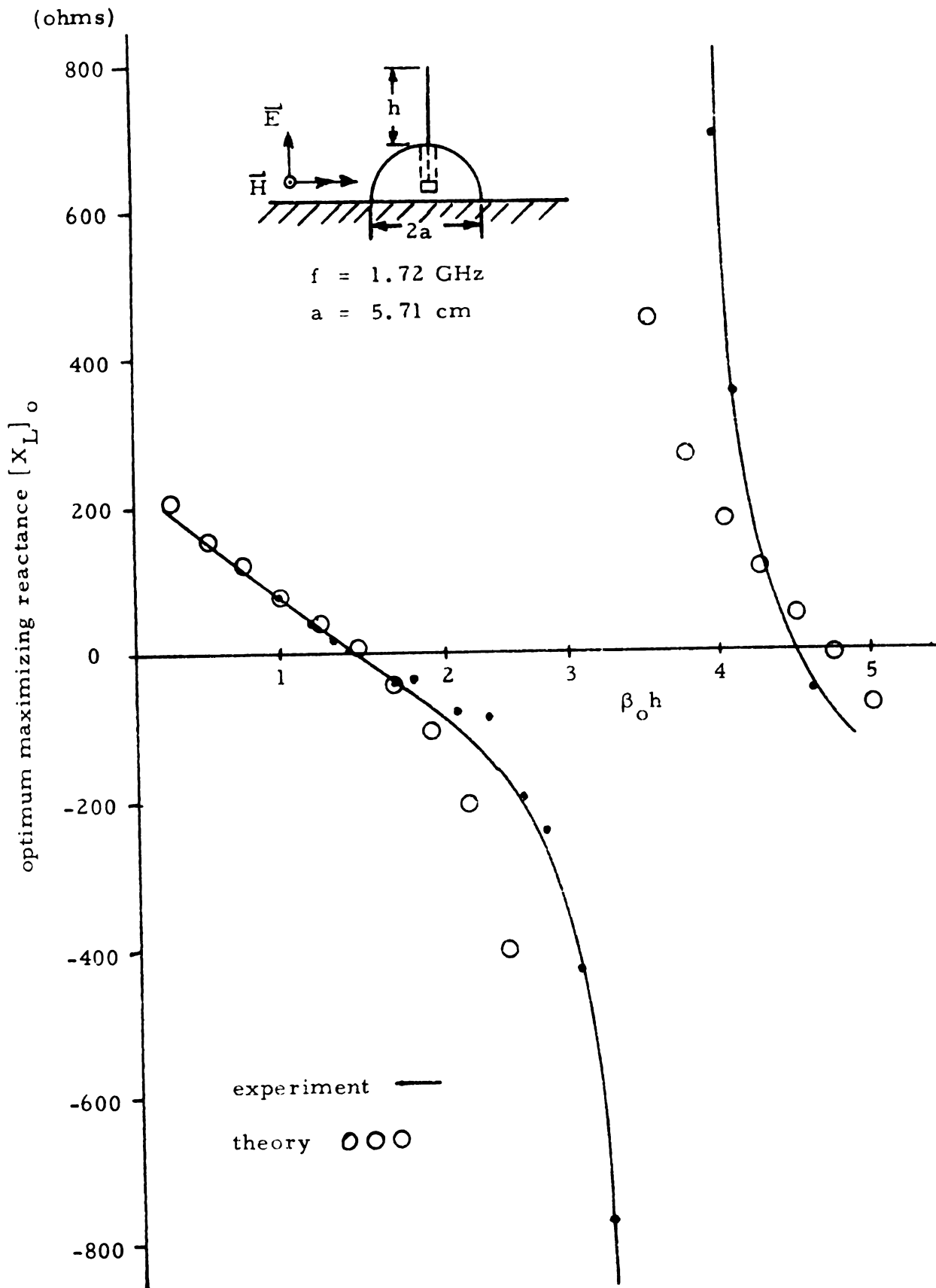


Figure 3.12. Optimum reactance for maximum backscatter from a sphere with loaded wires as a function of electrical length of wires.

CHAPTER IV

MODIFICATION OF BACKSCATTERING FROM METALLIC LOOPS

The results of an experimental investigation on the backscatter of a thin-wire, metallic loop, either circular or rectangular, are presented here. In a recent paper,¹² an experimental study on the resonances of loops was reported. It was shown that the resonant scattering cross sections of wire loops are dependent upon their shape and periferal dimensions. As an extension to this study, modification of the backscattering cross section of a loop by the impedance loading technique is investigated. Some results of this study has already been published elsewhere.¹³

4.1. Circular Loop

The impedance loading technique is applied successfully to modify the backscattered field of a circular, metallic loop. It is observed that, with an optimum impedance loading located at appropriate points on the loop, the amplitude and phase of the induced current can be controlled in such a way that the backscattered field maintained by the induced current is substantially modified. In this investigation, both minimization and enhancement on the backscatter are studied.

Figure 4.1 indicates the geometry of the impedance loaded, circular loop. An experimental model of this conducting loop (diameter = 5.15 cm) is constructed of cylindrical copper wire having a radius of 0.1 cm. In the experiment, the circular loop

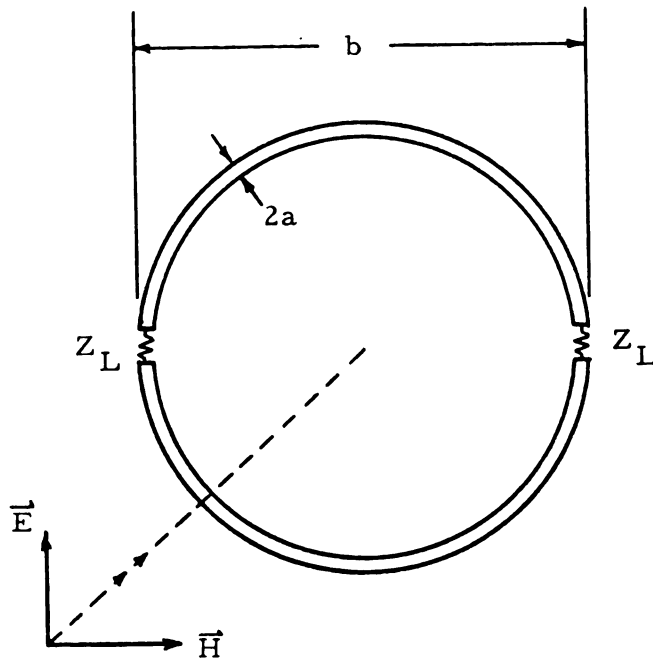
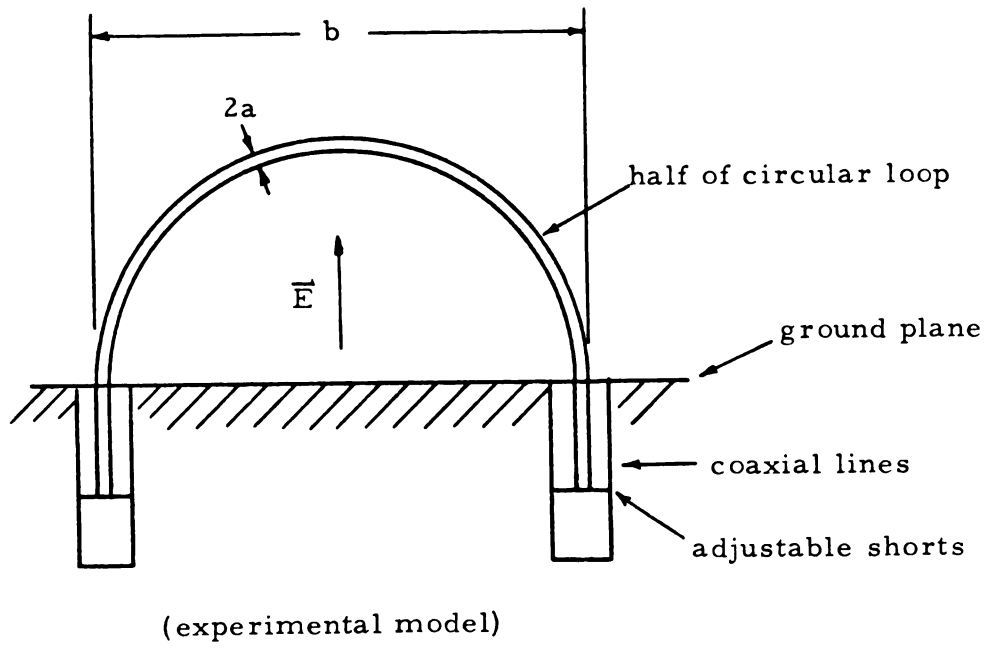


Figure 4.1. Loaded, circular wire loop.

is illuminated by a plane wave at normal incidence and at various frequencies. The cancellation technique described in section 2.2.2 is again employed to measure the backscattered field from the loops. The loop is symmetrically doubly loaded with a pair of identical purely reactive impedances which are realized experimentally by two adjustable coaxial cavities located beneath the ground plane.

In Figures 4.3 to 4.13, the backscattering cross section of the circular loop is plotted as a function of loading impedance for various specified frequencies (1.6 GHz - 2.5 GHz). A solid curve represents the cross section of the loaded loop while a solid straight line represents that of the solid one. It is observed that if the loading impedance (or the length of the coaxial cavity) is properly adjusted, the backscattered field of the loop can be minimized to the noise level of the measurement system. Similarly, the backscattered field of the loop can be maximized or enhanced considerably with another properly selected reactance loading. With the optimum minimizing reactance, up to 15 db reduction in the backscattering cross section is observed at each excitation frequency investigated.

For each specified frequency, an optimum minimizing or maximizing reactive loading impedance is obtained. These optimum impedances for a circular loop are plotted in Figures 4.14 and 4.15 as a function of the electrical loop circumference $\beta_0 b$, where b is the radius of the loop and β_0 is the free space wave number. The solid curve in each of the two figures represents the optimum minimizing impedance and the optimum enhancing impedance respectively for the loaded circular loop. For each of the optimum

reactive impedances obtained, the stray capacitance which exists at the terminal zone of the coaxial line or loop loading point is taken into account.

4.2. Rectangular Loop

The impedance loading technique is also applied successfully to modify the backscattered field of a rectangular, thin-wire loop. As observed for the case of a circular loop, proper choice of an optimum impedance loading located at appropriate points on the loop will control the amplitude and phase of the induced current in such a way that the backscattered field of the loop is significantly modified. A wide range of minimization or enhancement can be achieved by a suitable choice of loading impedance.

In Figure 4.2, the geometry of an impedance loaded, rectangular loop is indicated. Cylindrical copper wire of 0.1 cm radius is utilized in construction of the experimental rectangular loop model which has dimensions of 4.15 cm on each side. A plane wave at normal incidence and of various frequencies is employed to illuminate the rectangular wire loop. Measurement of the backscattered field is accomplished through use of the cancellation method (see section 2.2.2). The loop is loaded symmetrically with a pair of purely reactive impedances.

The backscattering cross section of the rectangular loop for various frequencies (1.6 GHz - 2.5 GHz) is plotted in Figures 4.3 to 4.13 as a function of the loading impedance. A dashed line curve represents the cross section of a loaded square loop while

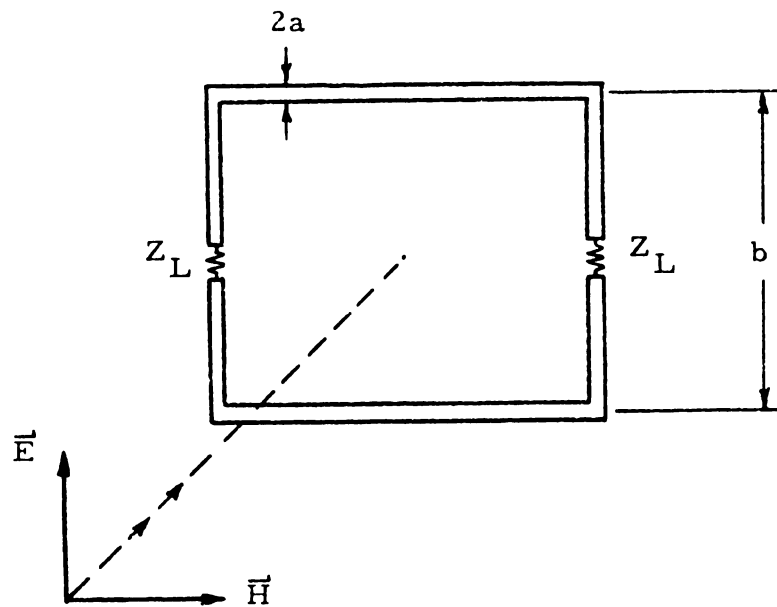
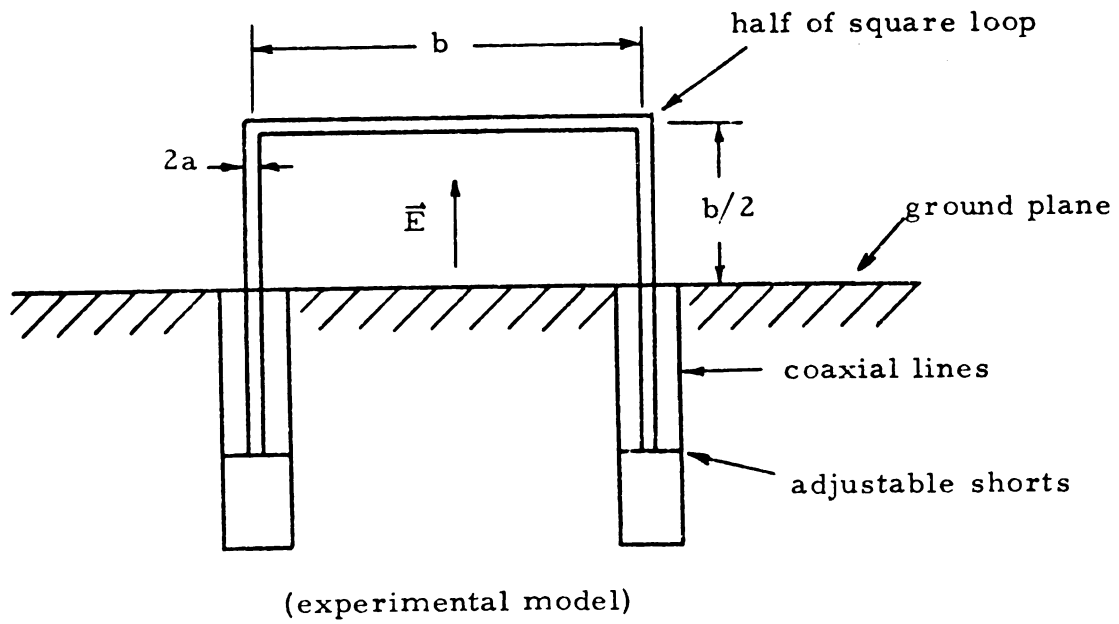


Figure 4.2. Loaded square wire loop.

a dashed straight line represents that of a solid one. Proper adjustment of the loading impedance will minimize the backscattered field to the noise level of the measuring system. It is also observed that another appropriate choice of loading impedance results in maximization of the backscatter by up to 12 dB. The optimum minimization impedance reduces the backscatter up to 15 dB at each particular frequency.

As for the case of a circular loop, an optimum minimizing or maximizing reactive impedance is obtained at each specified frequency. These optimum impedances for the loaded square loop are plotted in Figures 4.14 and 4.15 as a function of the electrical length $\beta_0 b$, where b is the side length of the loop and β_0 is the free space wave number. The dashed line plots in the two figures represent the optimum minimizing impedance and the optimum enhancing impedance respectively of the loaded square loop. These impedances are obtained with account taken for the stray capacitance existing at the input end of the coaxial cavity.

From Figures 4.3 to 4.13, it is observed for each specified frequency that the backscattering from a solid square loop is usually less than that of the solid circular loop (also observed by Lin and Chen¹²), although the maximum cross section above the noise level remains nearly the same for both loop shapes. This observation readily indicates that the backscattering cross section of a circular loop may be reduced more than that of a square loop, whereas for enhancement the opposite is true since the cross section of the square loop can be maximized more.

As a further comparison of the two loop shapes, the optimum reactive impedance for minimum and maximum backscatter indicated in Figures 4.14 and 4.15 may be compared. It is observed that the optimum minimizing reactances for the two loops as a function of loop sizes are positive, although those for the loaded square loop are about three times larger for $\beta_0 b/2$ equal to 0.94 and 1.05. For the optimum maximizing reactance of the circular and square loops, the values are mainly negative and small, although those for the circular loop of which $\beta_0 b/2$ is less than 0.95 are positive. The optimum reactance for the maximum enhancement of the backscatter of a square loop has a fairly sharp peak at $\beta_0 b/2$ equal 1.275 where the reactive impedance is about $x_L = -550$ ohms. A similar peak is seen for optimum maximizing reactance of the circular loop although of a much less magnitude. This observation readily suggests the reason for a rapid variation of the backscattering cross section as a function of coaxial line length ℓ of the loaded square loop near the point of maximum enhancement as shown in Figures 4.10 to 4.13 for example, since large impedances of a coaxial cavity vary rapidly for small variations in ℓ . The rapid change in the cross sections as a function of ℓ of both loop shapes near the point of optimum minimization for $\beta_0 b/2$ equal 1.25 to 1.4 may be explained in a like manner since the reactance is large there.

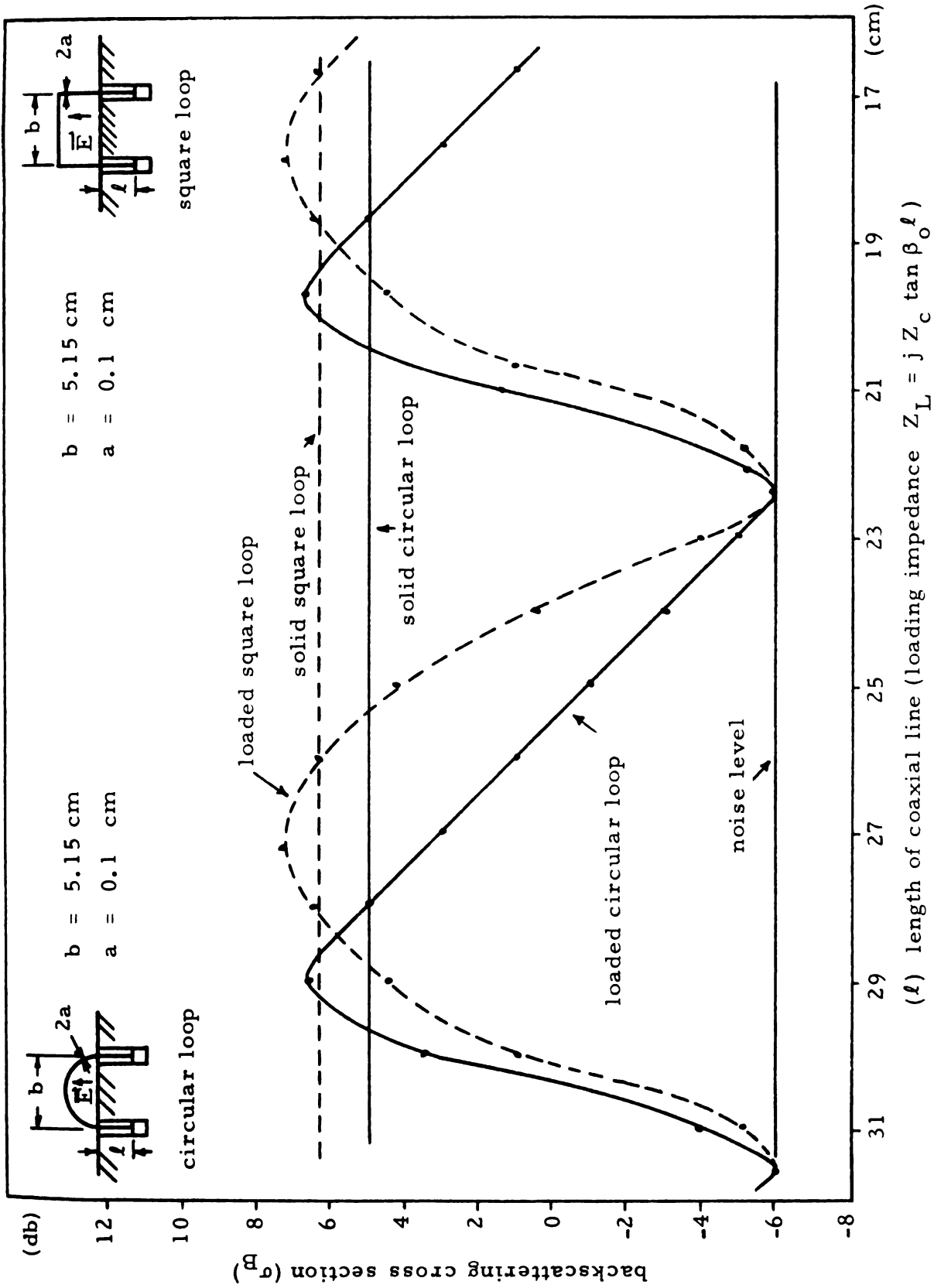


Figure 4.3. Backscattering cross section of a loaded loop as a function of loading impedance $Z_L = j Z_c \tan \beta_0 l$ (l) length of coaxial line (loading impedance $Z_L = j Z_c \tan \beta_0 l$) impedance ($f = 1.61$ GHz).

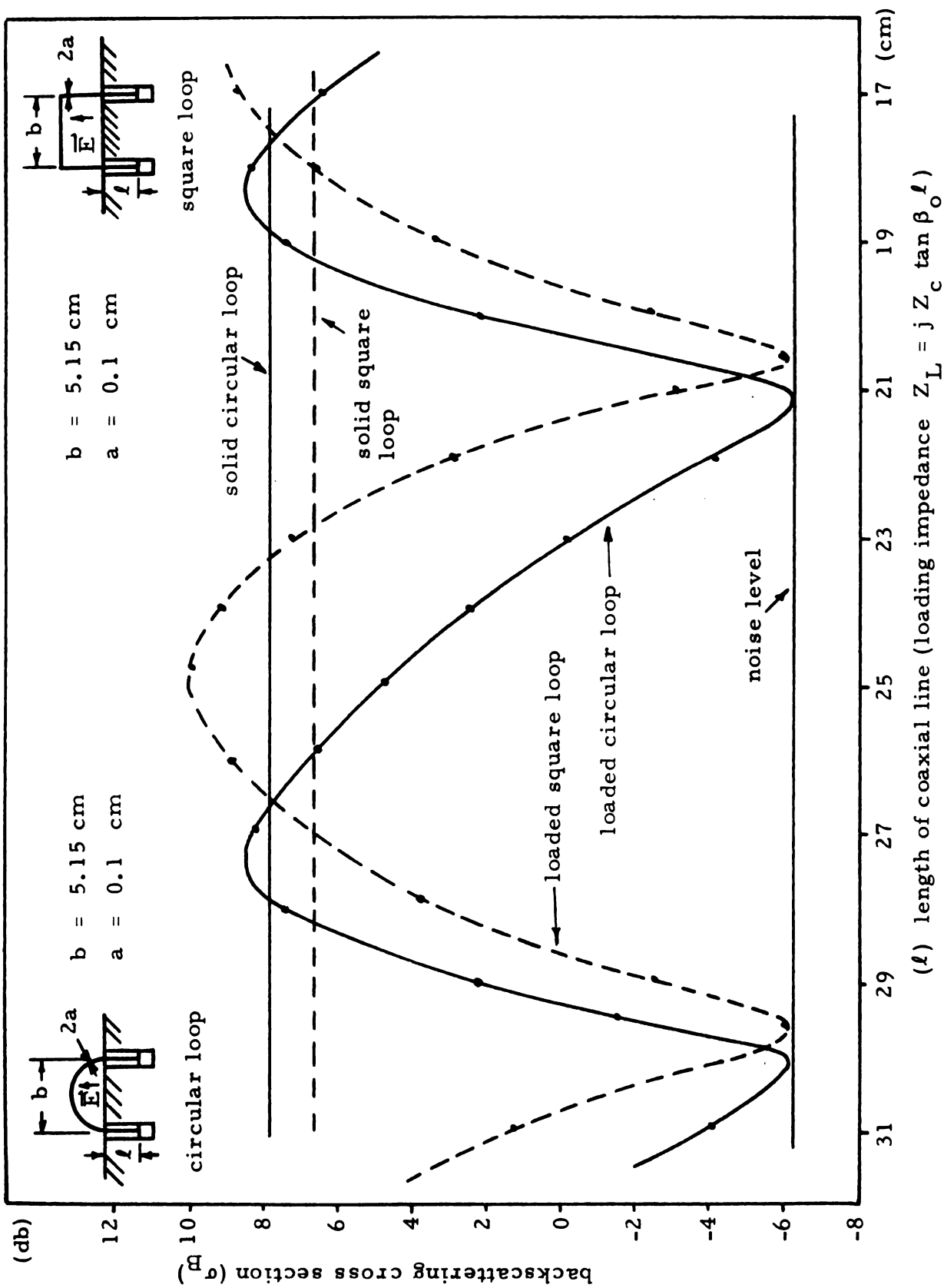
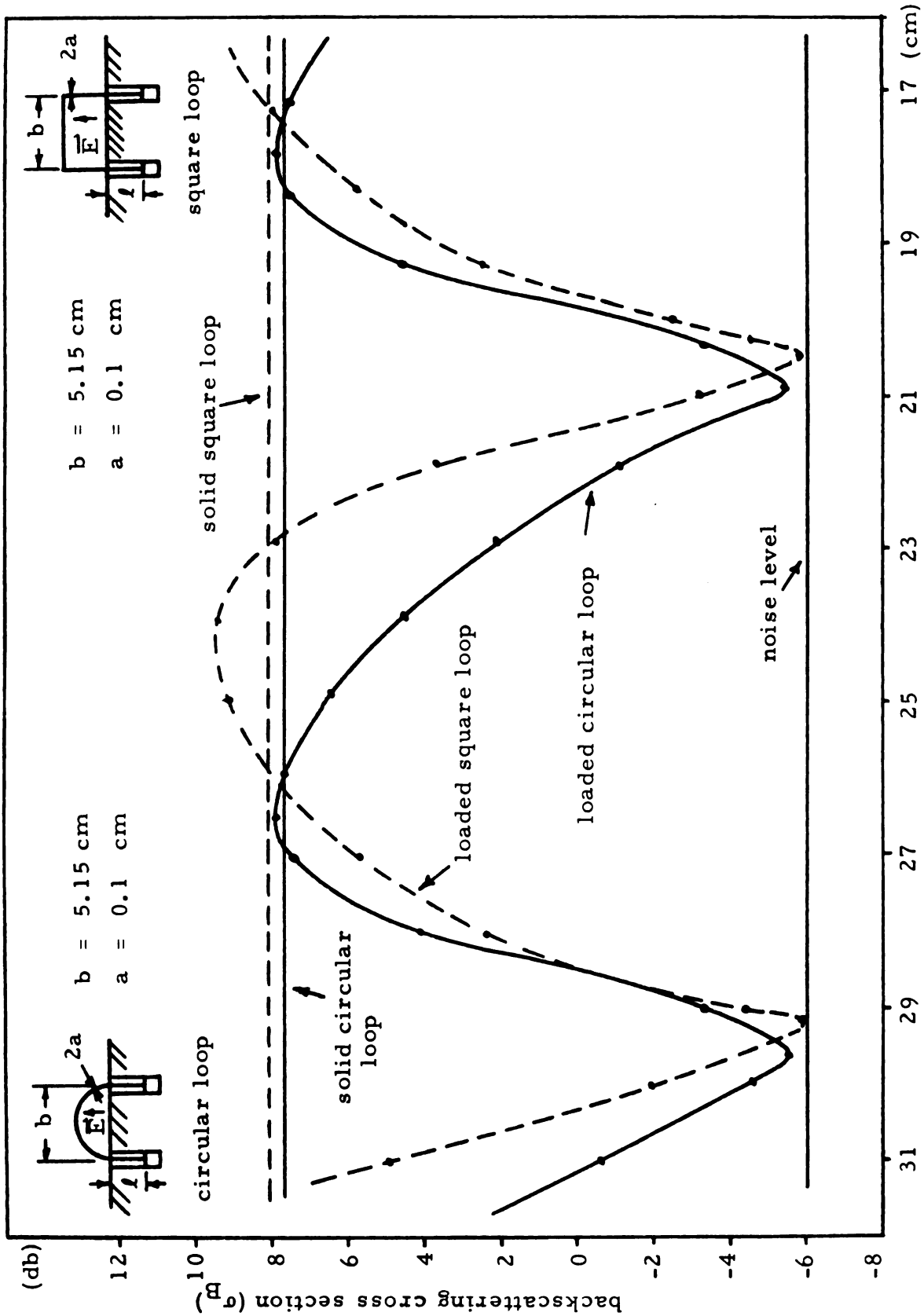


Figure 4.4. Backscattering cross section of a loaded loop as a function of loading impedance (f = 1.7 GHz).



(l) length of coaxial line (loading impedance $Z_L = j Z_C \tan \beta_0 l$)

Figure 4.5. Backscattering cross section of a loaded loop as a function of loading impedance ($f = 1.75$ GHz).

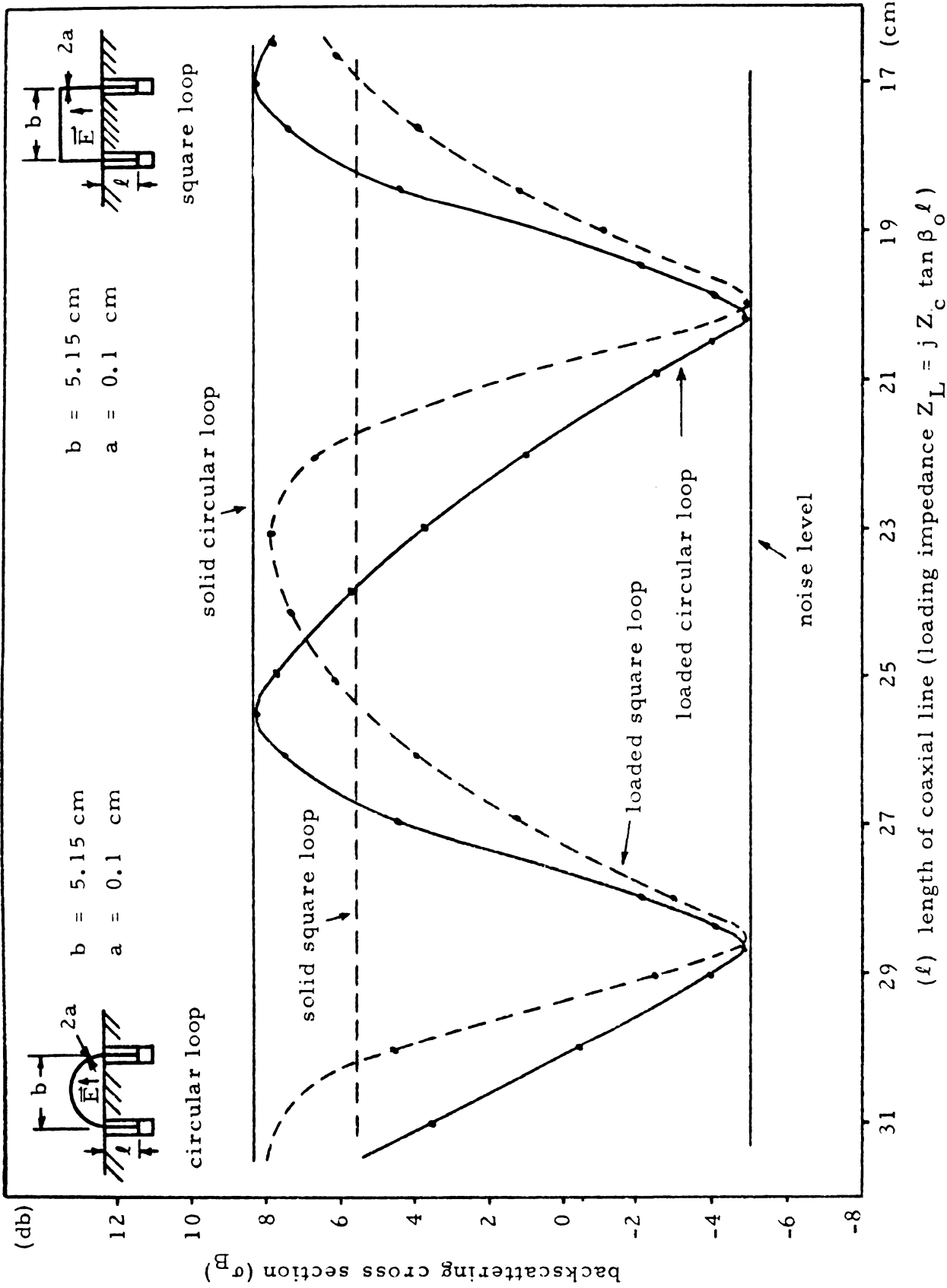


Figure 4.6. Backscattering cross section of a loaded loop as a function of loading impedance $Z_L = j Z_c \tan \beta_0 l$ (l length of coaxial line (loading impedance $Z_L = j Z_c \tan \beta_0 l$)).

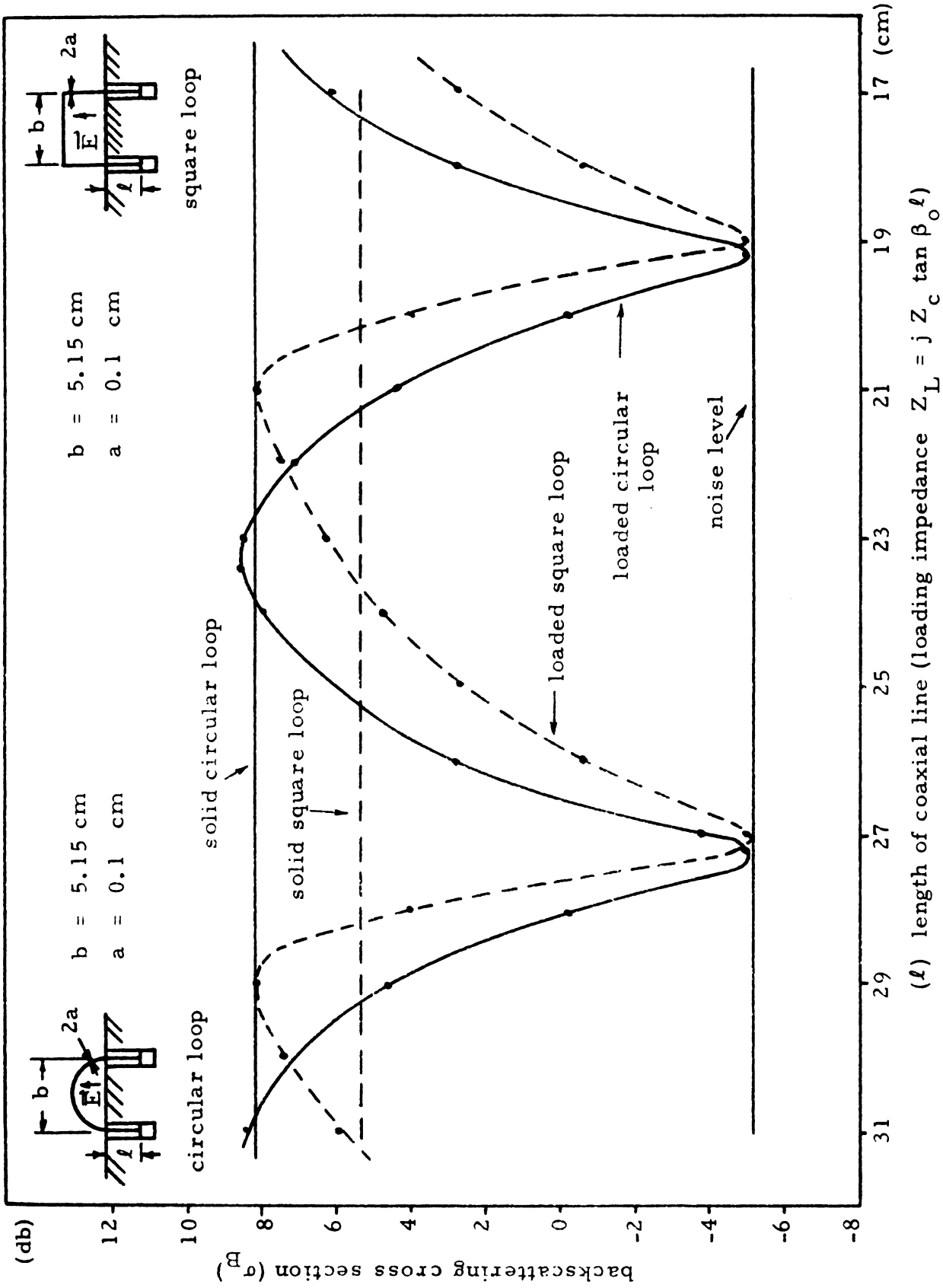


Figure 4.7. Backscattering cross section of a loaded loop as a function of loading impedance $Z_L = j Z_c \tan \beta_o \ell$ (length of coaxial line) (loading impedance $Z_L = j Z_c \tan \beta_o \ell$). impedance ($f = 1.9$ GHz).

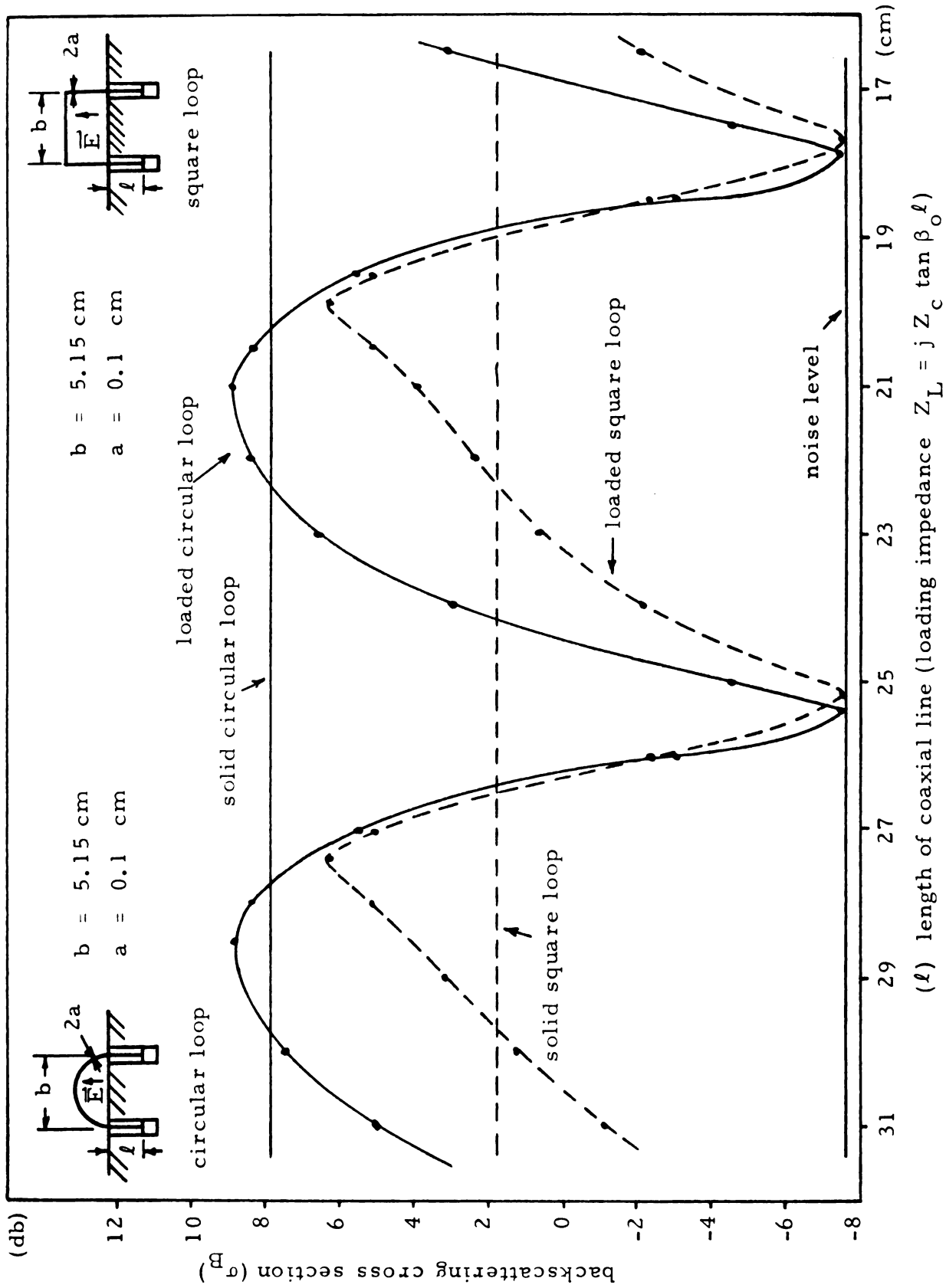


Figure 4.8. Backscattering cross section of a loaded loop as a function of loading impedance $Z_L = j Z_c \tan \beta_0 l$ (length of coaxial line) ($f = 2.0$ GHz).

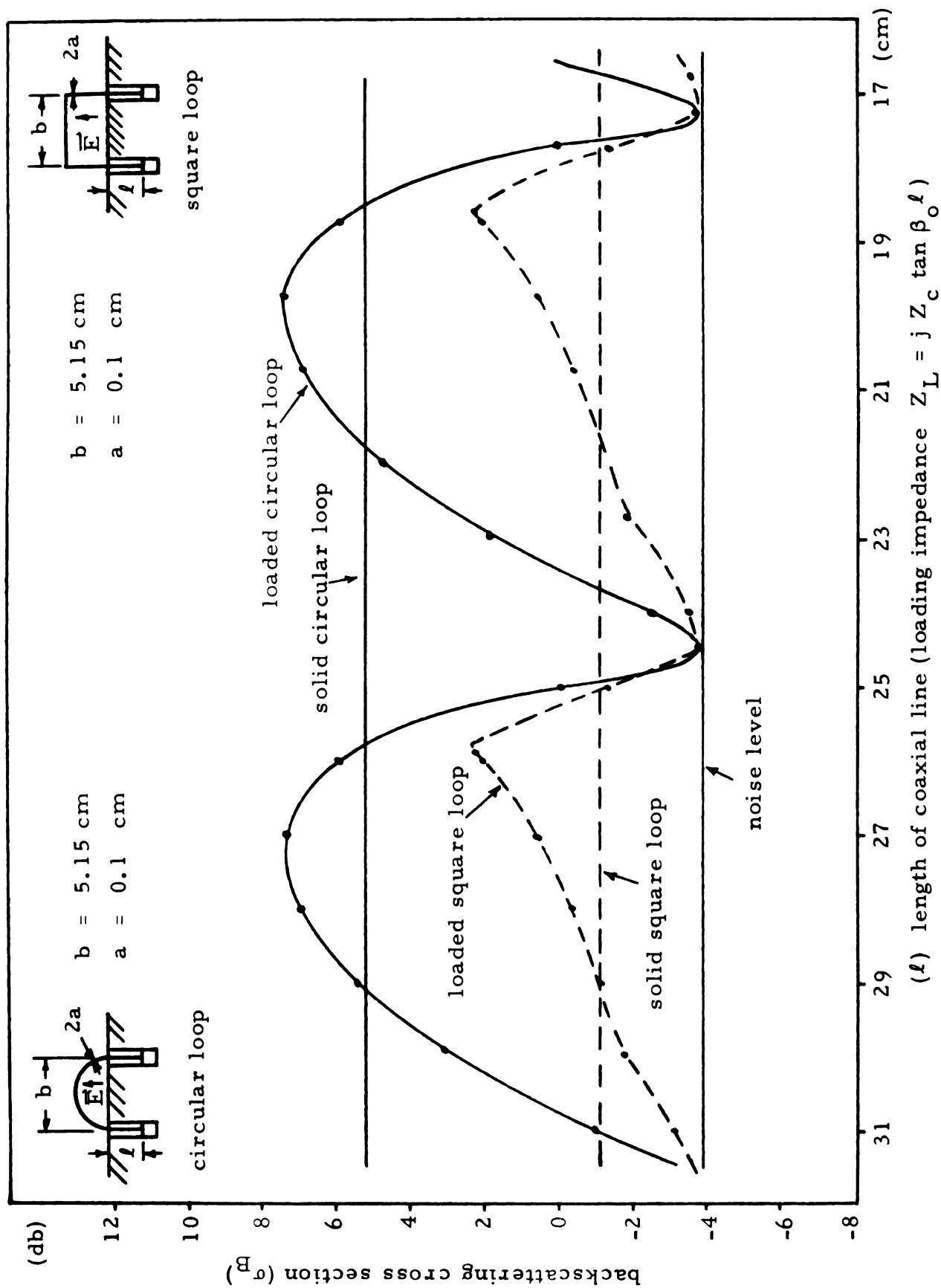


Figure 4.9. Backscattering cross section of a loaded loop as a function of loading impedance ($Z_L = j Z_C \tan \beta_0 l$)

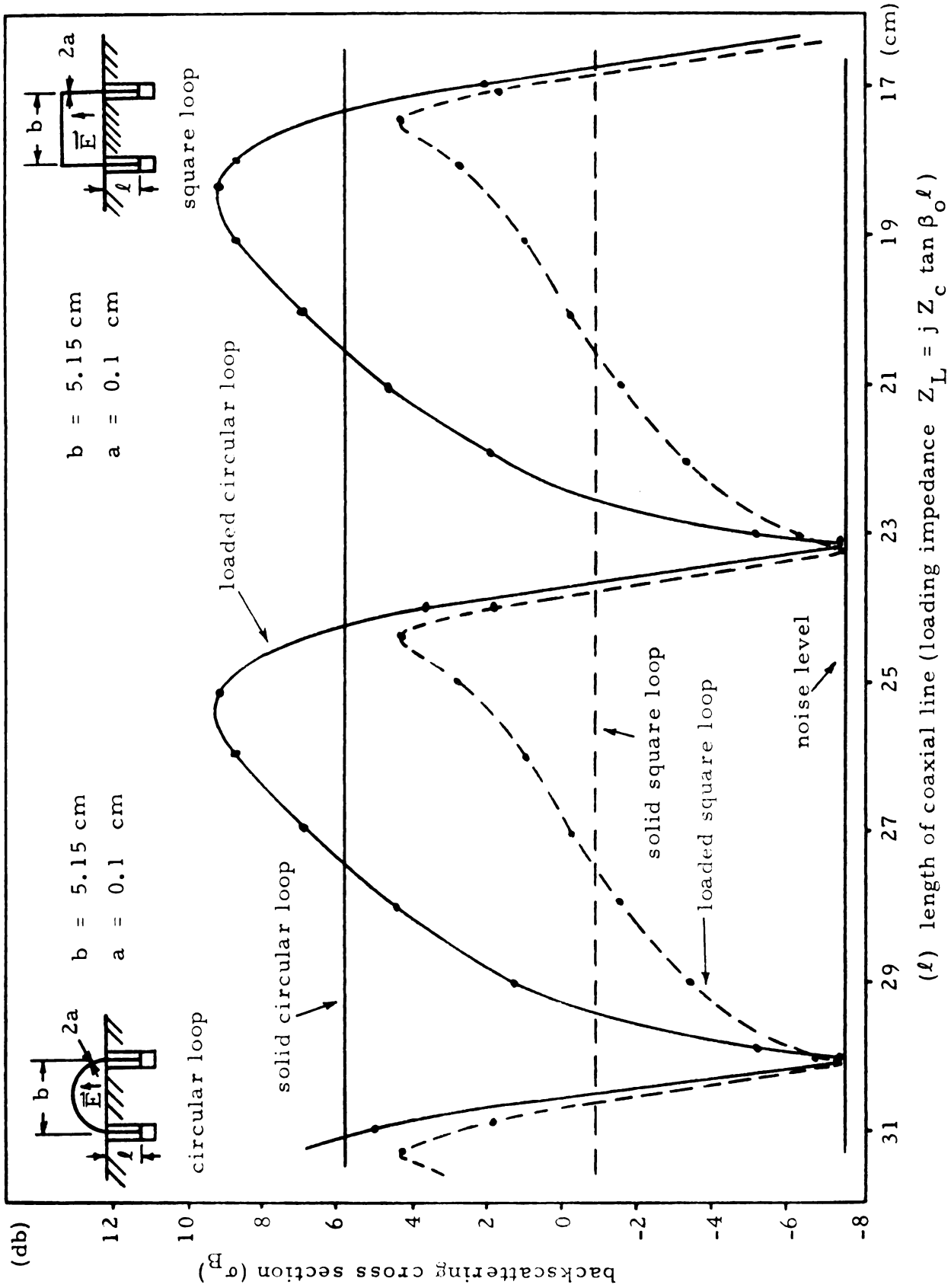


Figure 4.10. Backscattering cross section of a loaded loop as a function of loading impedance ($f = 2.2$ GHz).

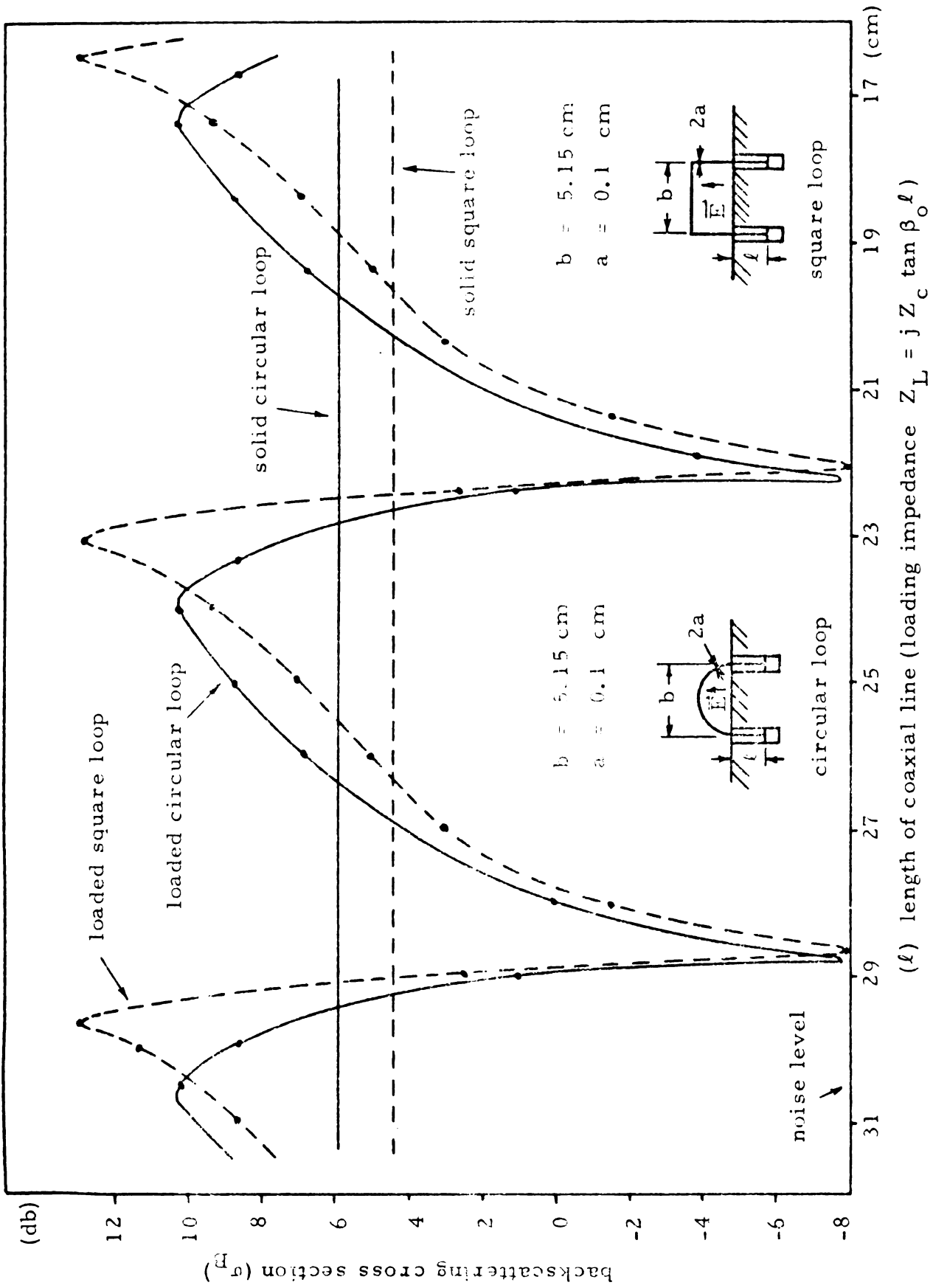


Figure 4.11. Backscattering cross section of a loaded loop as a function of loading impedance $Z_L = j Z_c \tan \beta_o l$ (l) length of coaxial line (loading impedance $Z_L = j Z_c \tan \beta_o l$) impedance ($f = 2.3$ GHz).

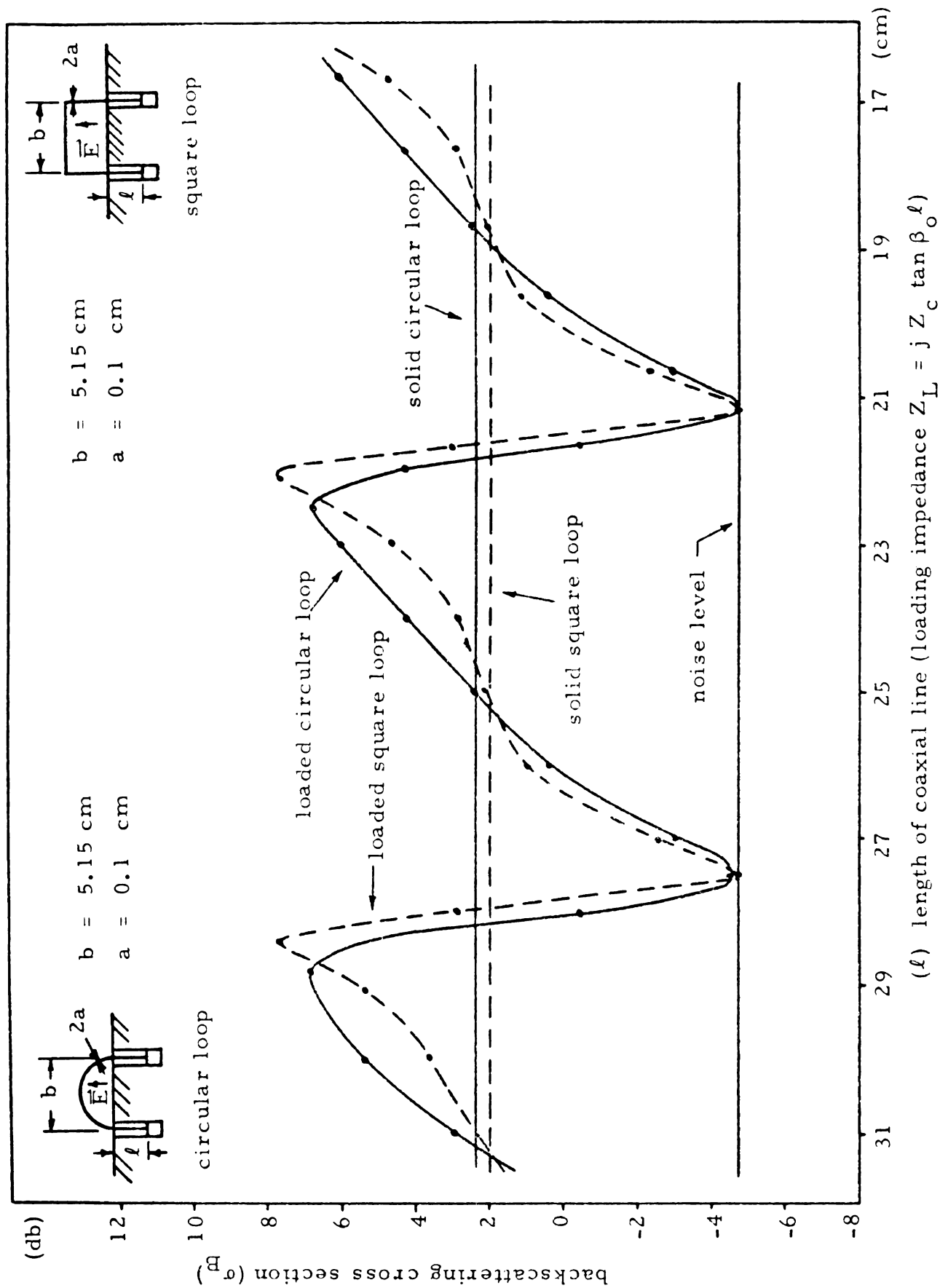
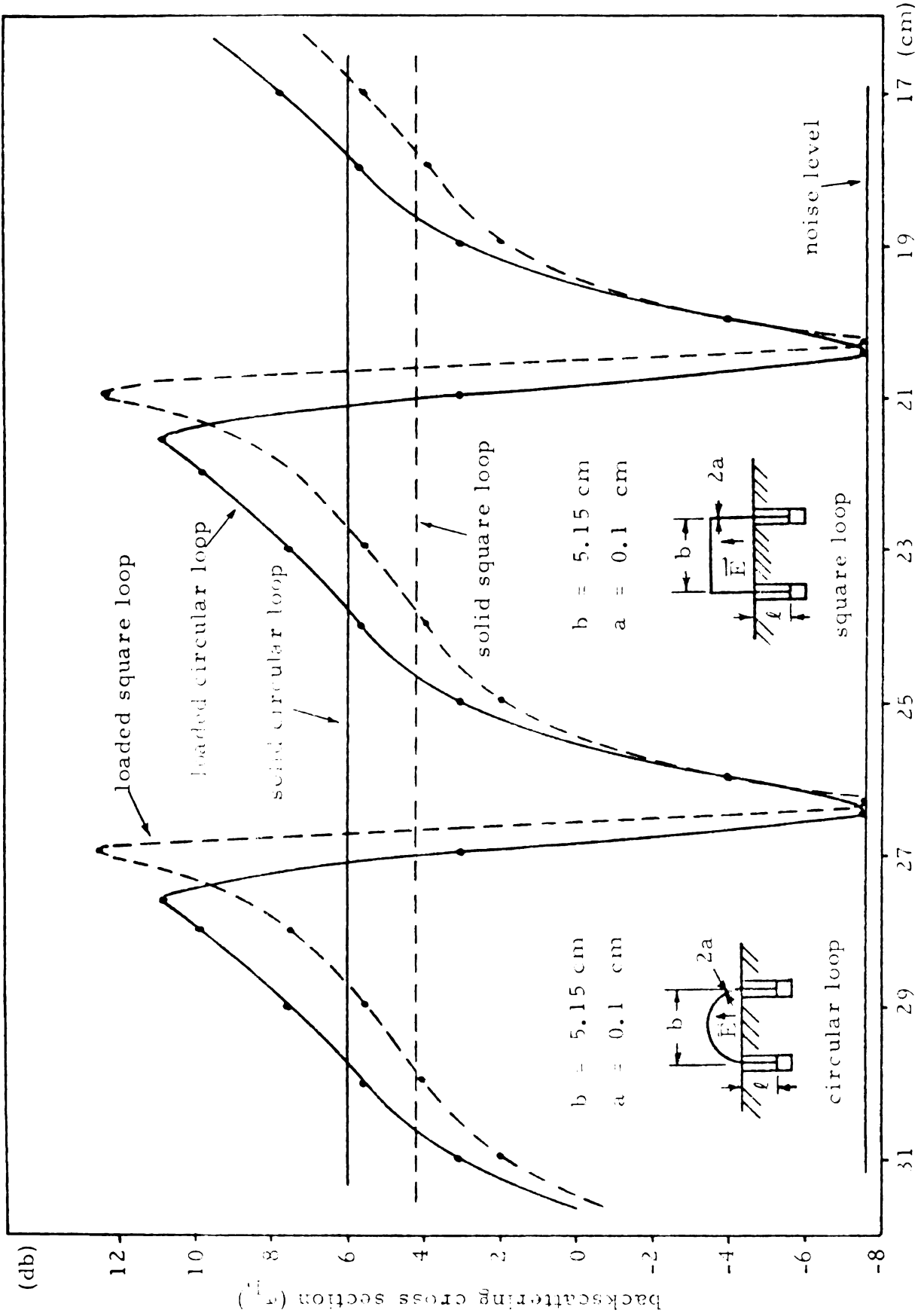


Figure 4.12. Backscattering cross section of a loaded loop as a function of loading impedance $Z_L = j Z_c \tan \beta_0 \ell$ (ℓ length of coaxial line (loading impedance $Z_L = j Z_c \tan \beta_0 \ell$ impedance ($f = 2.4$ GHz)).



(l) length of coaxial line (loading impedance $Z_L = j Z_c \tan \beta_o l$)

Figure 4.13. Backscattering cross section of a loaded loop as a function of loading impedance $Z_L = j Z_c \tan \beta_o l$ (impedance ($f = 2.5$ GHz)).

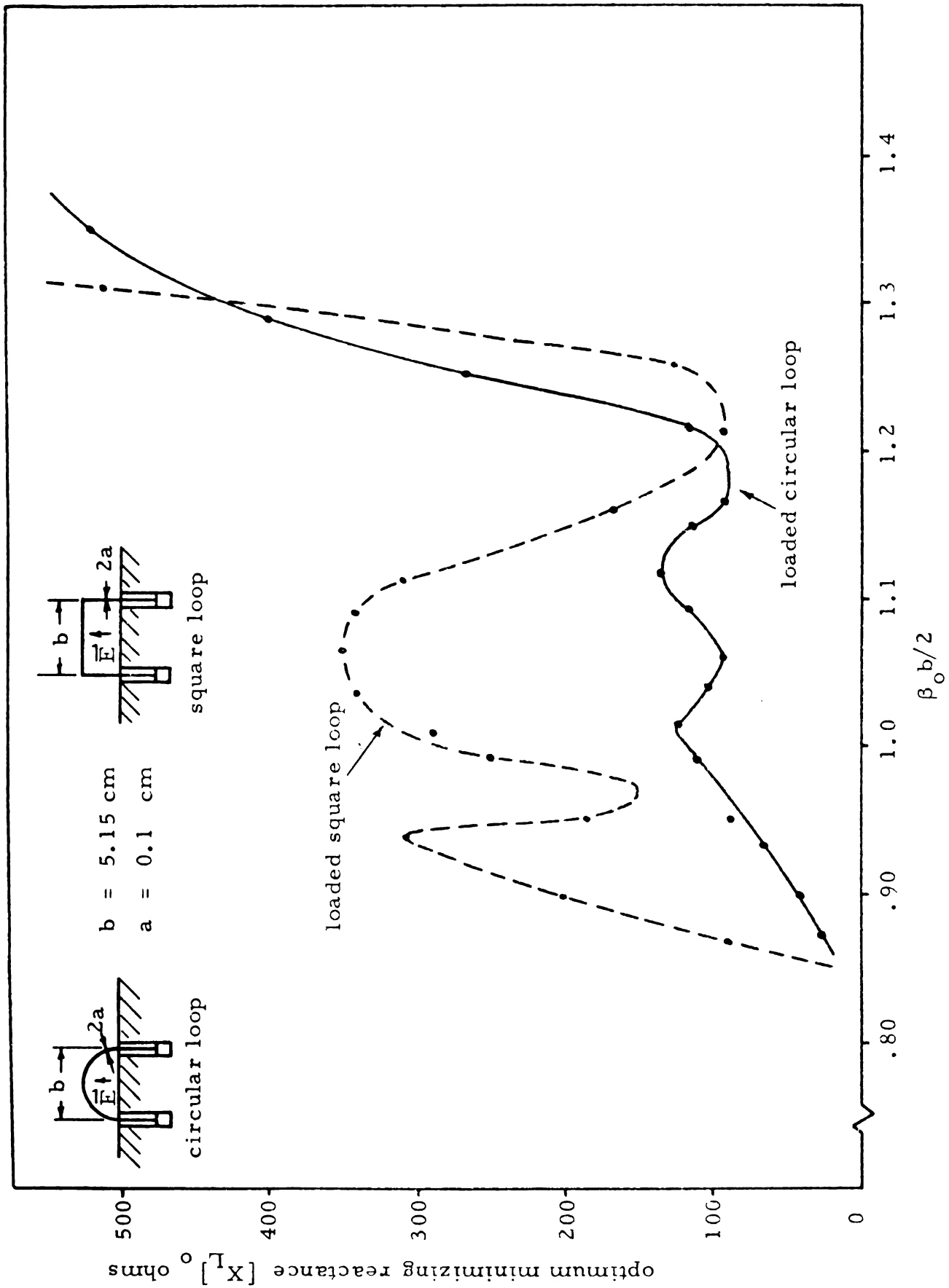


Figure 4.14. Optimum reactive impedance for minimum backscattering from a loaded loop illuminated by a plane wave at normal incidence.

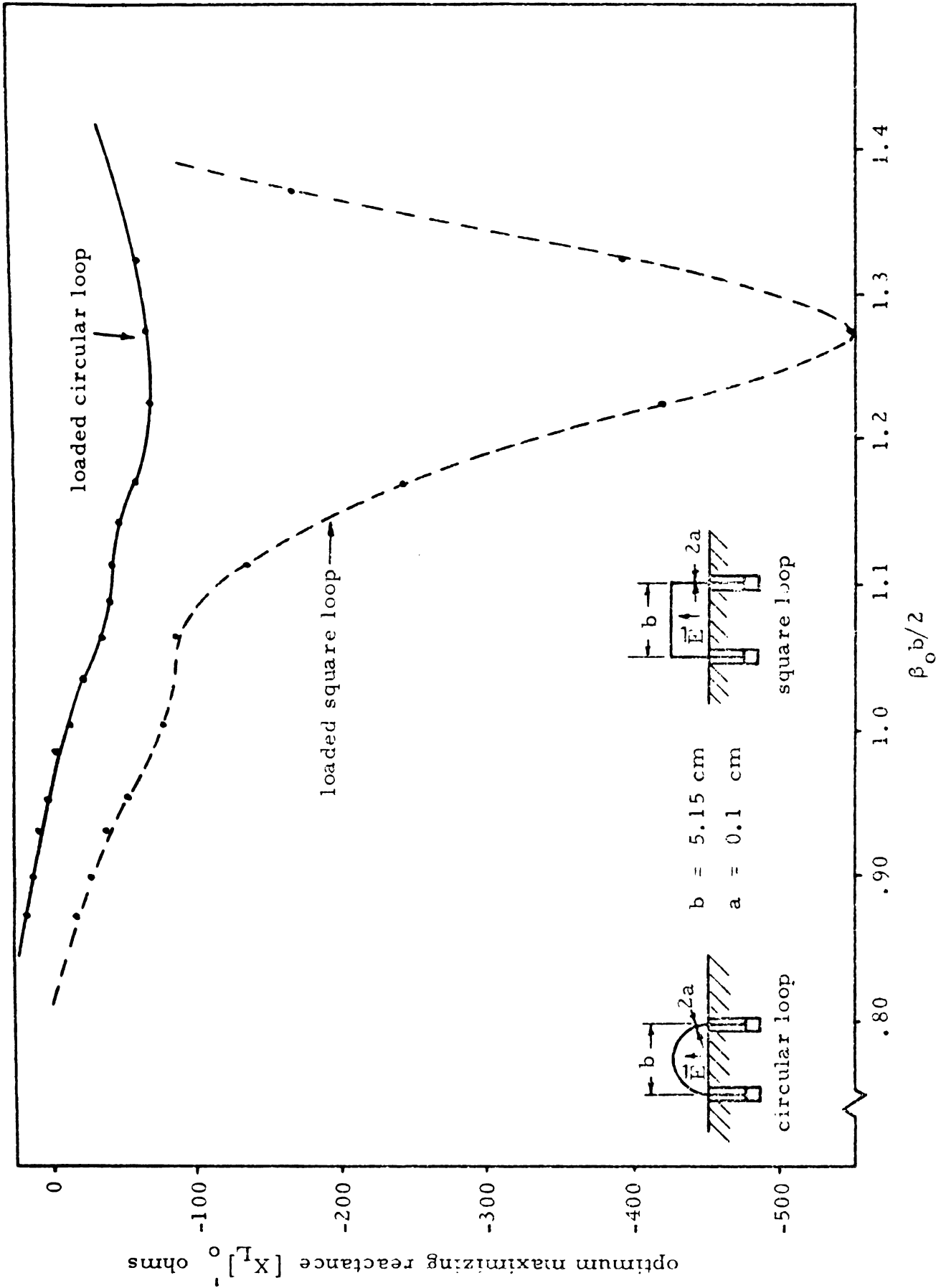


Figure 4.15. Optimum reactive impedance for maximum backscattering from a loaded loop illuminated by a plane wave at normal incidence.

CHAPTER V

MODIFICATION OF BACKSCATTERING FROM A CONDUCTING PLATE

In this chapter the modification of the backscattering cross section of another fundamental shape, the metallic plate, is studied. This shape has not been studied extensively. The only known methods of controlling the backscatter of a plate are to cut a resonant slot on the plate,⁷ or install a cavity-backed aperture on the plate. These methods can reduce the backscatter of the plate by not more than 15 dB and have the disadvantage of a requirement for cutting the plate. The method presented in this research offers a more effective means for backscatter reduction without the inherent disadvantages mentioned above. In some cases a reduction of about 25 dB is obtainable by this method. Part of this research has already been published elsewhere.¹⁴ Subsequently this method should have important practical applications.

5.1. Round Plate and Loop

The basic scheme of this method is to place a loaded circular loop directly in front of a round plate and parallel to it as indicated in Figure 5.1. The amplitude and phase of the induced current on the loop is controlled by a loading impedance in such a way that the backscatter produced by the loop cancels fully or partly the backscatter due to the induced currents on the plate. Thus the total backscatter produced by the composite plate and the loop structure is minimized. In a similar manner, the backscatter field from the composite structure may be enhanced.

large plate $d = 12.7$ cm
 medium plate $d = 10.2$ cm
 small plate $d = 7.6$ cm

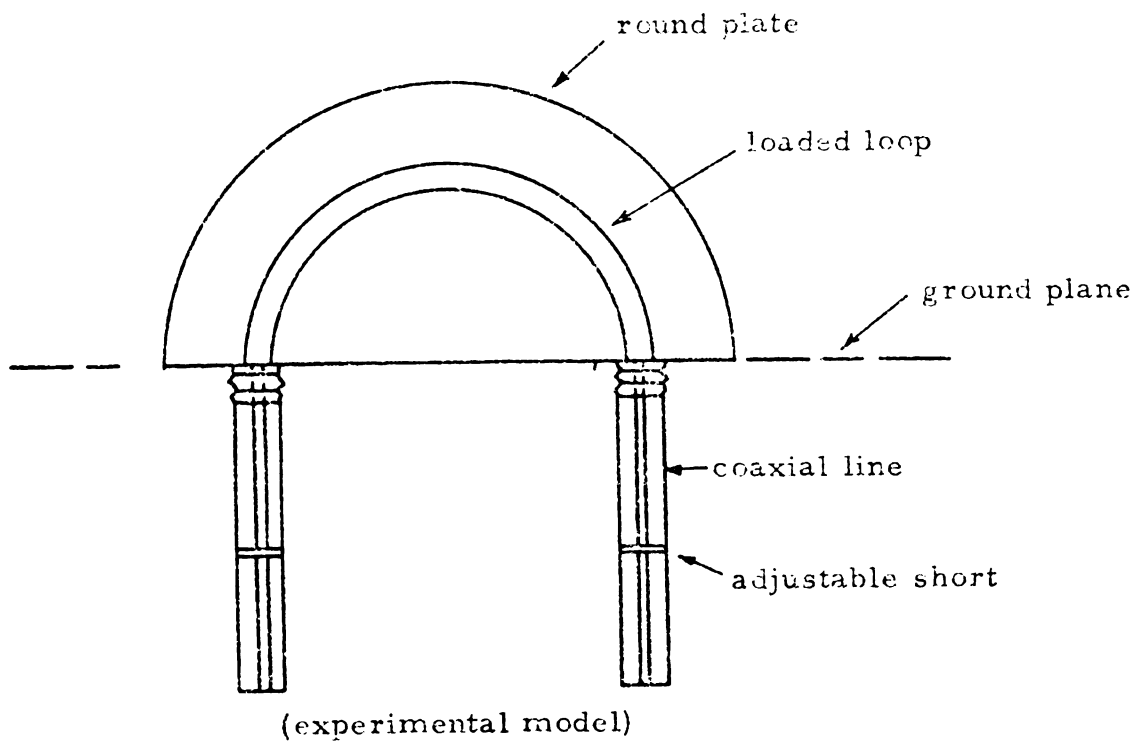
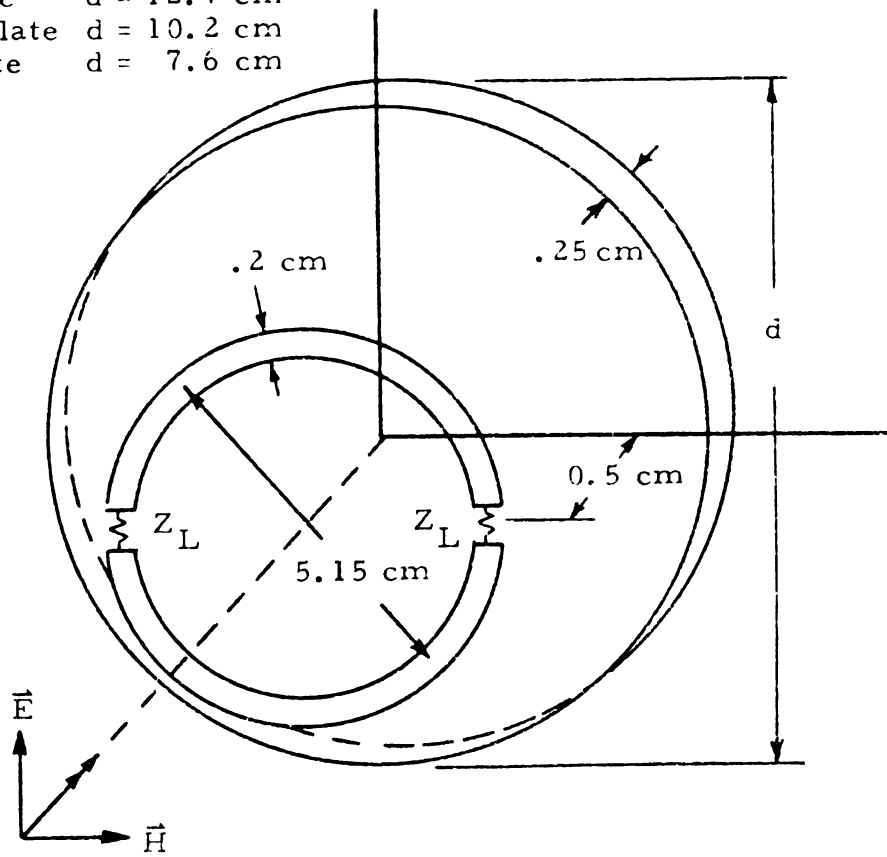
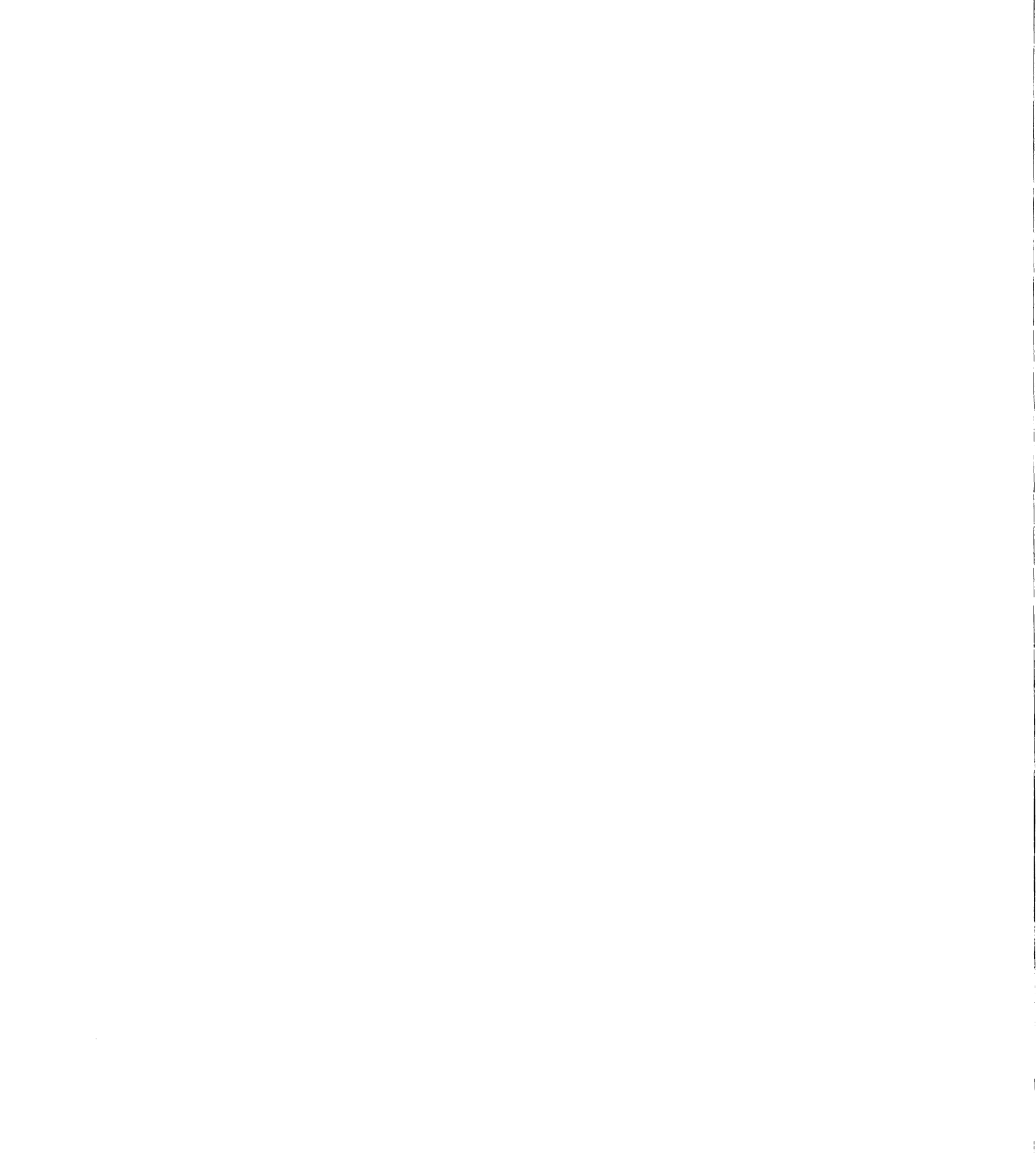


Figure 5.1. Circular plate and loaded loop.



In the experimental arrangement, a circular wire loop loaded symmetrically with a pair of identical reactive impedances, as described previously in section 4.1, is placed 0.5 cm in front of and parallel to a solid circular metallic plate. The plate and loop are illuminated by a plane wave at normal incidence. The experiment is performed at various frequencies and with circular plates of various diameters. Throughout the experiment, the diameter of the wire loop (diameter = 5.15 cm with wire radius = 0.1 cm) is held constant.

The experimental results are presented in Figures 5.2 to 5.20. In Figures 5.2 to 5.6 the backscattering cross sections of the small plate (diameter = 7.6 cm) and loaded circular loop are plotted as a function of the impedance loading of the loop. The backscatters of the medium plate (diameter = 10.2 cm) and loaded loop are indicated in Figures 5.7 to 5.14, while those of the large plate (diameter = 12.7 cm) and loaded loop are presented in Figures 5.15 to 5.20, all as a function of the loop loading impedance. In each Figure, the cross section of the plate alone is represented by a solid straight line and that of the plate and a solid circular loop by a dashed straight line. The cross sections of the loaded loop alone as a function of its loading impedance are indicated by dashed curves.

It is observed that the backscattered field of a circular conducting plate can be reduced by approximately 25 dB in some cases if the loading impedances (i. e., the length of the coaxial lines) are properly adjusted. On the other hand, another appropriate impedance can, in some cases, enhance the radar cross sections of the plate

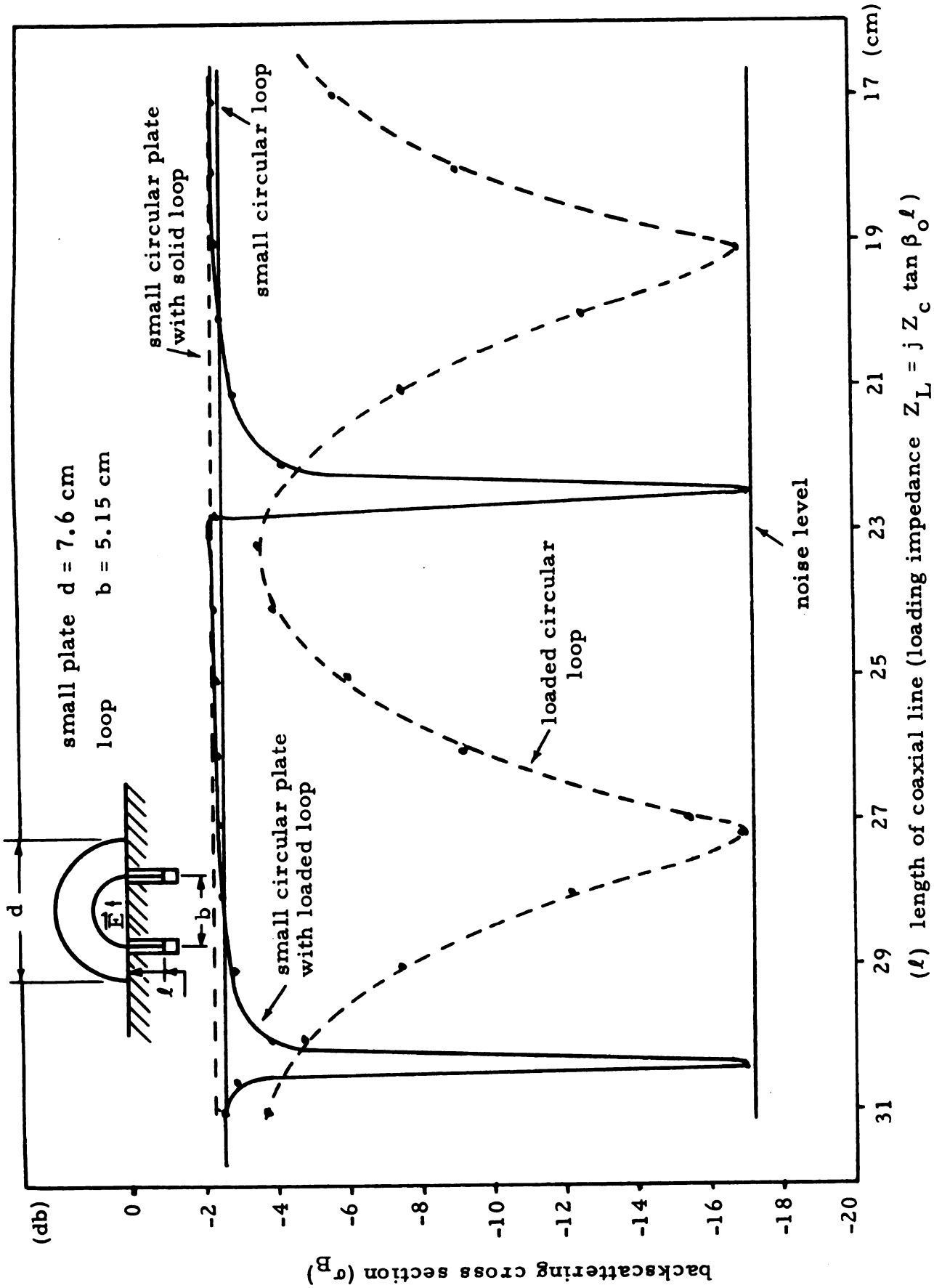


Figure 5.2. Backscatter of the small circular plate with a loaded loop as a function of loop loading ($f = 1.9$ GHz).

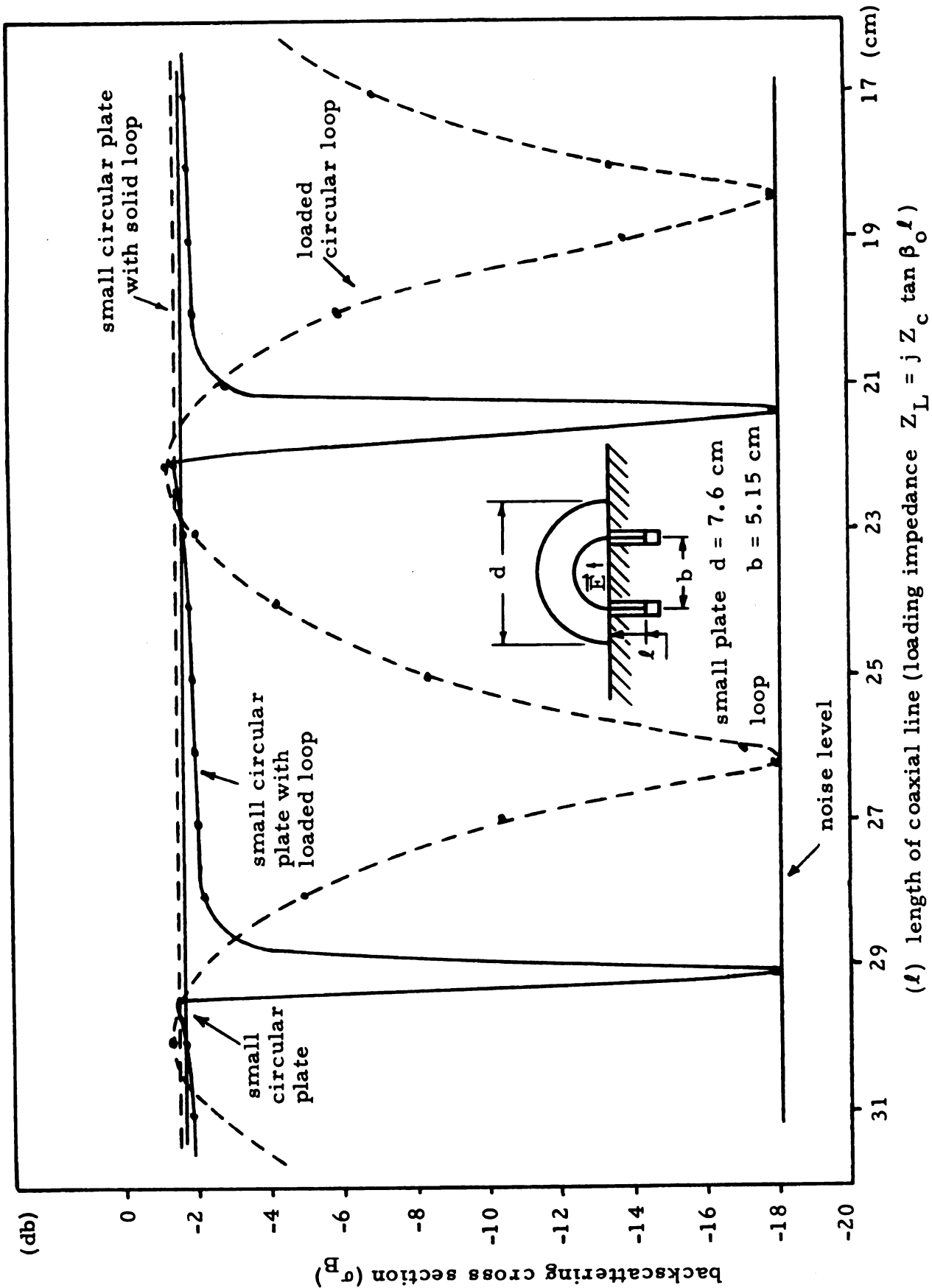


Figure 5.3. Backscatter of the small circular plate with a loaded loop as a function of loop loading ($f = 1.97$ GHz).

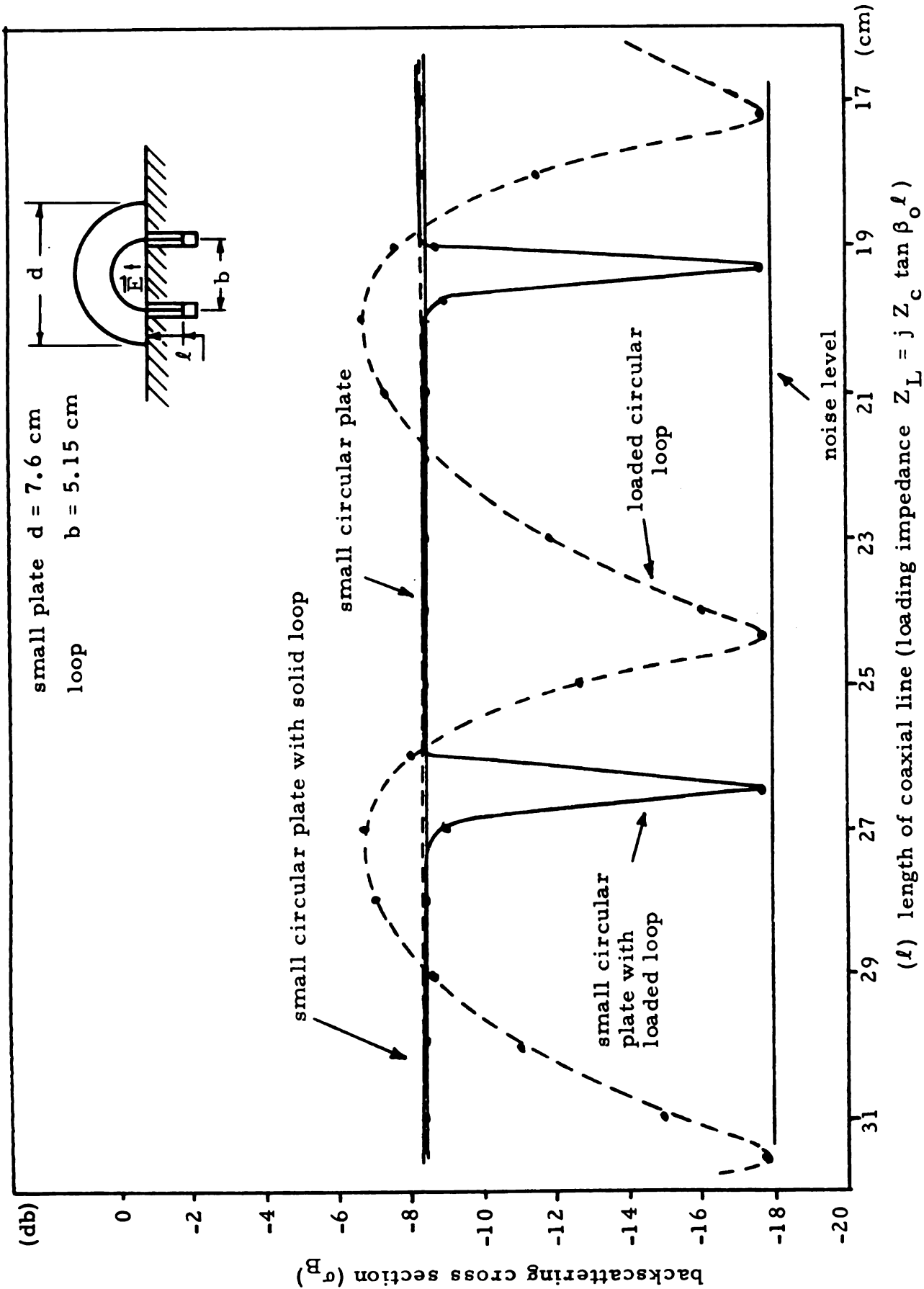


Figure 5. 4. Backscatter of the small circular plate with a loaded loop as a function of loop loading ($f = 2.1$ GHz).

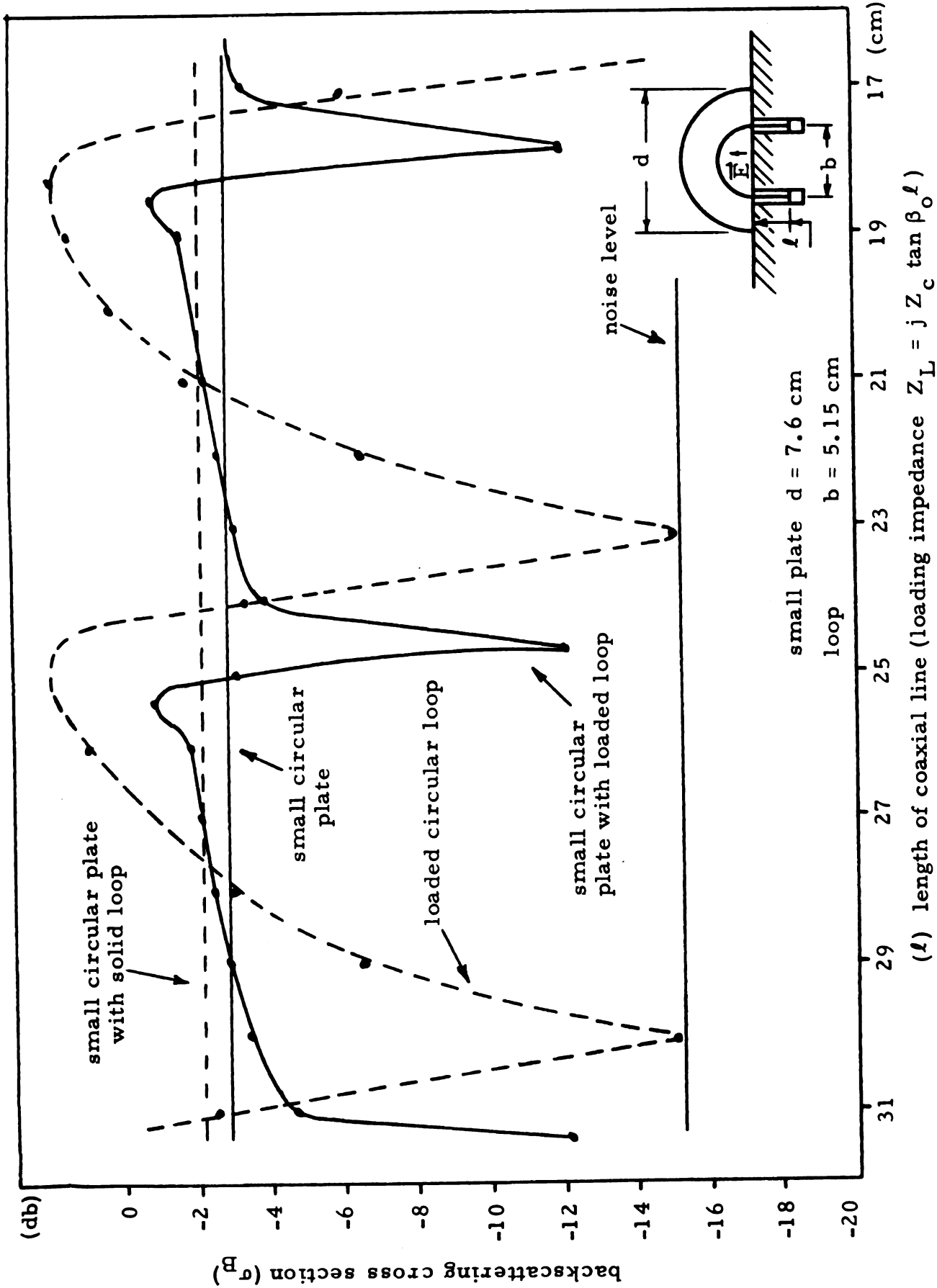


Figure 5.5. Backscatter of the small circular plate with a loaded loop as a function of loop loading ($f = 2.2$ GHz).

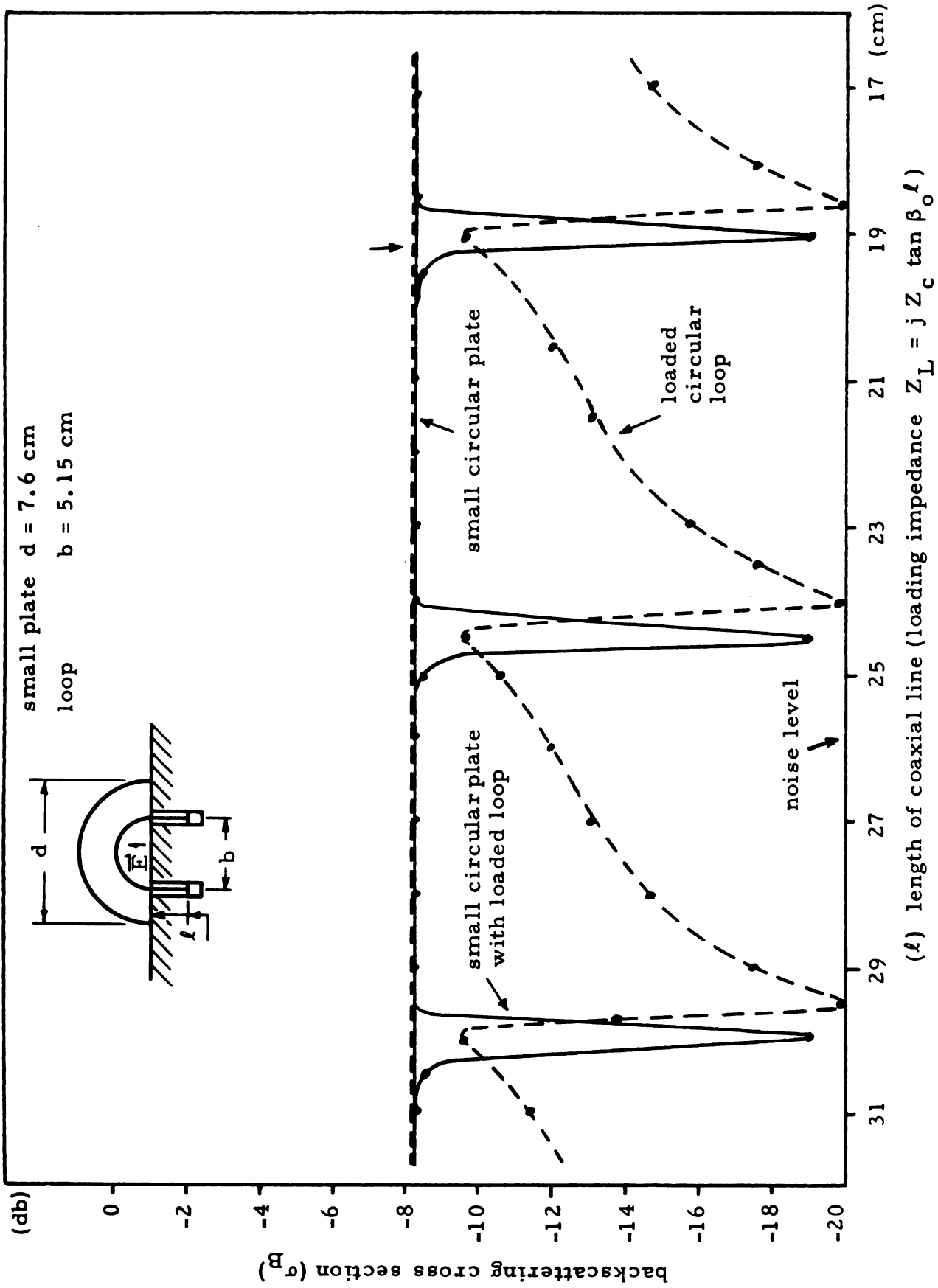


Figure 5.6. Backscatter of the small circular plate with a loaded loop as a function of loop loading ($f = 2.78$ GHz).

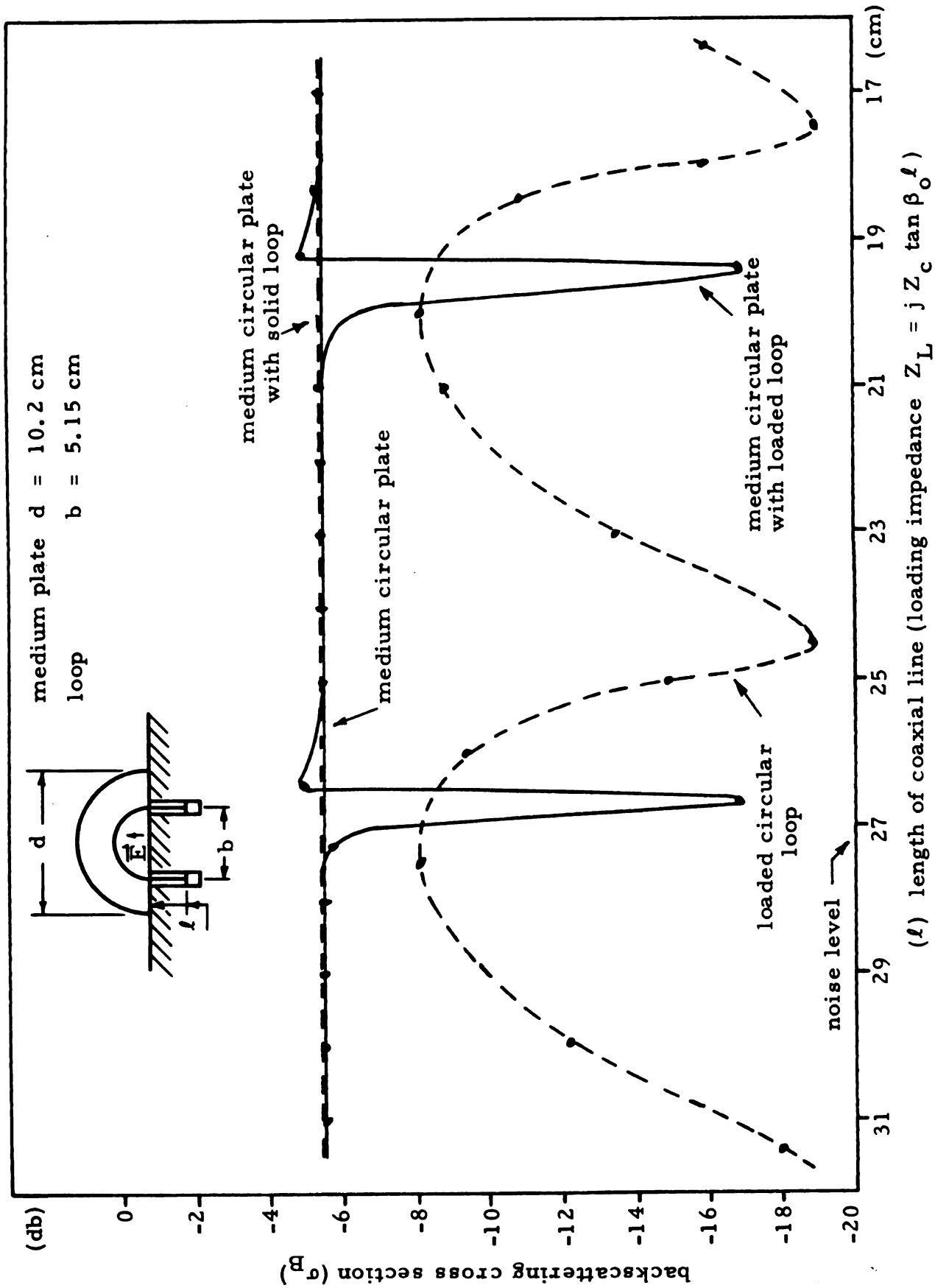


Figure 5.7. Backscatter of the medium circular plate with a loaded loop as a function of loop loading ($f = 2.1$ GHz).

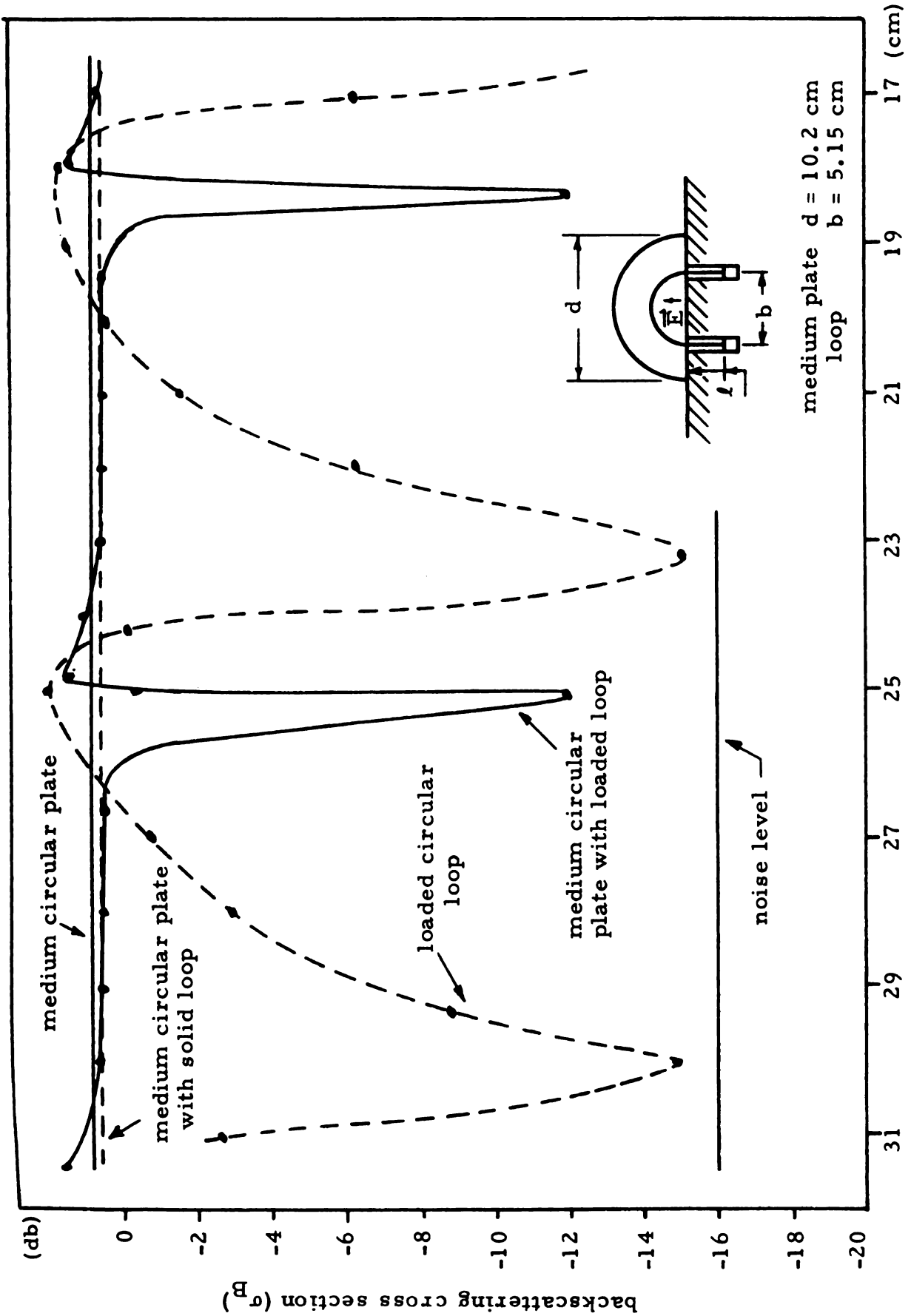


Figure 5.8. Backscatterer of the medium circular plate with a loaded loop as a function of loop loading ($f = 2.2$ GHz).

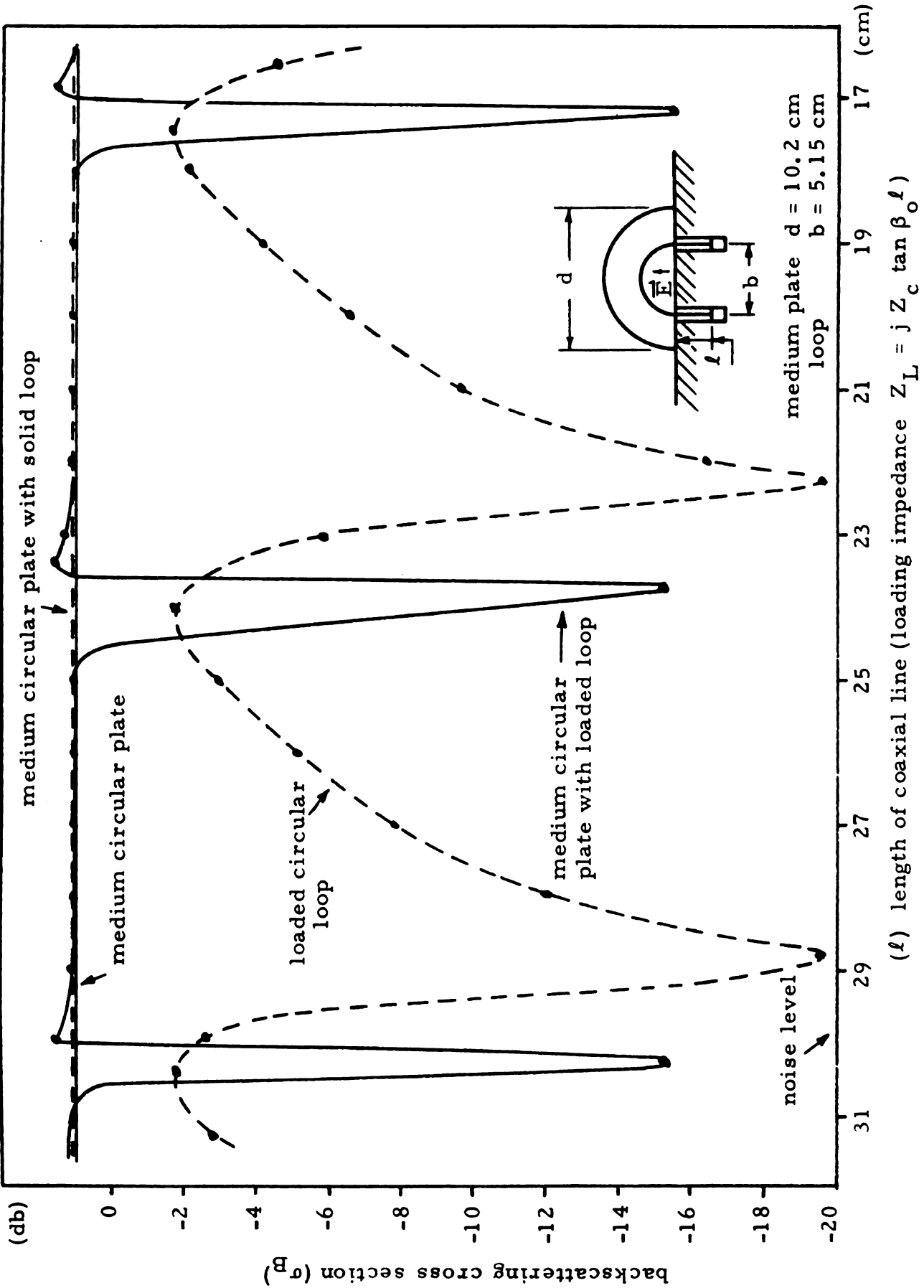


Figure 5.9. Backscatter of the medium circular plate with a loaded loop as a function of loop loading ($f = 2.3$ GHz).

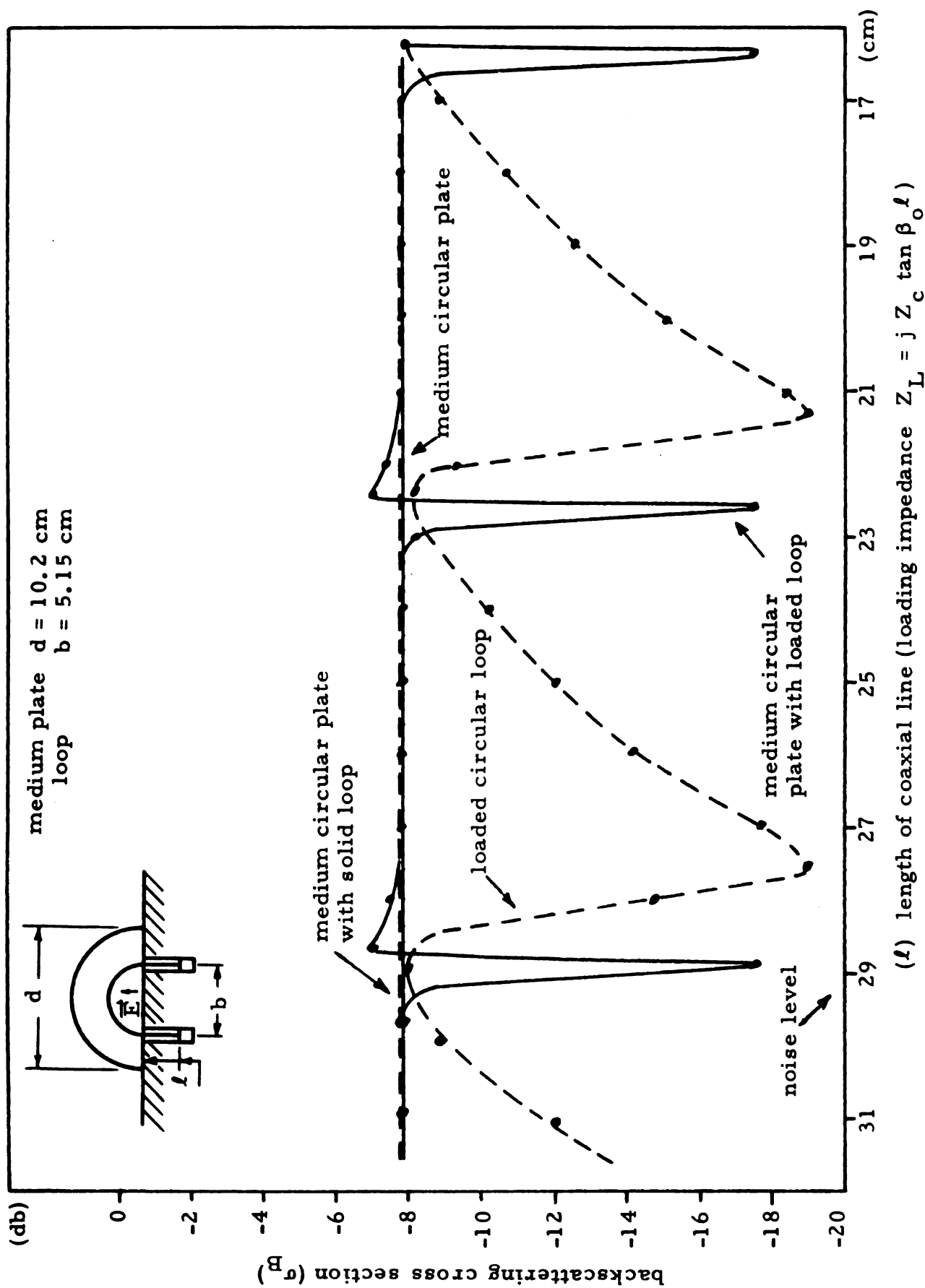
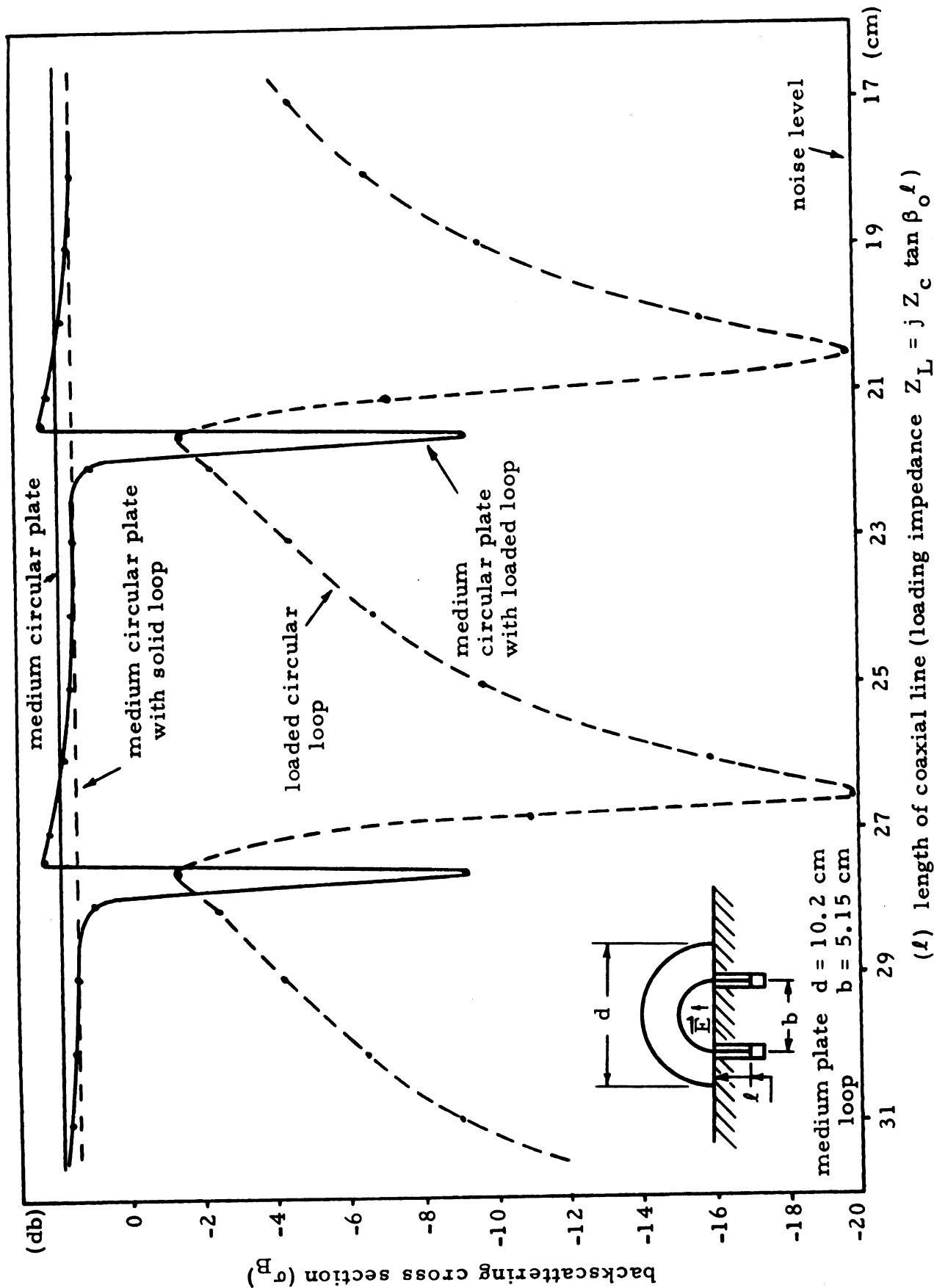


Figure 5.10. Backscatter of the medium circular plate with a loaded loop as a function of loop loading ($f = 2.4$ GHz).



(l) length of coaxial line (loading impedance $Z_L = j Z_C \tan \beta_0 l$)

Figure 5.11. Backscatter of the medium circular plate with a loaded loop as a function of loop loading ($f = 2.5$ GHz).

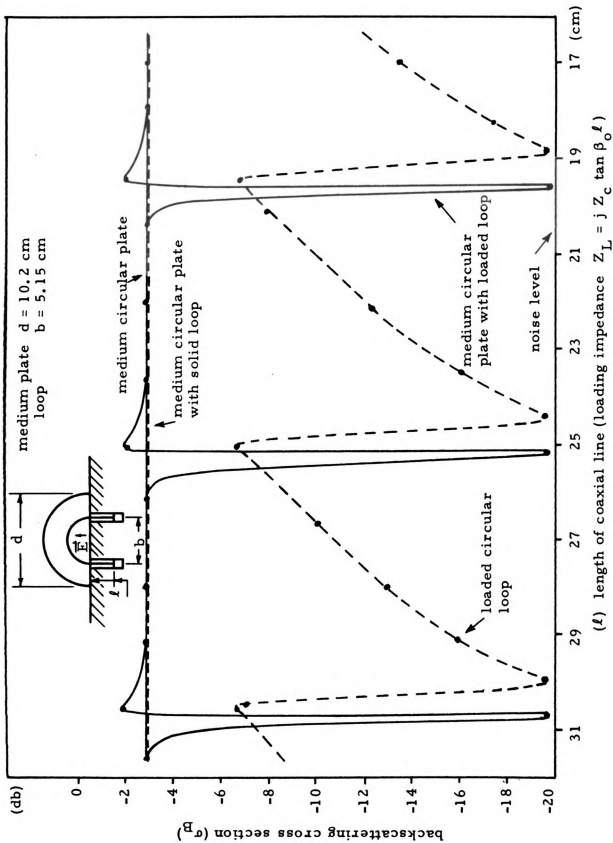


Figure 5.12. Backscatter of the medium circular plate with a loaded loop as a function of loop loading ($f = 2.7$ GHz).

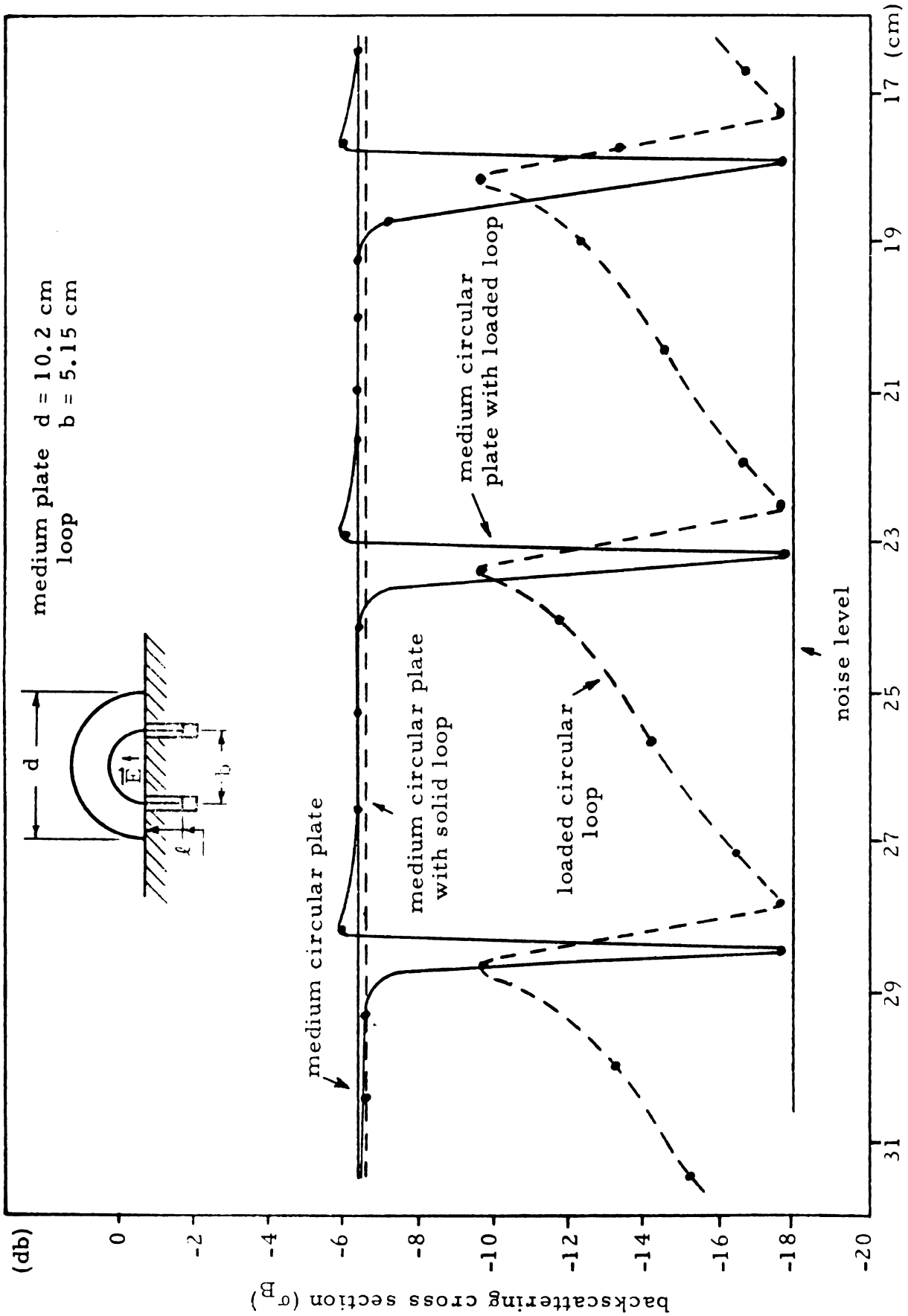
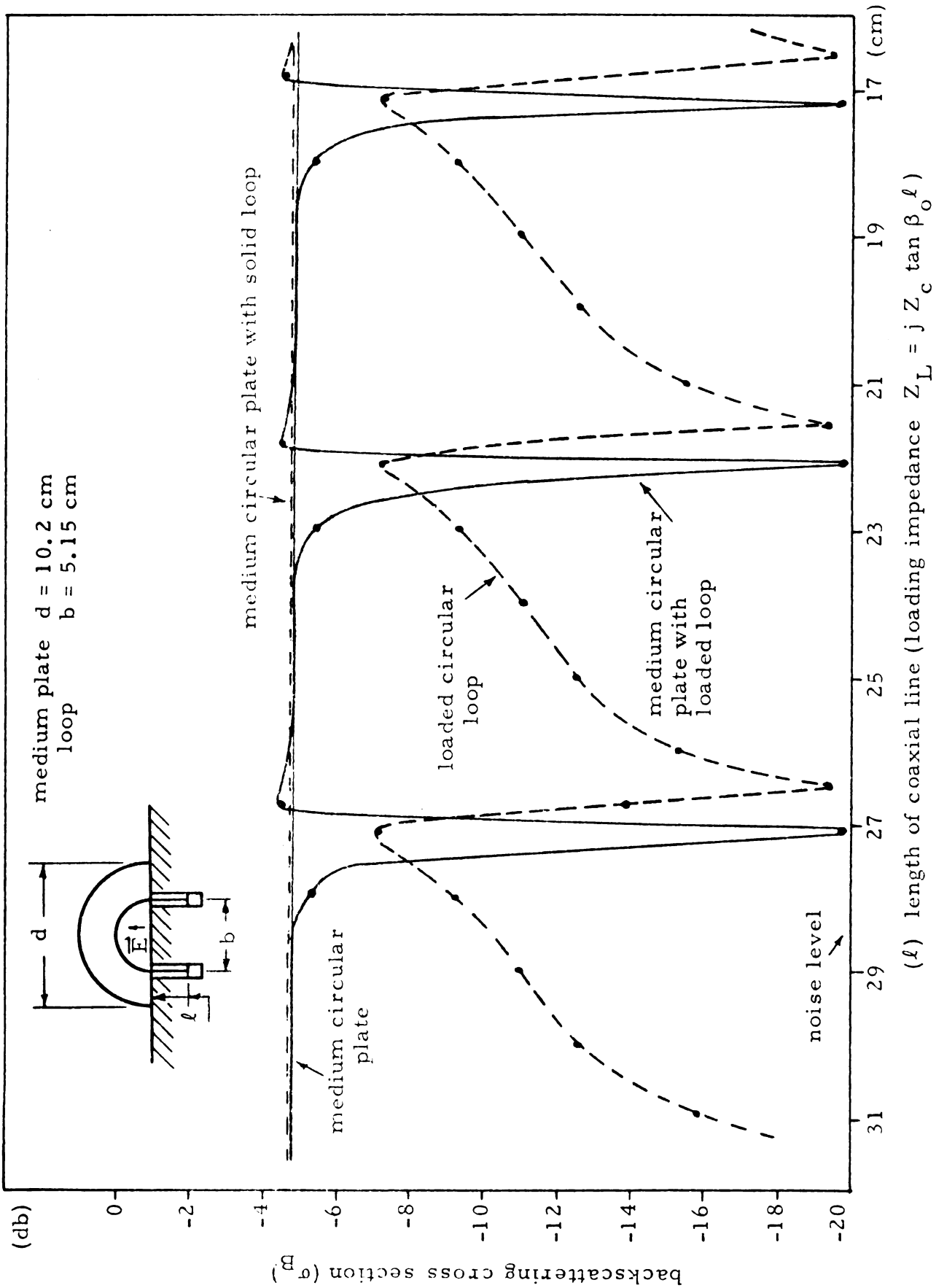


Figure 5.13. Backscatter of the medium circular plate with a loaded loop as a function of loop loading ($f = 2.9$ GHz).



(l) length of coaxial line (loading impedance $Z_L = j Z_c \tan \beta_o l$)

Figure 5.14. Backscatter of the medium circular plate with a loaded loop as a function of loop loading ($f = 3.04$ GHz).

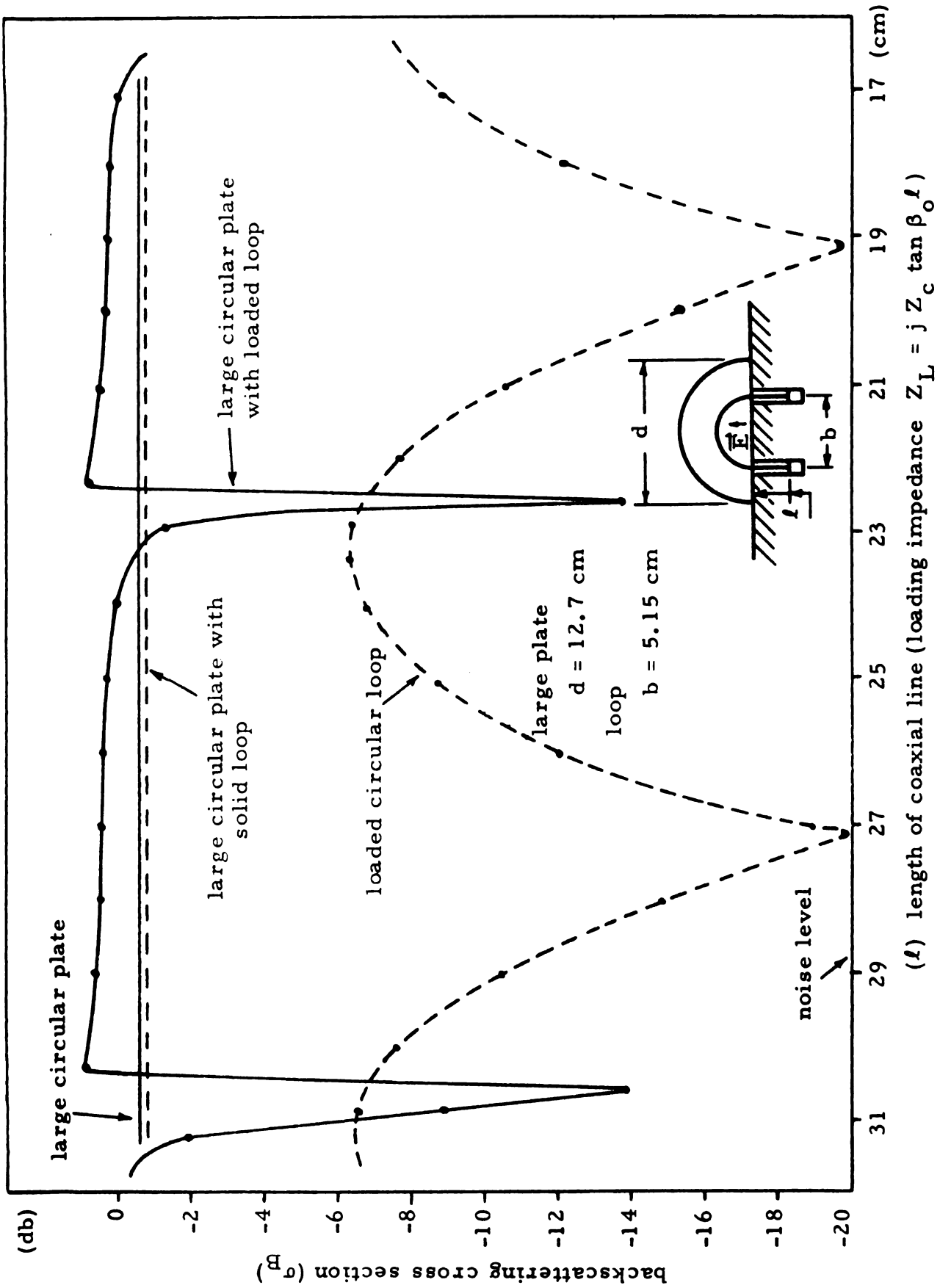


Figure 5.15. Backscatter of a large circular plate with a loaded loop as a function of loop loading ($f = 1.9$ GHz).

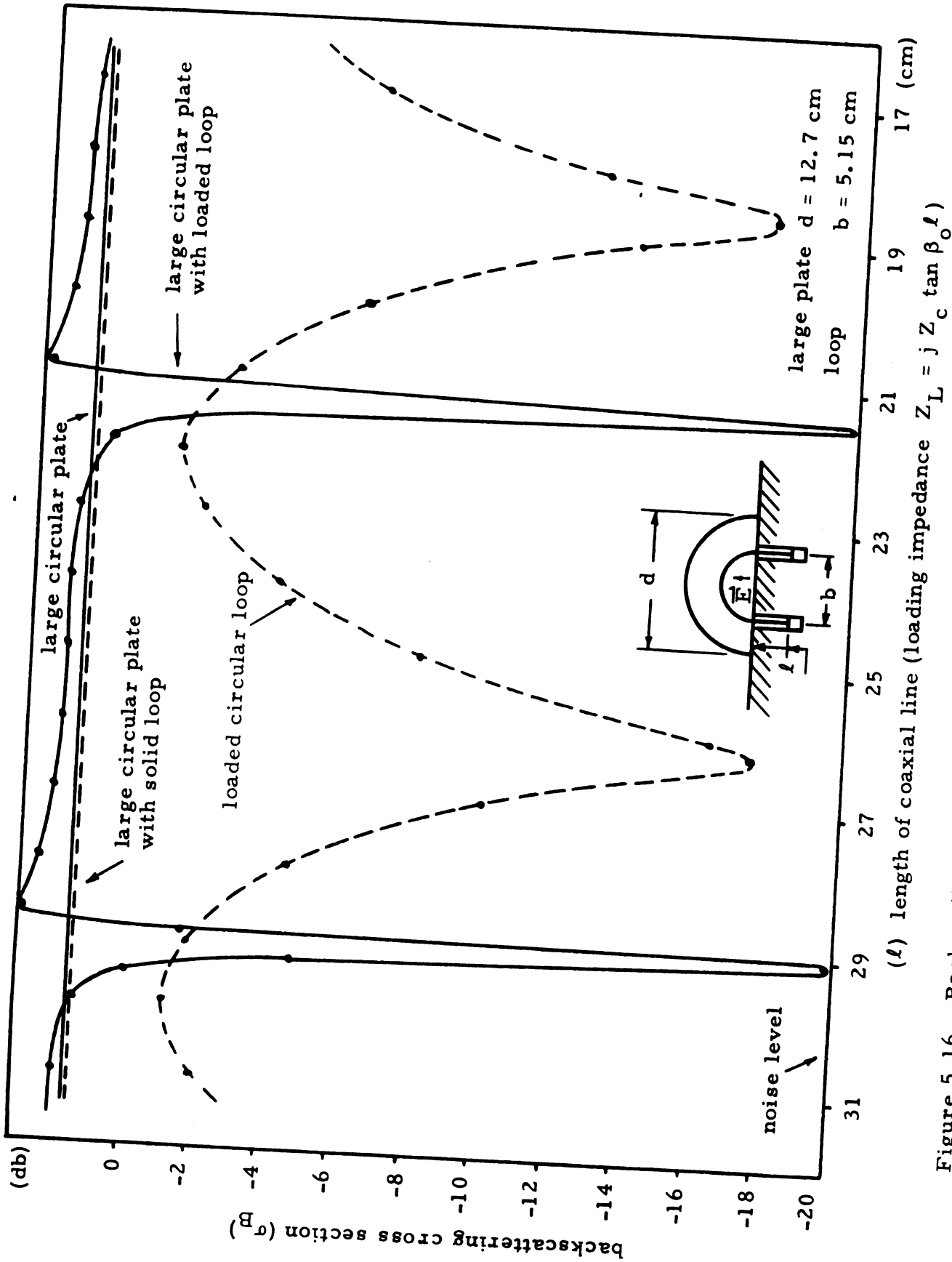


Figure 5.16. Backscatter of a large circular plate with a loaded loop as a function of loop loading ($f = 1.97$ GHz).

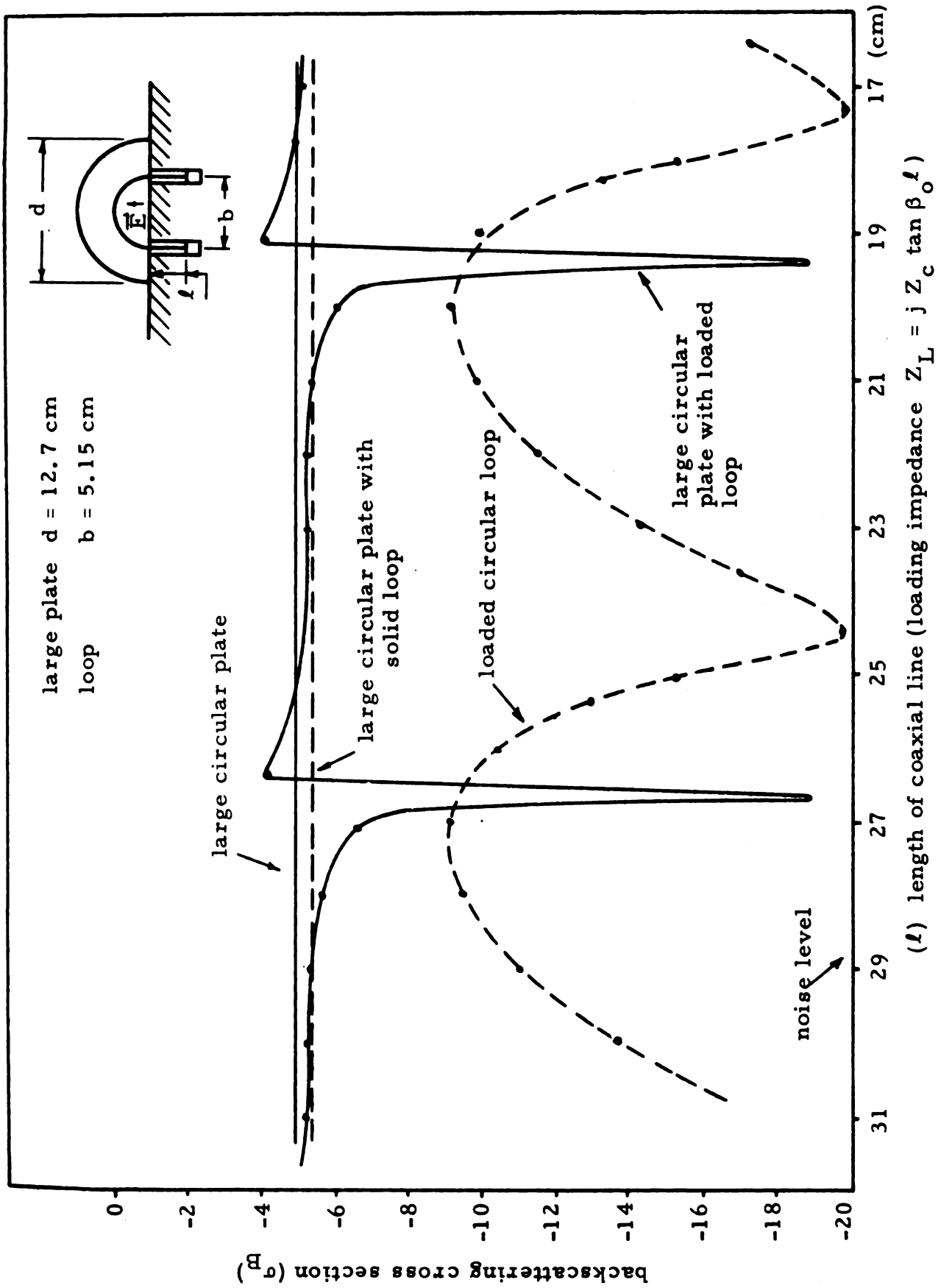


Figure 5.17. Backscatter of a large circular plate with a loaded loop as a function of loop loading ($f = 2.1$ GHz).

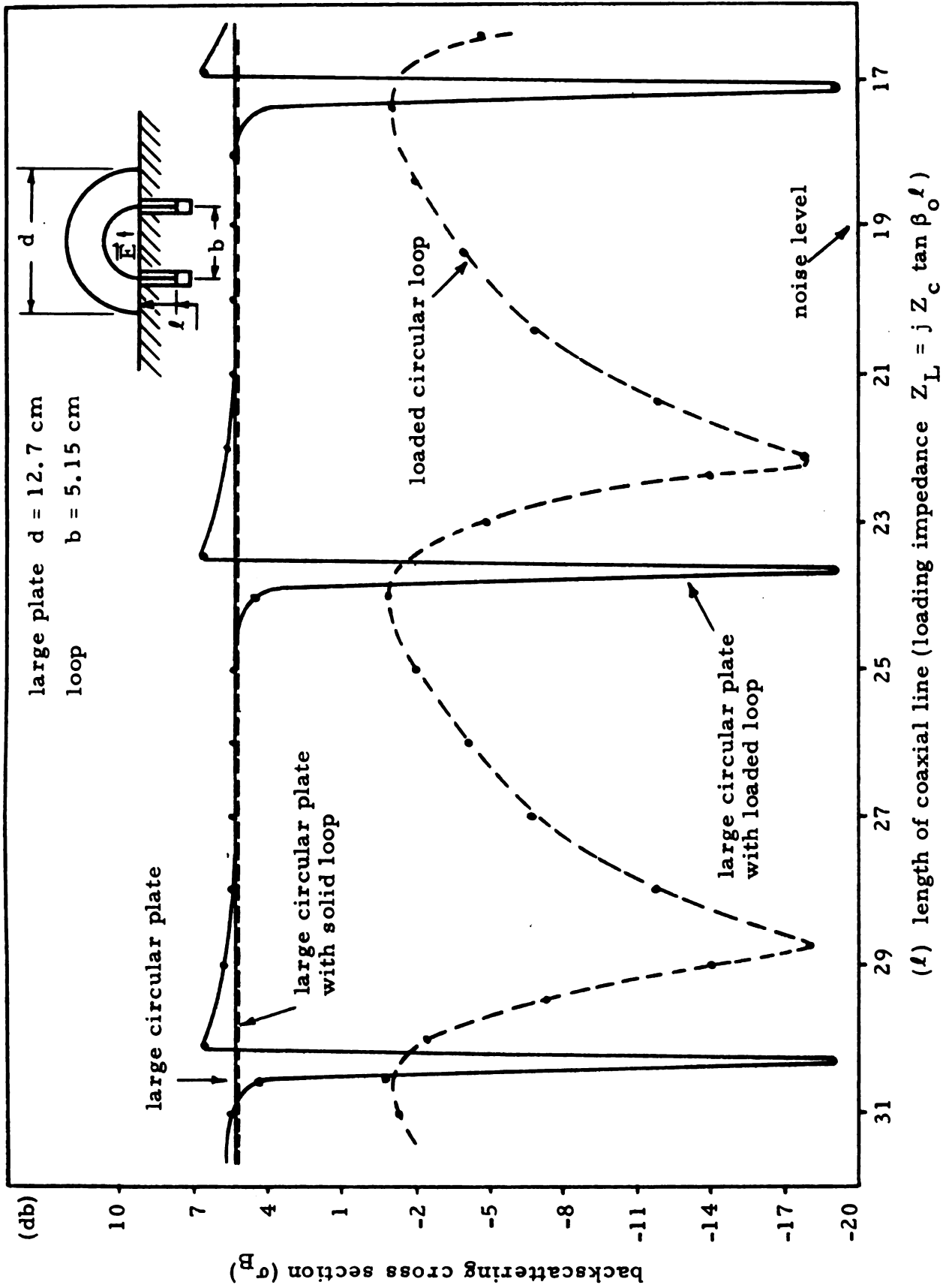
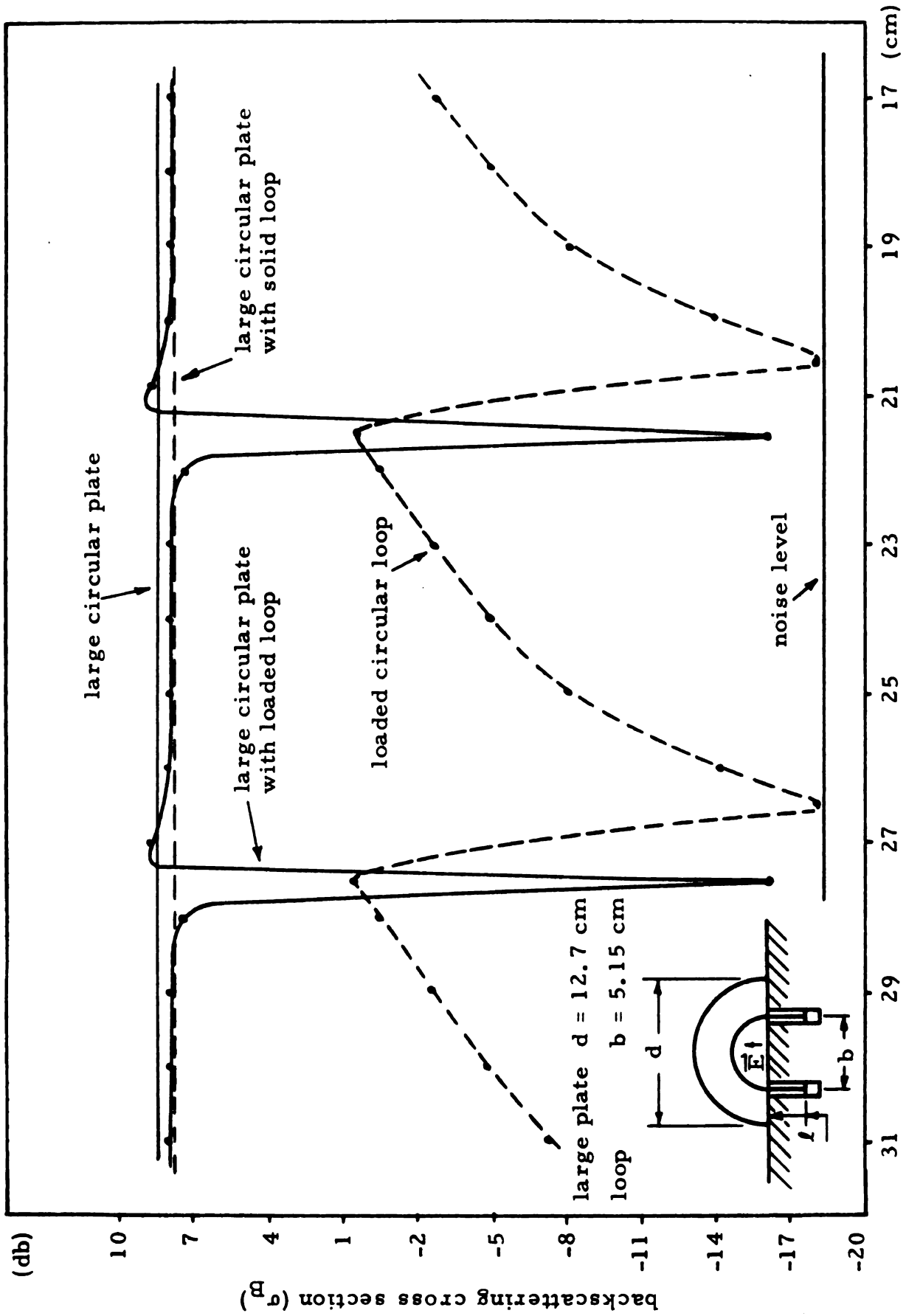


Figure 5.18. Backscatter of a large circular plate with a loaded loop as a function of loop loading ($f = 2.3$ GHz).



(l) length of coaxial line (loading impedance $Z_L = j Z_C \tan \beta_0 l$)

Figure 5.19. Backscatter of a large circular plate with a loaded loop as a function of loop loading ($f = 2.5$ GHz).

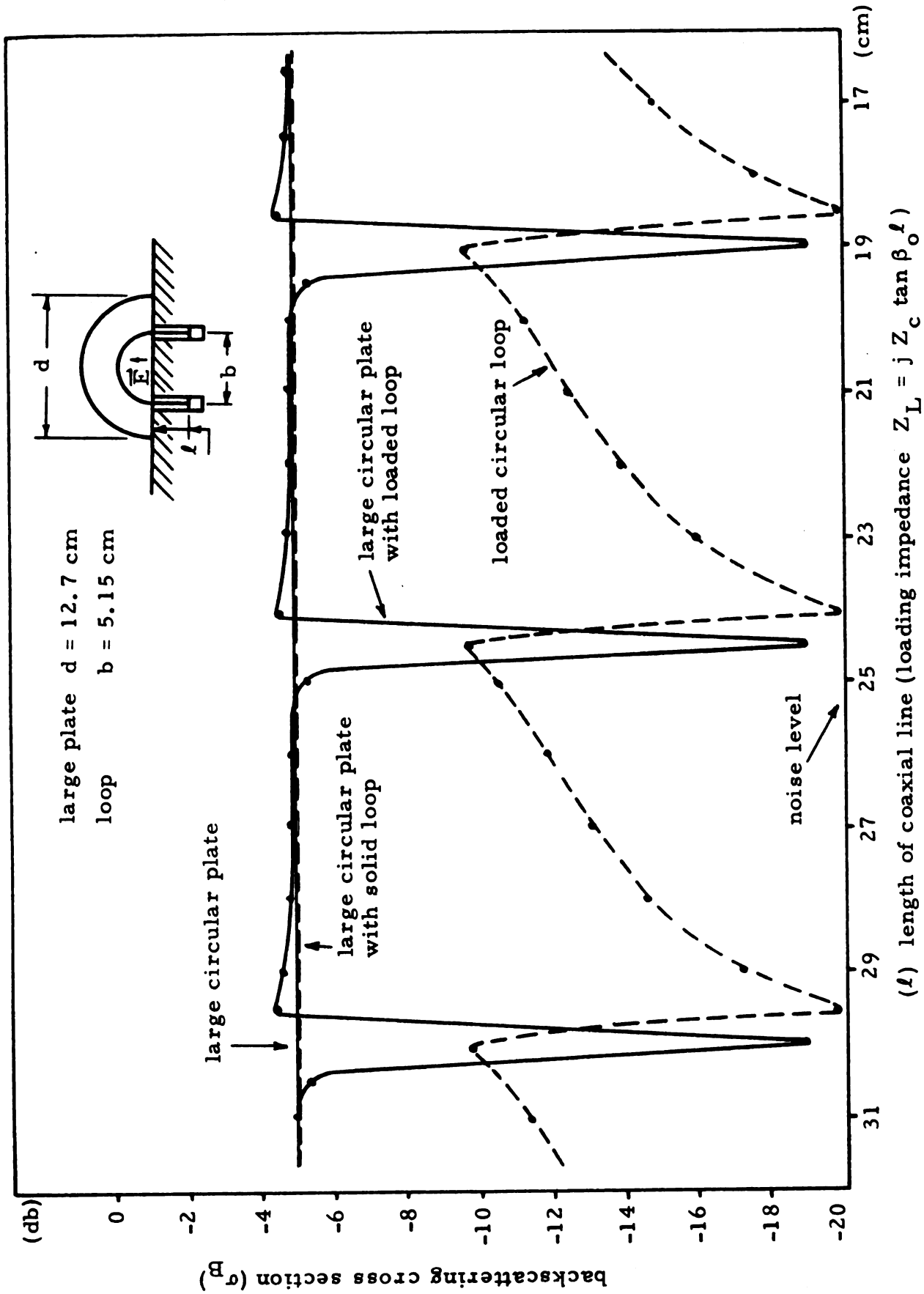


Figure 5.20. Backscatter of a large circular plate with a loaded loop as a function of loop loading ($f = 2.78$ GHz).

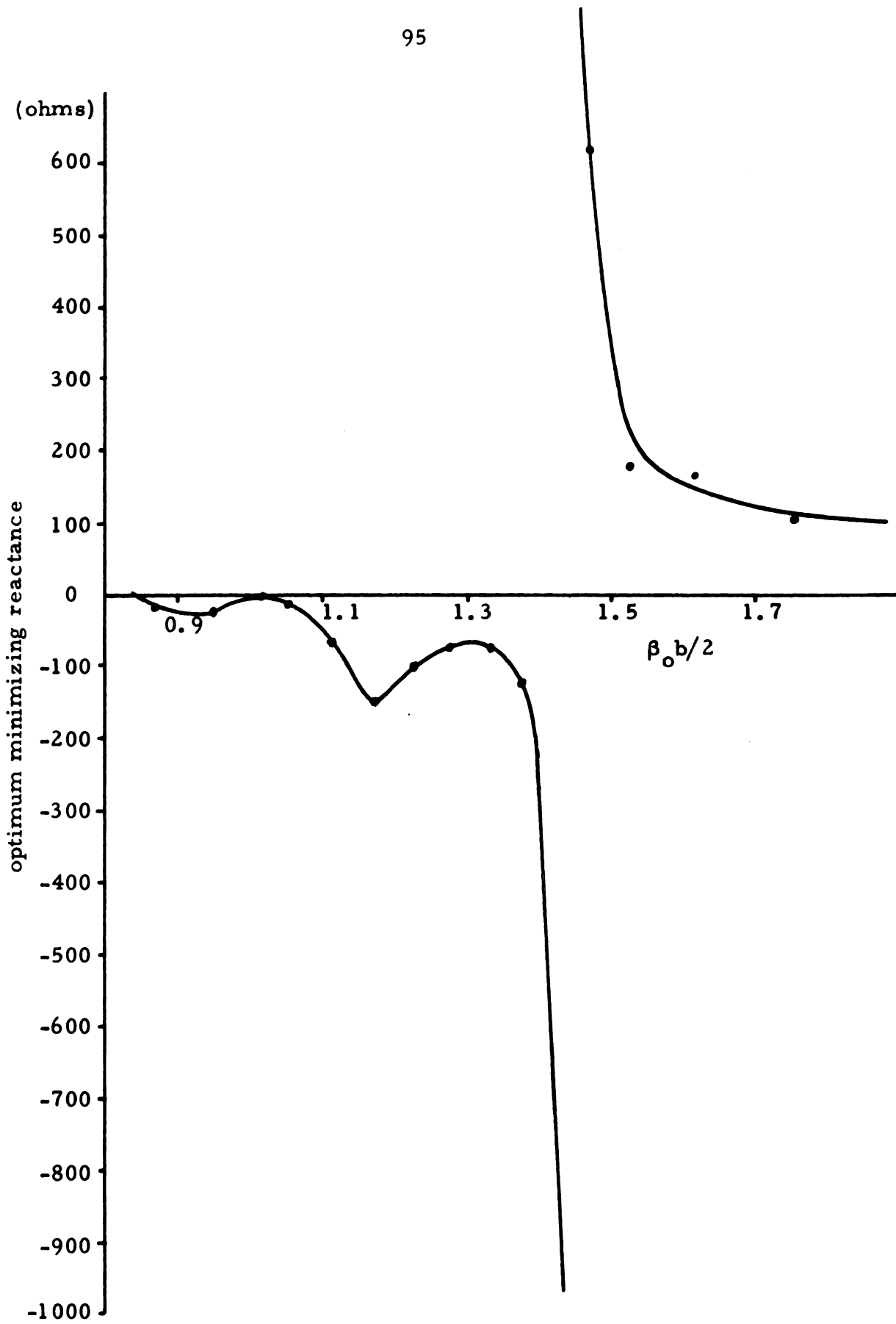


Figure 5.21. Optimum impedance for minimum backscattering from a circular plate with a loaded circular loop.

by up to 5 dB. It is readily obvious that this technique for modifying the backscatter from metallic plates is much more effective for minimization of the backscatter of a circular plate than for its enhancement. In fact, it is noted that for certain of the frequencies utilized, the backscatter from the plate-loaded loop structure can be reduced to the noise level of the measuring system.

In the experiment, there were more frequencies used than mentioned above. These experimental results tend to indicate that there exists an optimum relation between the plate diameter d and loop diameter b for a maximum reduction of the backscatter field. For example, to obtain the maximum backscatter reduction at the frequencies of 1.97 GHz, 2.1 GHz, and 2.5 GHz, the optimum ratio d/b should be 1.47, 1.98, and 2.47, respectively.

Another interesting observation from the Figures is that the optimum reactive impedances for minimum backscatter for the three variations in round plate-loaded loop structures are nearly the same at each specified frequency. This optimum reactance for minimum radar cross section of the composite structure is plotted in Figure 5.21 as a function of electrical loop circumference $\beta_0 b/2$, where b is the loop diameter and β_0 is the free space wave number. As in section 4.1, the stray capacitance at the terminal end of the coaxial line is considered.

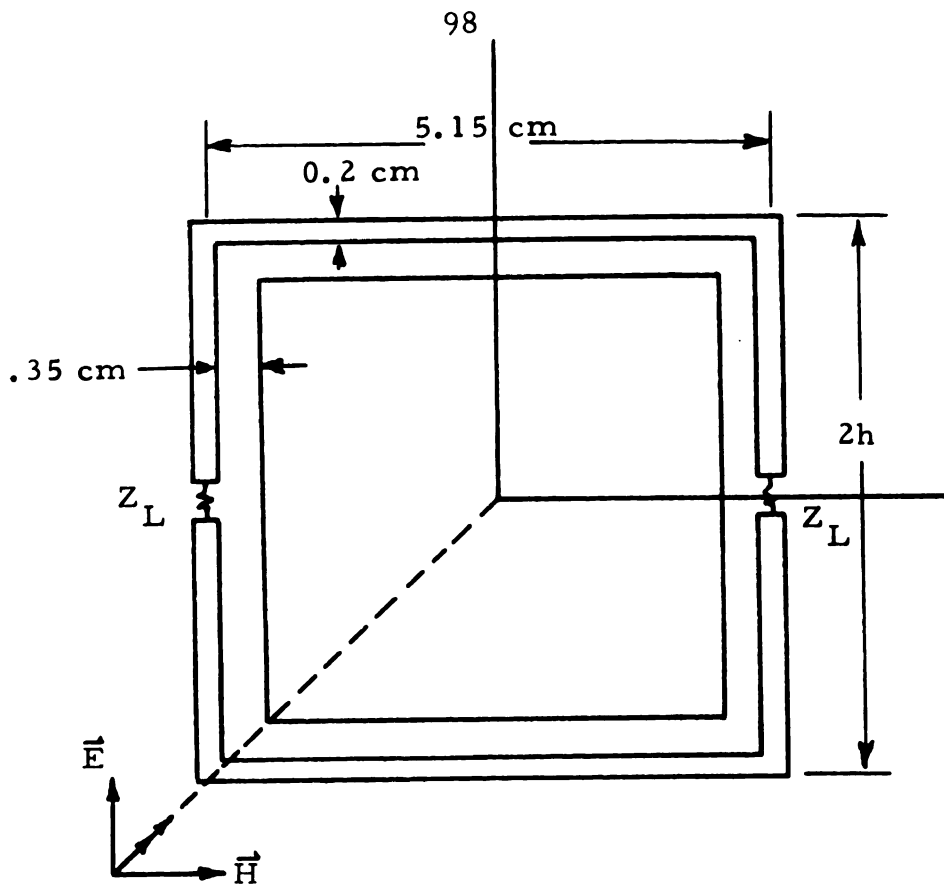
5.2. Rectangular Plate and Loop

A technique similar to that employed in section 5.1 for modifying the backscatter from a metallic plate is applied here for the case of

a conducting rectangular plate. The scheme of this method is to place a slightly larger loaded rectangular loop in the same plane with the plate, as indicated in Figure 5.22. Again, as in the case of the circular plate, the amplitude and phase of the induced current on the loop is controlled by a loading impedance in such a way that the backscatter field produced by the loop may either partially cancel or enhance the backscatter field due to the induced currents on the plate. Either minimization or enhancement of the backscattering cross section of the rectangular plate may therefore be achieved, depending upon which of the two appropriate loading impedances is selected.

In the experiment, various sizes of rectangular plates and correspondingly larger rectangular loops (wire radius = 0.1 cm) are used. Each plate and corresponding loop are placed in the same plane and are illuminated by a plane wave at normal incidence. The wire loops are loaded symmetrically with a pair of identical reactive impedances, obtained experimentally by means of adjustable shorted coaxial line sections beneath the ground plane. Throughout the experiment, the width ($b = 5.15$ cm) of the loops is held constant.

The results of this experiment are presented in Figures 5.23 to 5.28. Figures 5.23 to 5.25 indicate the backscattering cross sections of the small rectangular plate ($h = 2.8$ cm) and loaded loop as a function of the loop loading impedance. The backscatters of the large rectangular plate ($h = 5.6$ cm) and loaded loop are given in Figures 5.26 to 5.28, plotted also as a function of the loop loading impedance. In each Figure, the cross section of the rectangular



large plate $h = 5.6 \text{ cm}$
 small plate $h = 2.8 \text{ cm}$

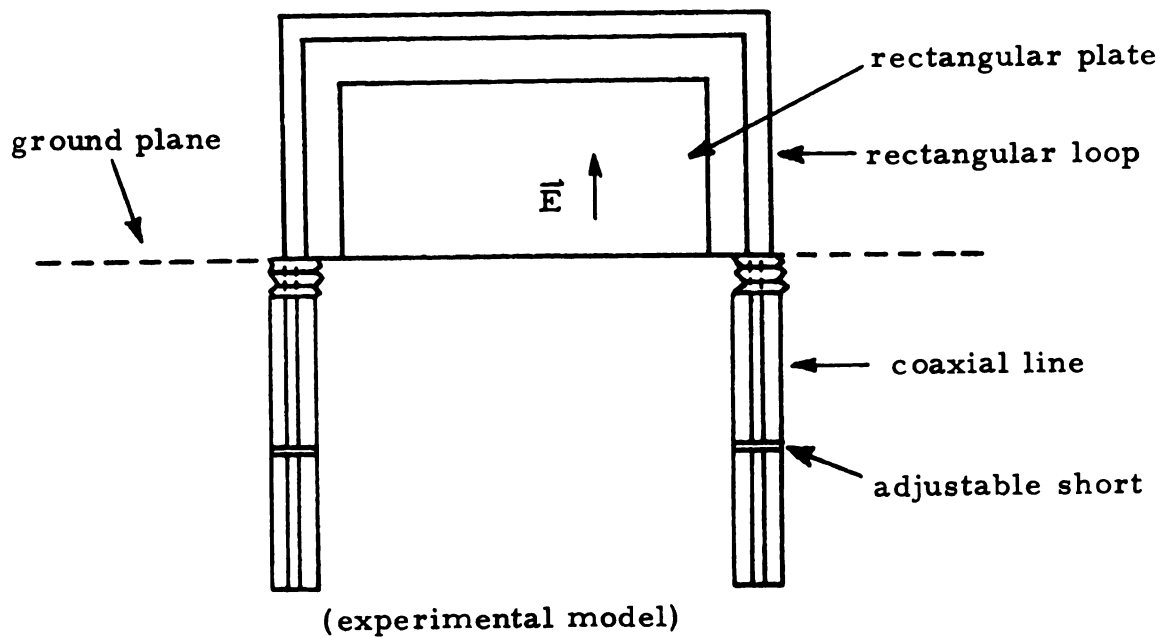


Figure 5.22. Rectangular plate and loaded loop.

plate alone is represented by a solid straight line and that of the rectangular plate and solid loop by a dashed straight line. Additionally, the radar cross sections of the loaded loop alone are designated by dashed curves, which are also plotted as a function of its loading impedances.

It is observed that the backscatter from a rectangular metallic plate can be reduced by about 11 dB in certain cases if the loading impedances (i. e., the length of the coaxial lines) are properly adjusted. Correspondingly, enhancement is even more successful since the cross sections of the rectangular plate can be enhanced by nearly 10 dB in many cases. In most cases, furthermore, the magnitude of enhancement is larger than that of the reduction.

In the experiment, there are various other sizes of rectangular plates and frequencies utilized, but with much less success. These experimental results seem to indicate that this technique has limited applications since modification of the backscatter field of rectangular plates of certain sizes is small. For this reason, the optimum reactance for either minimization or enhancement is not given, although it can be obtained in exactly the same manner as those for the circular plate and loaded loop.

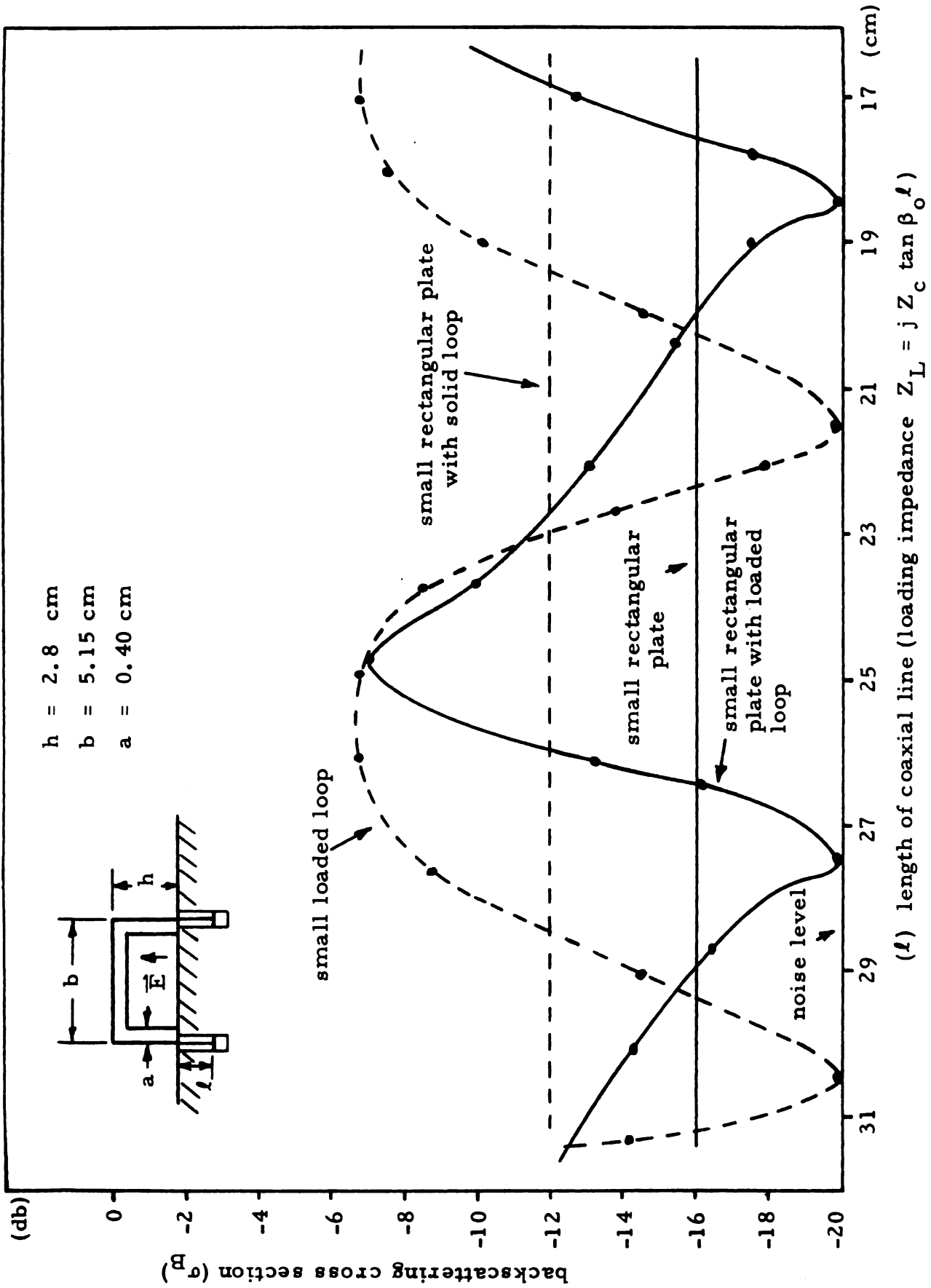


Figure 5.23. Backscatter of the small rectangular plate with a loaded loop as a function of loop loading ($f = 1.72 \text{ GHz}$).

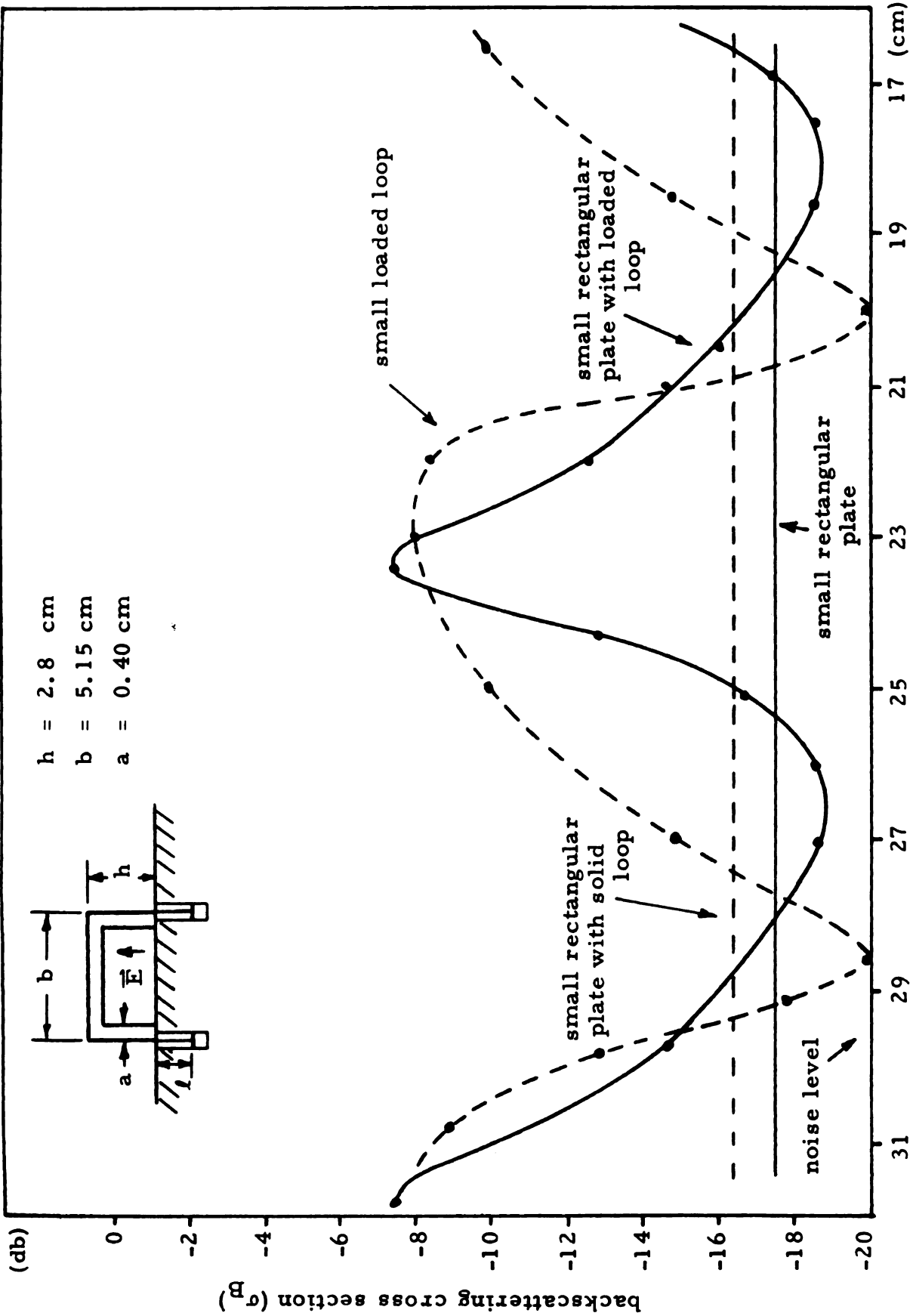


Figure 5.24. Backscatter of the small rectangular plate with a loaded loop as a function of loop loading ($f = 1.8 \text{ GHz}$).

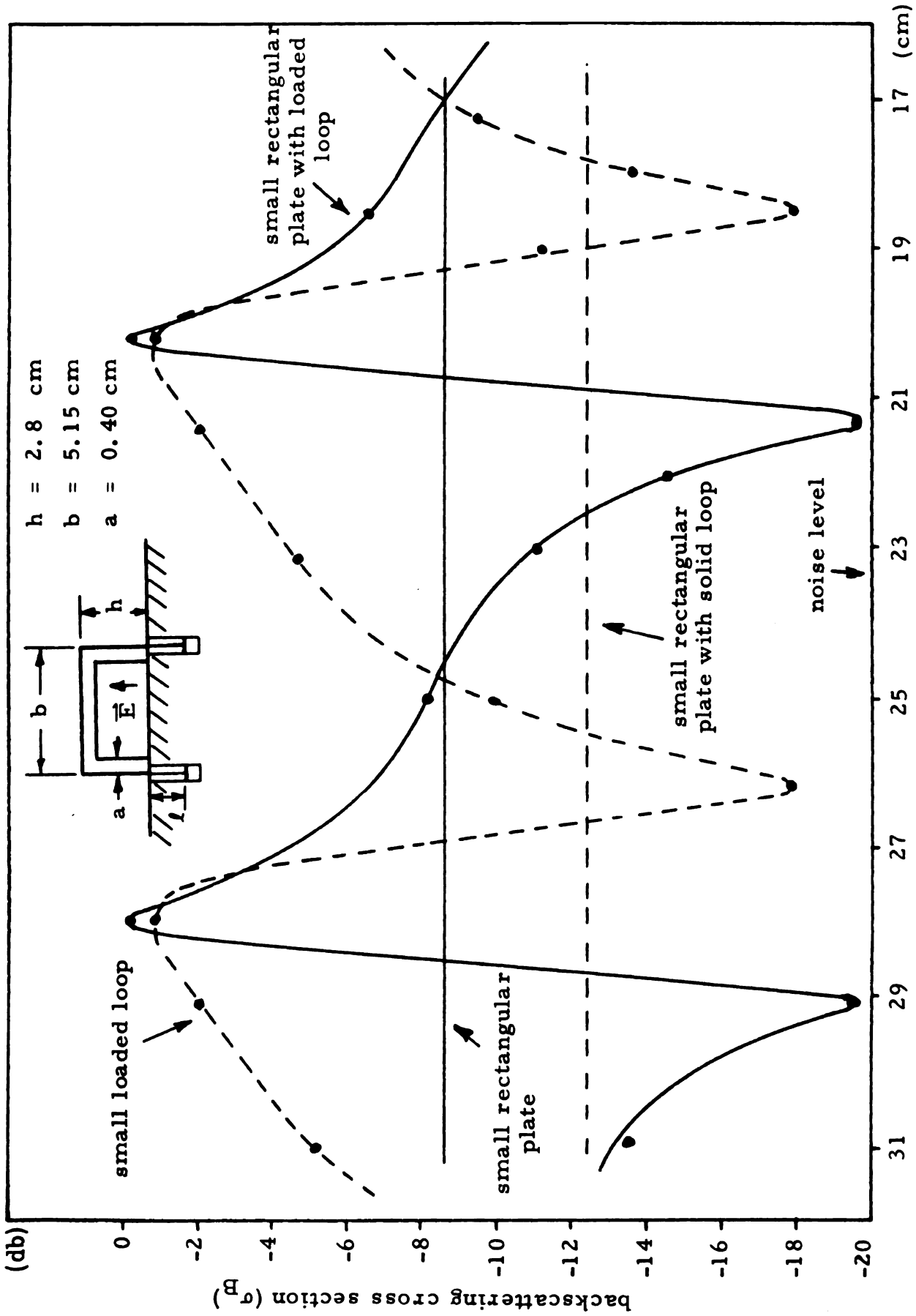


Figure 5.25. Backscatter of the small rectangular plate with a loaded loop as a function of loop loading ($f = 1.97$ GHz).

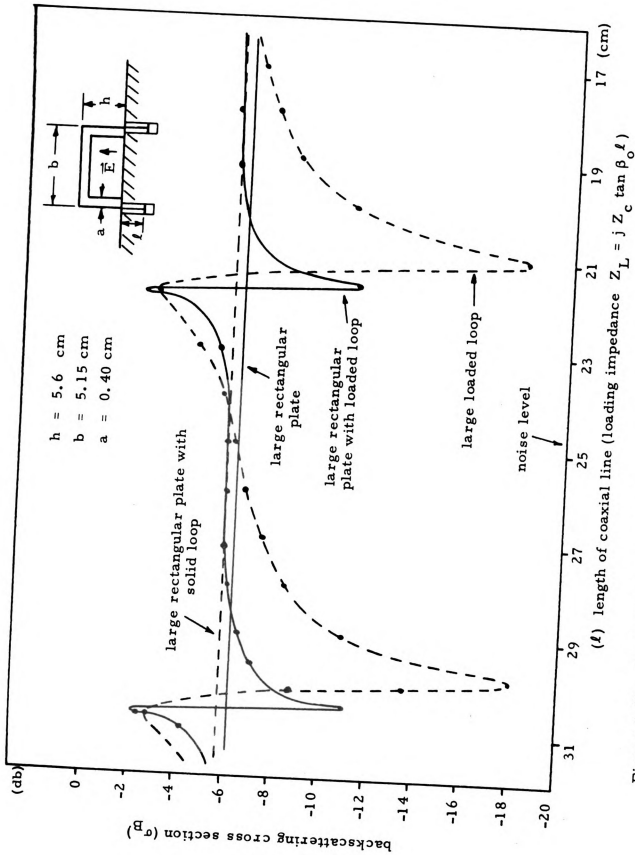


Figure 5.26. Backscatter from a large rectangular plate with a loaded loop as a function of loop loading ($f = 1.72$ GHz).

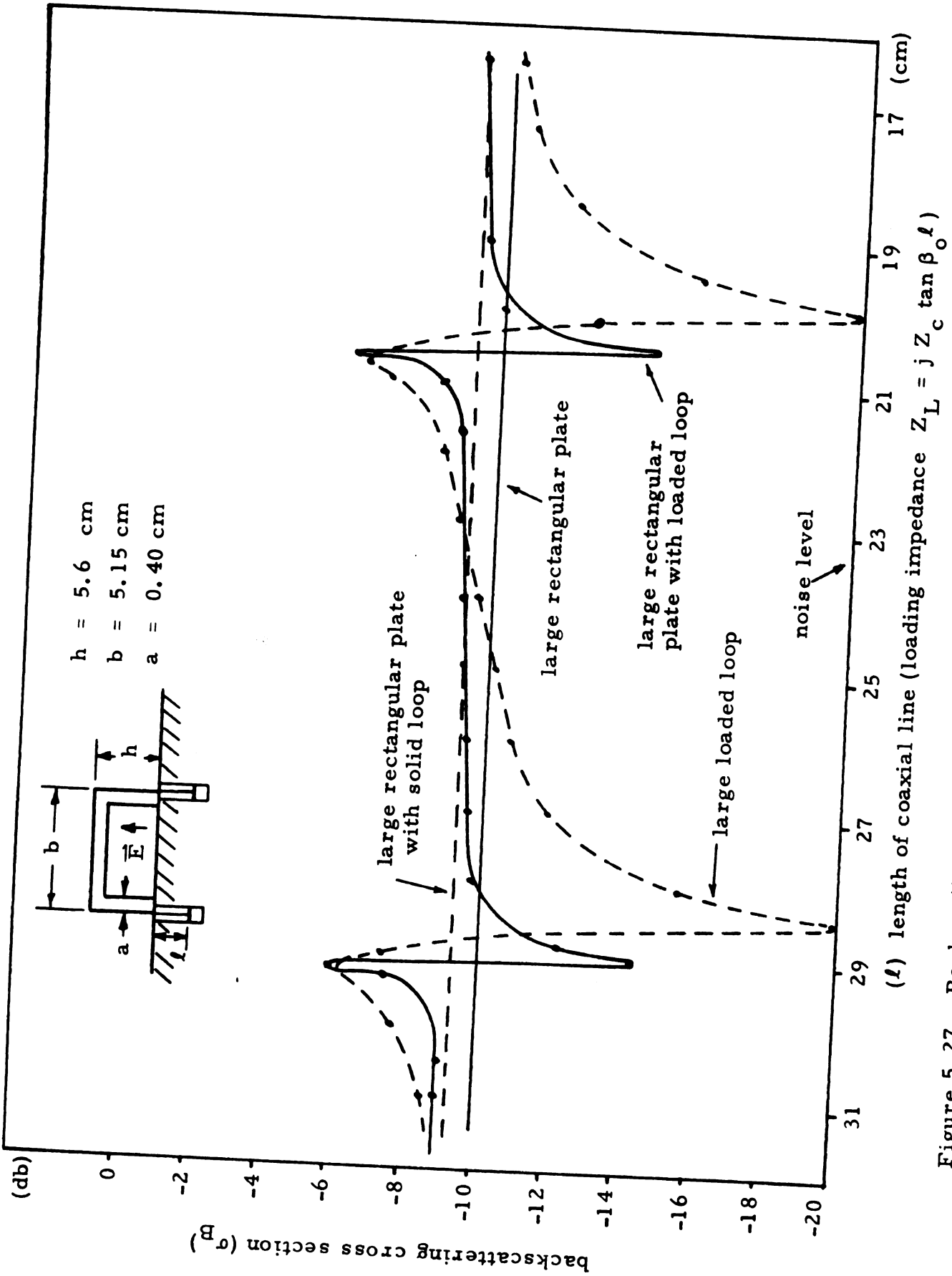


Figure 5.27. Backscatter from a large rectangular plate with a loaded loop as a function of loop loading ($f = 1.8$ GHz).

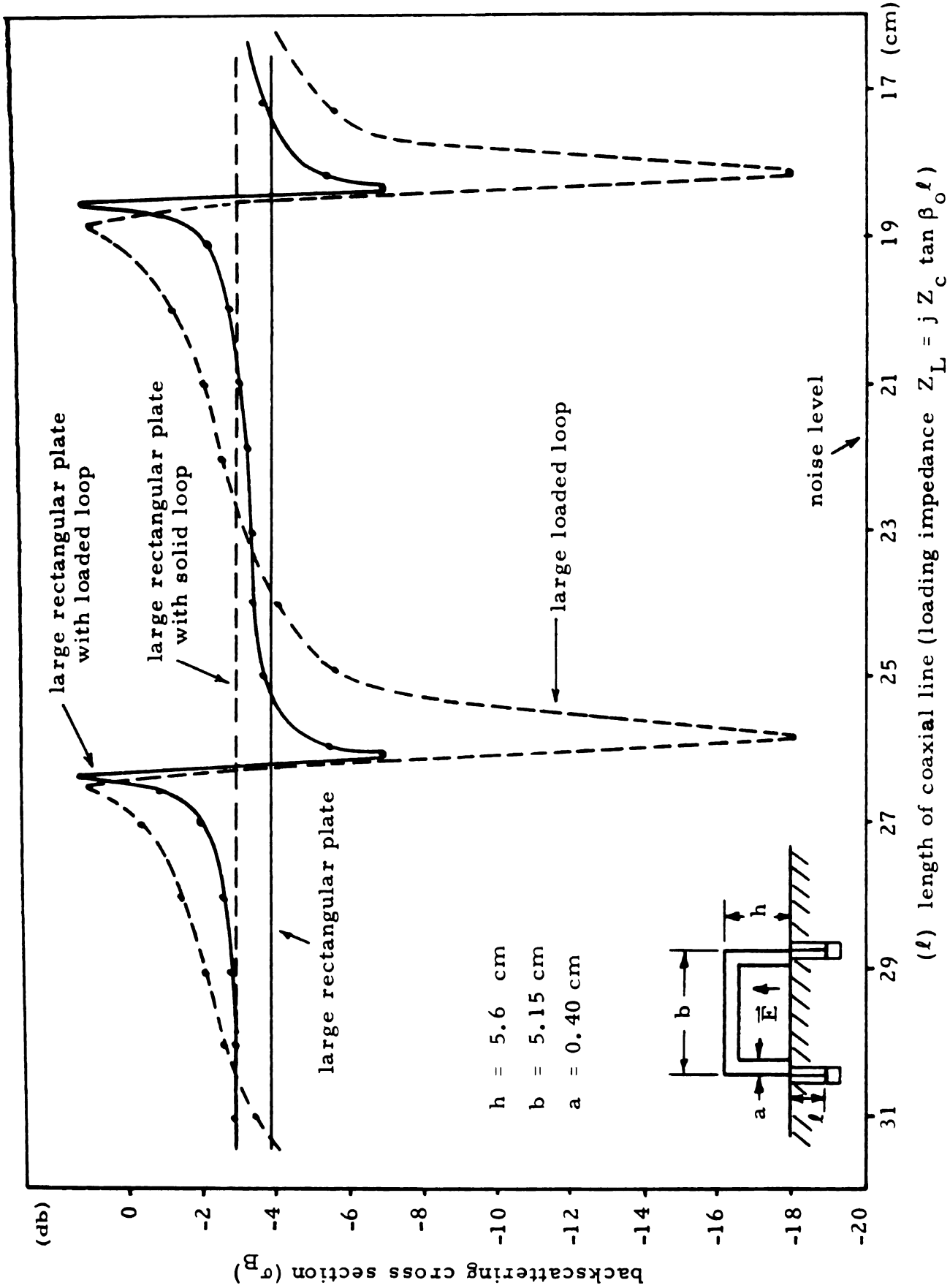


Figure 5.28. Backscatter from a large rectangular plate with a loaded loop as a function of loop loading ($f = 1.97 \text{ GHz}$).

CHAPTER VI

MODIFICATION OF BACKSCATTERING FROM CYLINDERS

The backscattering of a circular cylinder has been studied rather conclusively by theoretical techniques.³ As an extension, Chen¹⁵ studied the backscatter from the combination of a thick cylinder and a parallel, impedance loaded thin-wire element. Experimental investigations of the backscattering cross sections of a single cylinder and combinations of parallel cylinders are performed to demonstrate the reliability of these techniques, and to study new problems which are much too complex for theoretical study.

6.1. Solid and Loaded Cylinders

For comparison purposes, the backscattering cross section of cylinders, both thick and thin, are studied here. The scattered field from an unloaded cylinder, as well as loaded cylinder, is investigated experimentally.

6.1.1. Solid or Unloaded Cylinder

The relative backscattering cross section of the solid cylinder (zero loading) is experimentally determined by use of the cancellation technique described in section 2.2.2. The 1 kHz amplitude modulation technique is used here for detection. For each cylinder thickness (diameter = $2a$), the relative radar cross section is determined as a function of electrical cylinder half-length h/λ_0 (see Figure 6.1). The backscattering cross section of the thick cylinder is represented

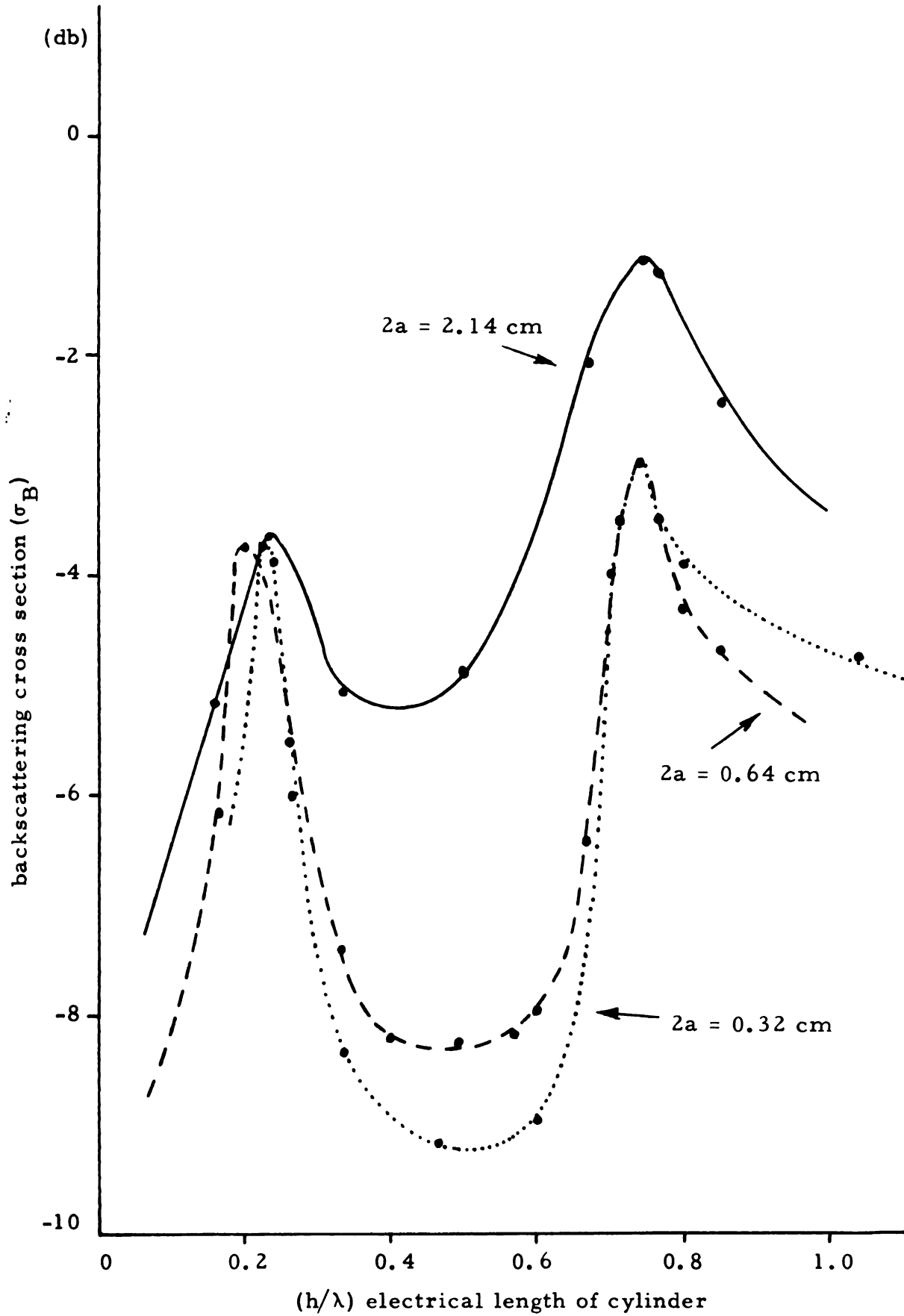


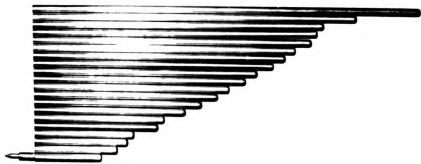
Figure 6.1. Backscattering cross sections of solid cylinders as a function of cylinder half-length h .

by a solid curve, the medium one by a dashed line, and the thin cylinder by a dotted line. This experiment is performed at a frequency of 2 GHz. Three different thicknesses are used: $2a = 2.14$ cm, $2a = 0.64$ cm, and $2a = 0.32$ cm. Physical dimensions of two of these cylinders ($2a = 2.14$ cm and $2a = 0.32$ cm) are described in Figure 6.2. It is observed from Figure 6.1 that the backscatter from the thick cylinder is approximately 5 dB greater than the two thinner cylinders. Furthermore, the resonant peaks of the thick cylinder are not as distinct, since there is only about 2 dB variation between the resonant and antiresonant points.

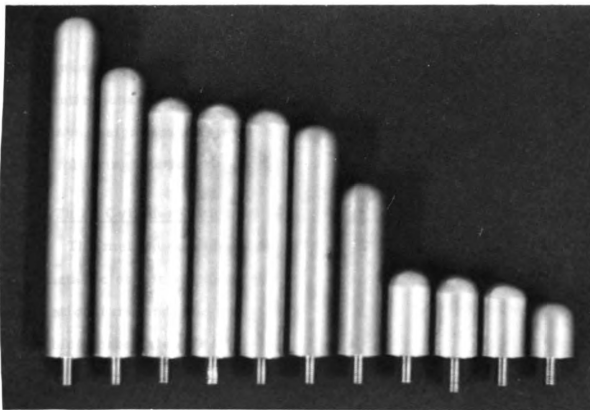
6.1.2. Impedance Loaded Cylinder

As a means of modifying the scattering cross sections of the above mentioned thin cylinder ($2a = 0.32$ cm), the cylinder is loaded at its center by a lumped impedance. In general, both resistive and reactive impedance components are required to produce a maximum variation of the radar backscattering. The problem becomes very complex when the required resistance is negative. To simplify this problem, only reactive loading is considered. This is accomplished by means of a coaxial cavity located beneath the ground plane (Microline adjustable coaxial shorted line). As before, the cancellation method is employed for measurement of the radar cross section of the loaded cylinder.

The experimental results for several lengths of thin cylinders are indicated in Figures 6.4 to 6.6. In each of these Figures, the scattering cross section of a thin, loaded cylinder, represented by



thin cylinder ($2a = 0.32$ cm)



thick cylinder ($2a = 2.14$ cm)

Figure 6.2. Physical description of cylinders.

dashed lines, is plotted as a function of the loading impedance of the cylinder. A coaxial cavity is utilized as the loading device, therefore providing a purely reactive impedance. The approximate impedance of the coaxial cavity can be calculated from the expression $Z_L = j Z_c \tan \beta_o \ell$ where Z_c is the characteristic impedance of the coaxial cavity, β_o is the wave number, and ℓ is its length.

In most cases above, both minimization and enhancement can be achieved to some degree for particular values of loading reactance. The minimization of the scattering should have direct application to space vehicle radar camouflage. It is observed that the radar cross section of the cylinder can be minimized to the noise level for each case, (up to 15 dB). Enhancement is also observed for most cylinder lengths, with the exception of resonant lengths, but generally to a much lesser degree. It is a noteworthy observation that scattering from antiresonant cylinders can be enhanced to the greatest extent; this plays a significant role in the compensation method discussed in the following section.

6.2. Thick Cylinder With a Parallel, Impedance Loaded Thin Cylinder

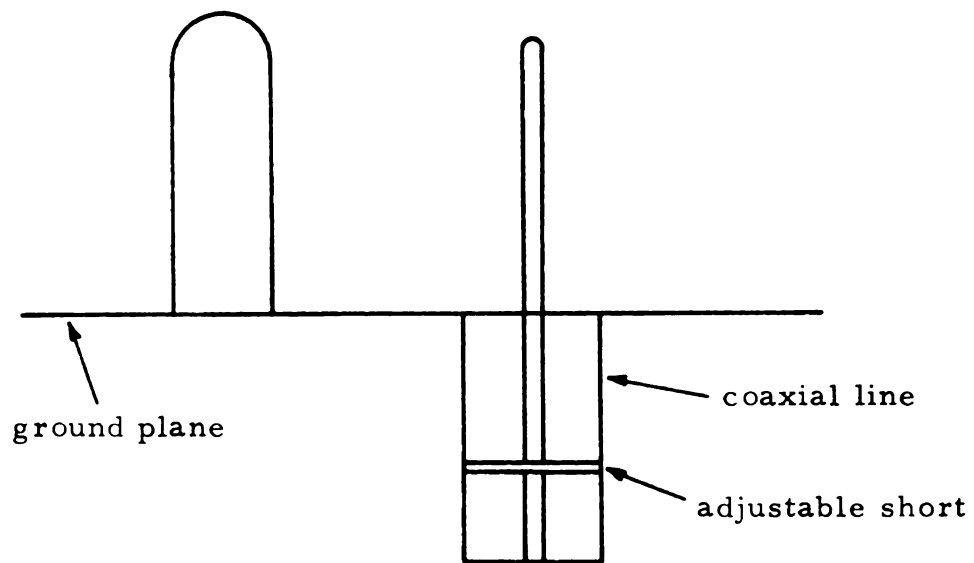
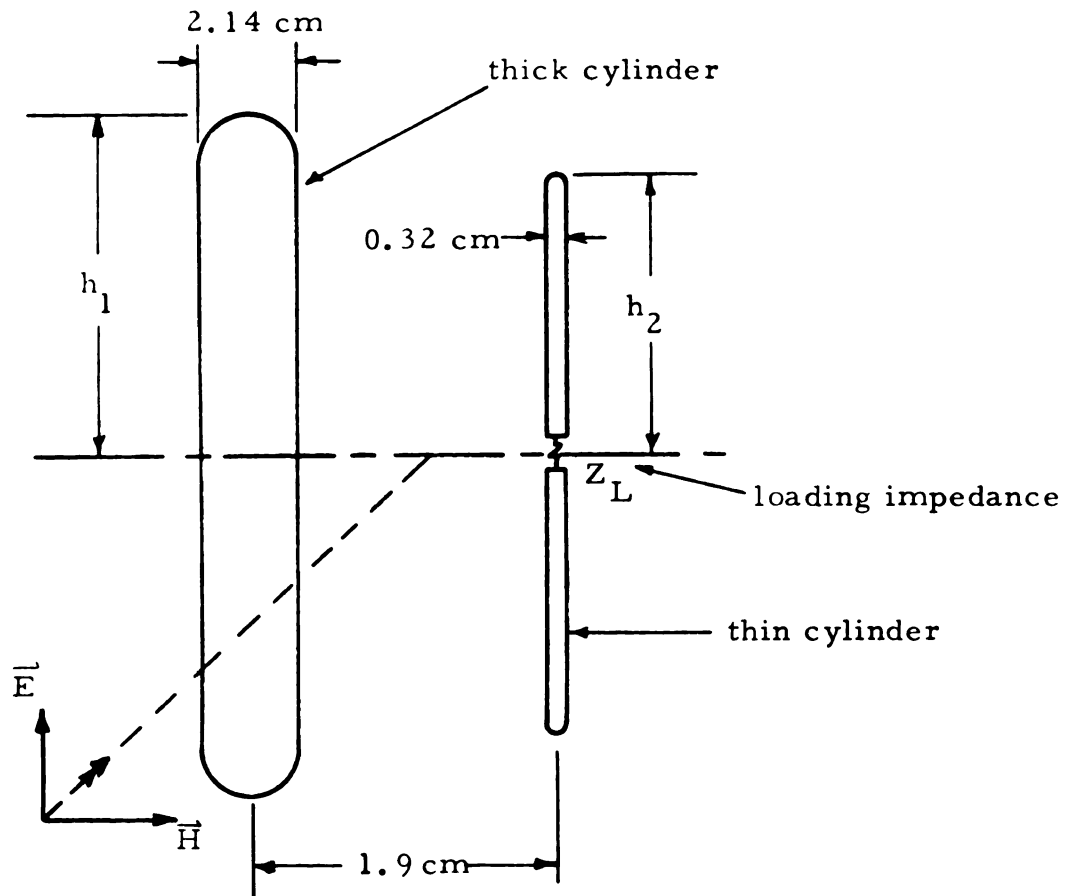
The method considered thus far for modifying the backscattering of a metallic object utilizes an impedance loading technique. Other conventional methods include the techniques of employing radar absorbing materials and of reshaping the body. In some cases none of these techniques are permissible for mechanical reasons. A relatively new technique, the compensation method, is investigated for possible use on those metallic bodies for which an impedance

loading technique cannot be applied.

The compensation method consists of adding a small metallic body, such as a thin wire loaded with appropriate impedances, to the main metallic body. When the main body and added thin wires are illuminated by an electromagnetic wave, currents are induced on either element. If the amplitude and phase of the induced current on the thin wire can be properly adjusted by means of an appropriate impedance loading, it can cancel or add to the radiation field due to the induced current on the main body; thus the total backscatter field from the main body and thin wire is modified.

The experiment involves a solid cylinder and a thin, center-loaded wire placed parallel to one another, with a plane electromagnetic wave assumed to be incident broadside upon them, as indicated in Figure 6.3. Minimization of the radar cross section of this combination is the primary goal of the research, although enhancement is considered as well.

The experimental results are shown in Figures 6.4 to 6.6. Solid lines represent scattering from the thick cylinder ($a = 1.07$ cm) combined with the loaded, thin cylinder ($b = 0.16$ cm), for which the scattering cross sections are plotted as functions of the cylinder loading impedance. A frequency of 1.72 GHz is used for the experiment of Figures 6.4 to 6.6, although various other frequencies are considered in this research. Various combinations of cylinder lengths $2h$ are utilized for this study. It is observed that certain combinations of lengths produce more minimizations or enhancement than others. Figures 6.7 to 6.13 indicate the maximum and minimum



(experimental model)

Figure 6.3. Thick cylinder with a loaded thin cylinder.

backscatters from each combination of thick with optimum loaded thin cylinders, plotted as functions of the thin cylinder half-length h_2 . In each figure the length of the thick cylinder h_1 is held constant while h_2 is varied. The backscatter of the thick cylinder only is represented by a solid straight line, while the minimum and maximum backscatters of the combined thick with loaded thin cylinders are represented by solid and dashed line curves, respectively.

It is noted that the largest variation in the backscatters occur when the thin cylinder is considerably longer than the thick cylinder, and also when the length of the thick cylinder is small compared with the wavelength. Addition of resistive components, both positive and negative, to the reactive loading should make the application of this technique more successful.

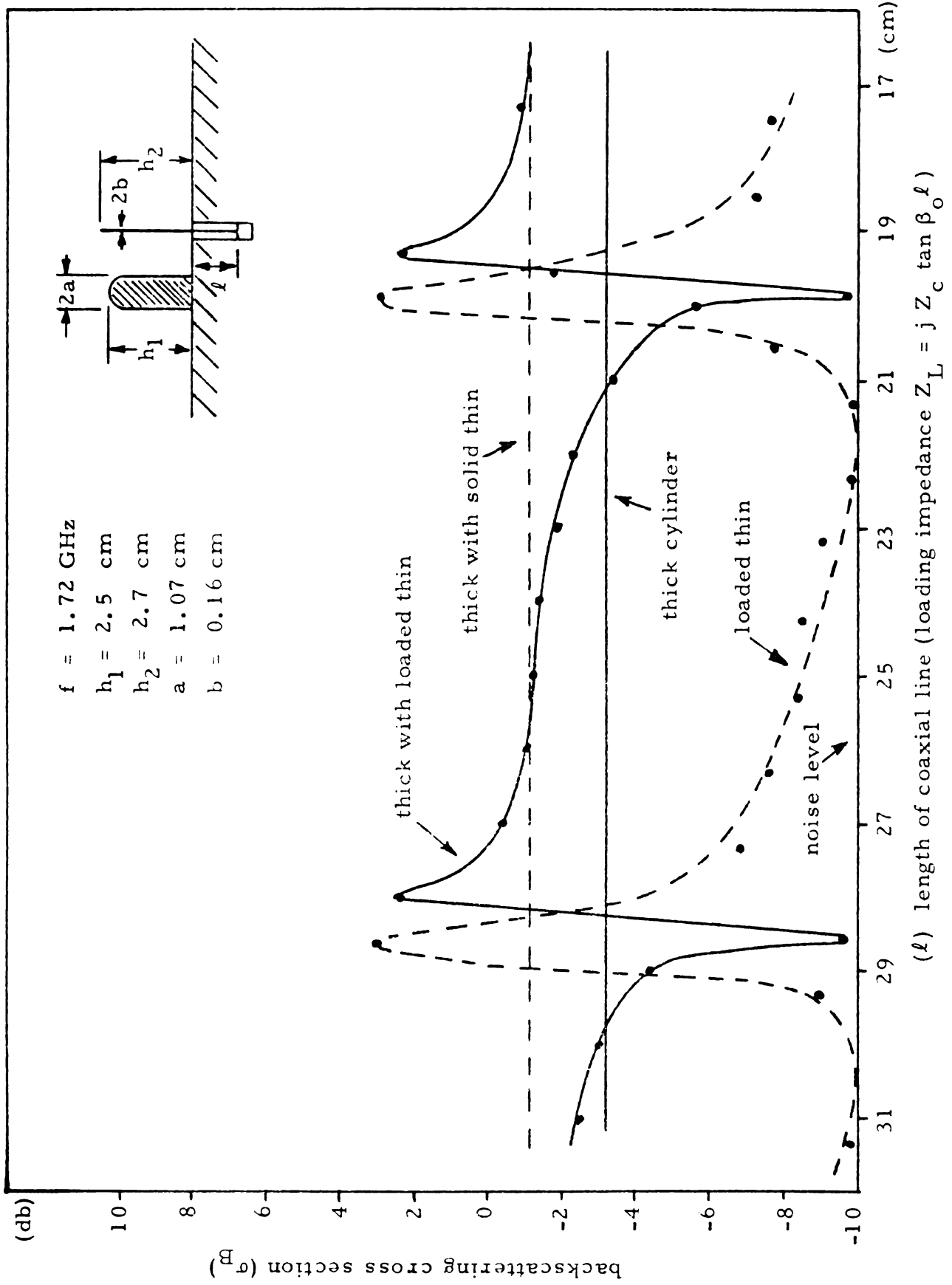


Figure 6.4. Backscattering cross section of a thick with a loaded thin cylinder as a function of loading impedance of thin cylinder ($h_1 = 2.5 \text{ cm}$, $h_2 = 2.7 \text{ cm}$).

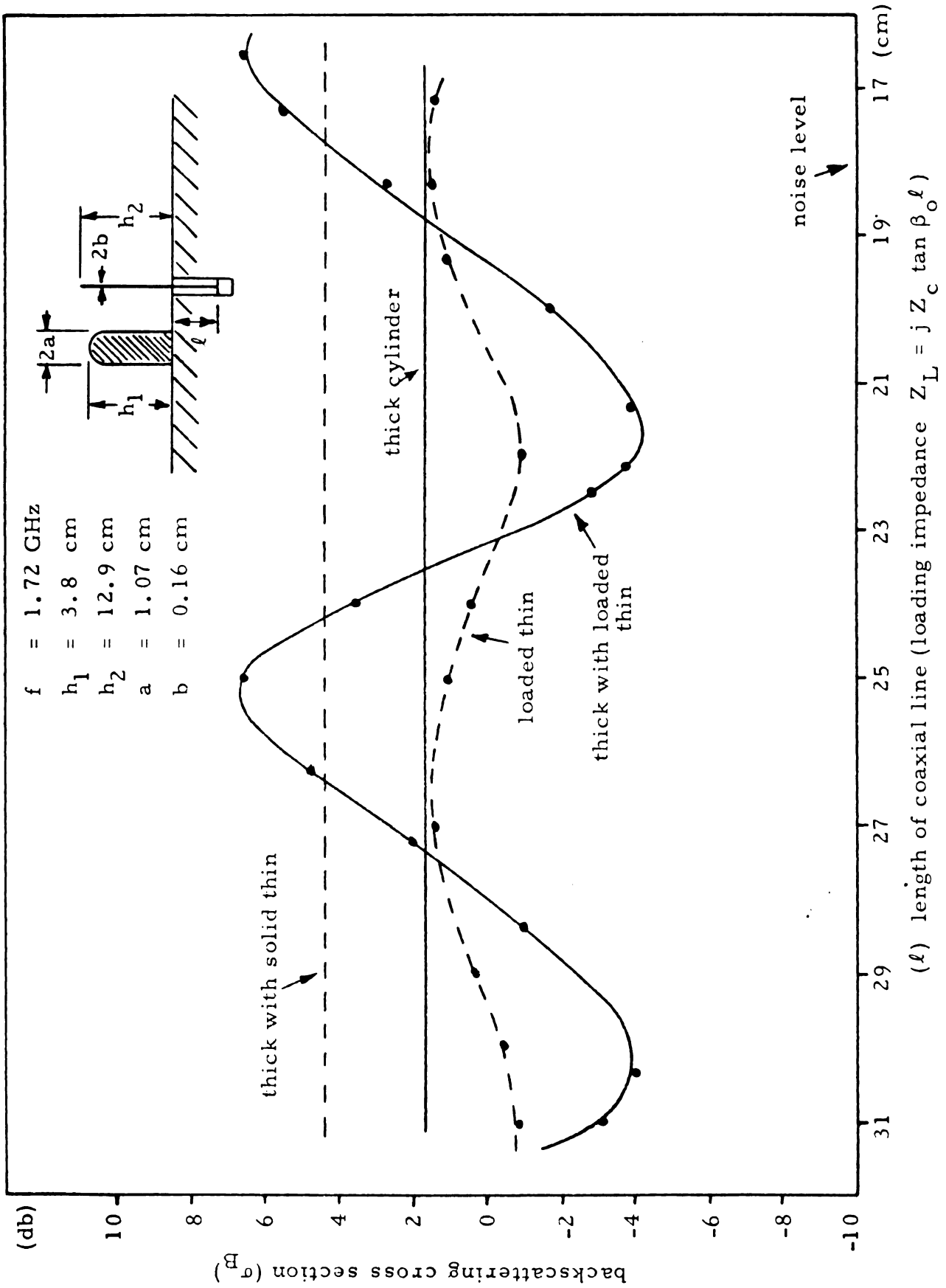


Figure 6.5. Backscattering cross section of a thick with a loaded thin cylinder as a function of loading impedance of thin cylinder ($h_1 = 3.8 \text{ cm}$, $h_2 = 12.9 \text{ cm}$).

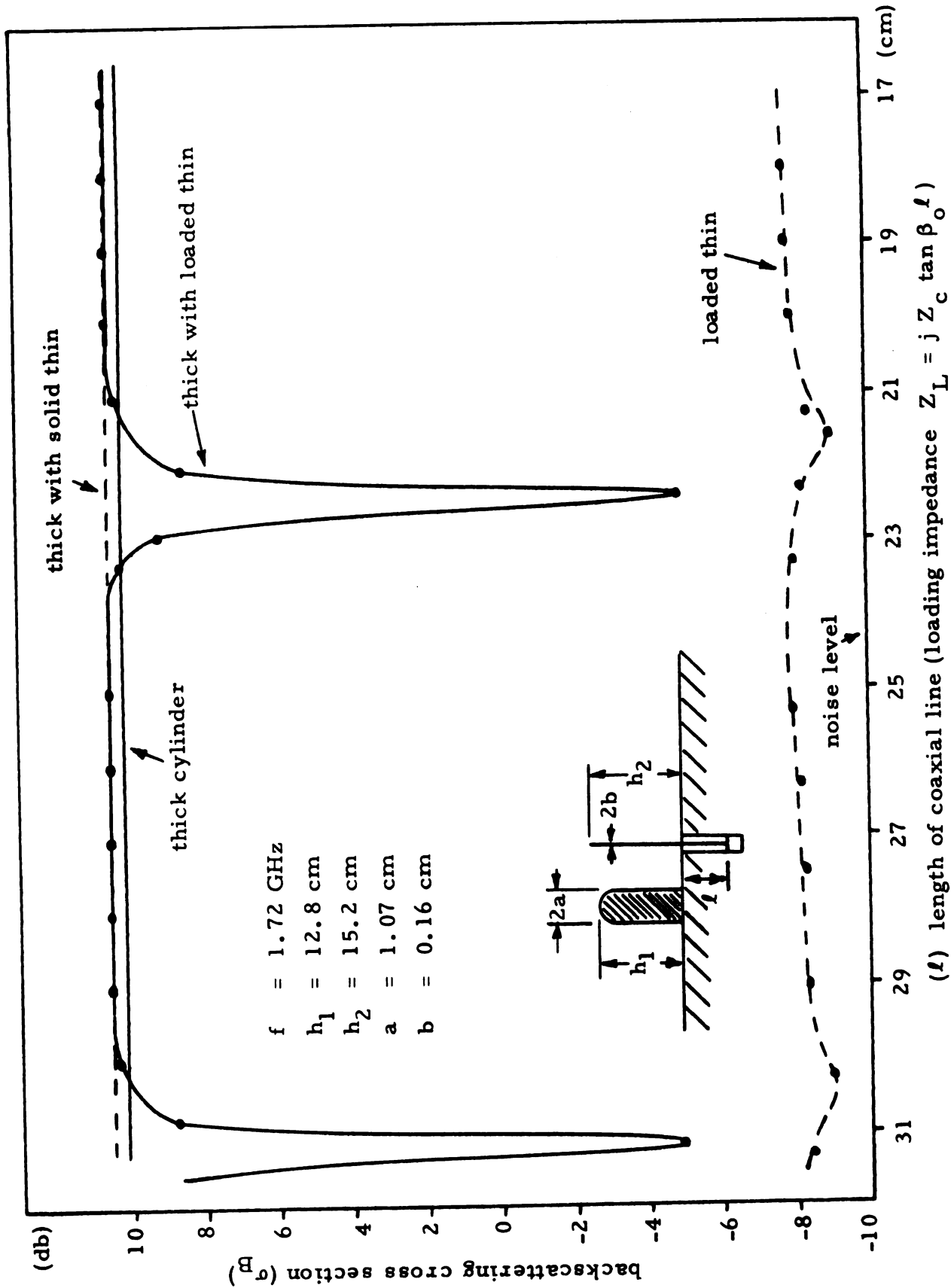


Figure 6.6. Backscattering cross section of a thick with a loaded thin cylinder as a function of loading impedance of thin cylinder ($h_1 = 12.8 \text{ cm}$, $h_2 = 15.2 \text{ cm}$).

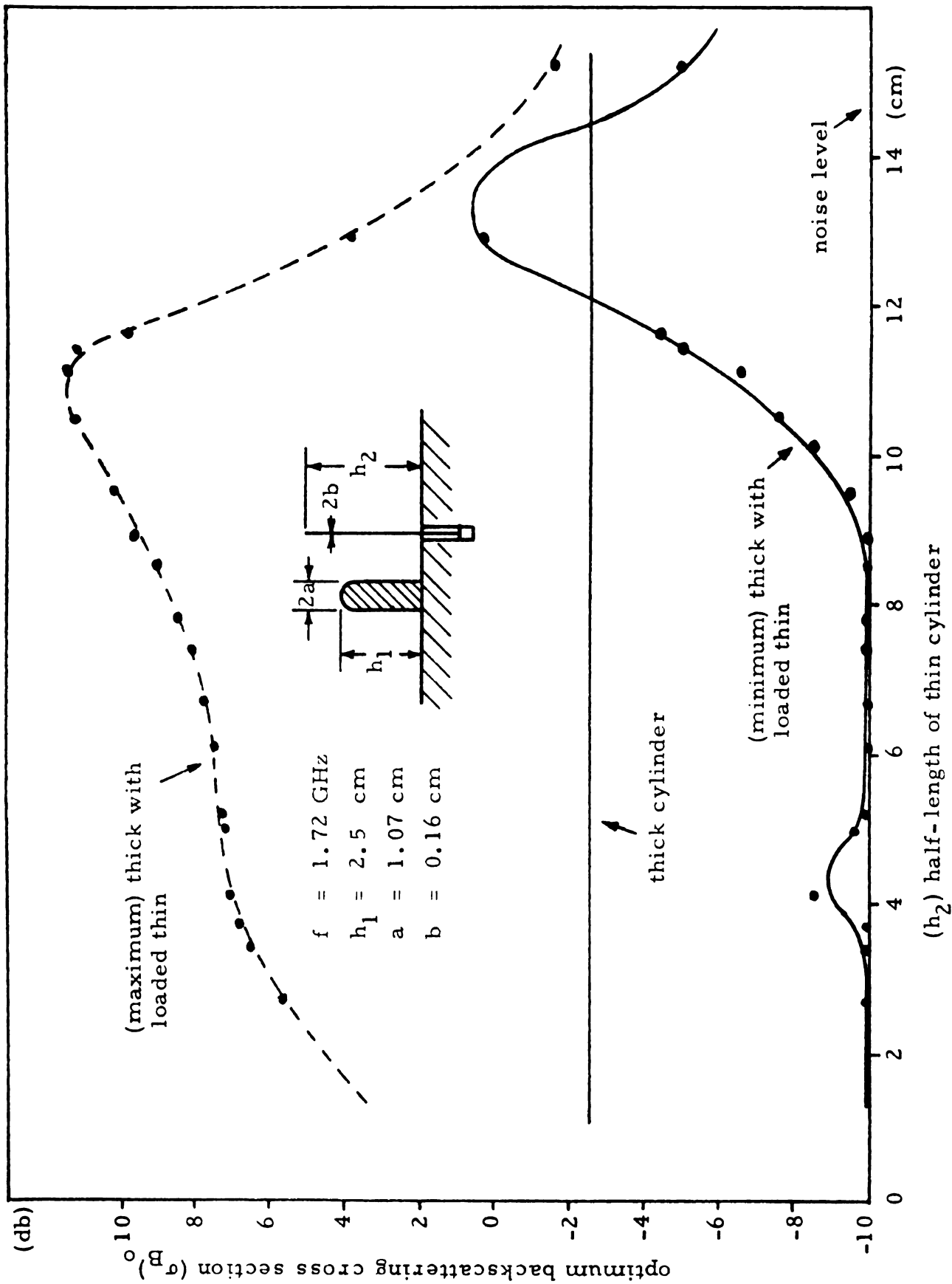


Figure 6.7. Maximum and minimum backscatters from a thick with a loaded thin cylinder as a function of thin cylinder half-length h_2 ($h_1 = 2.5 \text{ cm}$).

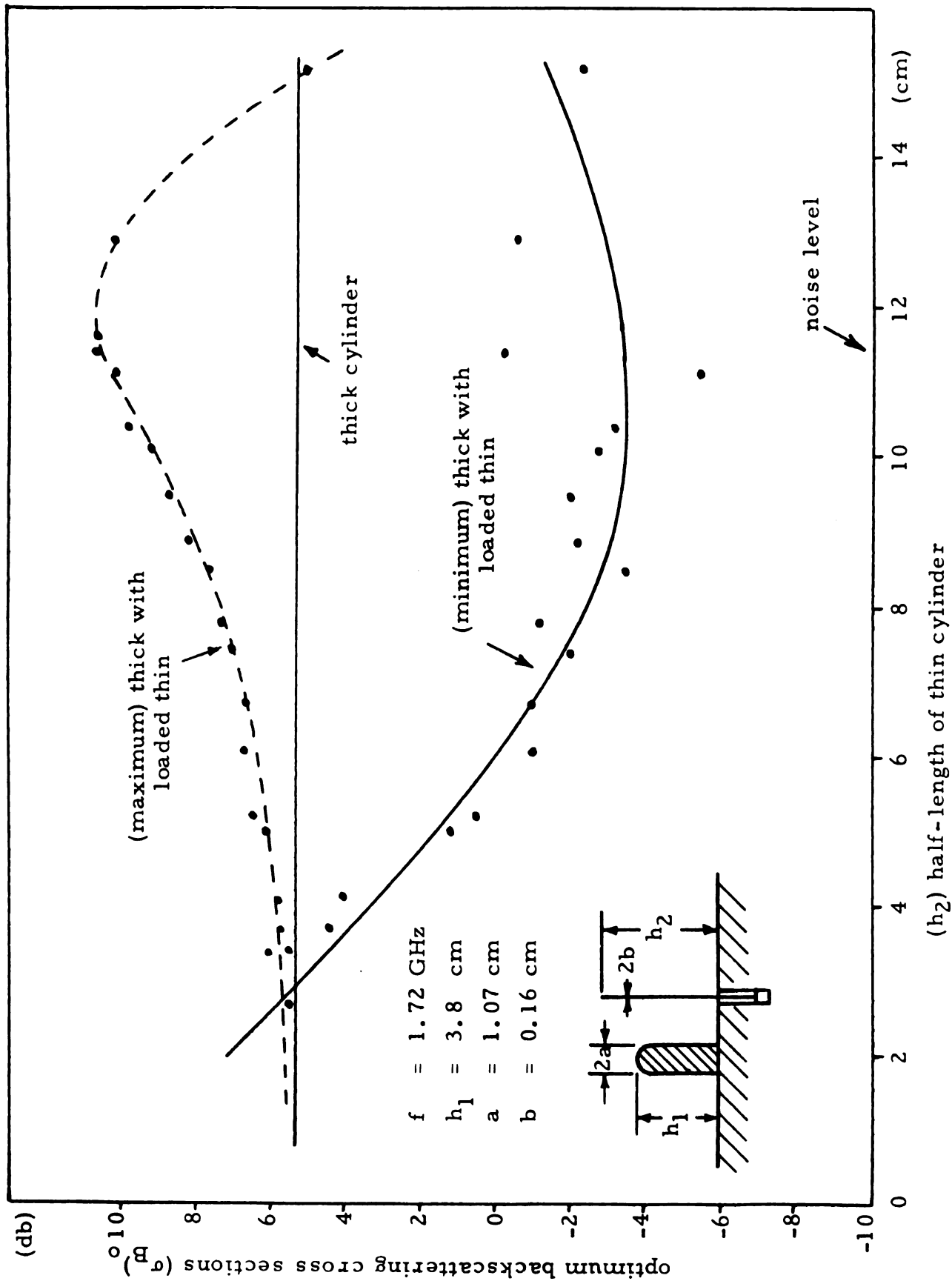


Figure 6.8. Maximum and minimum backscatters from a thick with a loaded thin cylinder as a function of thin cylinder half-length h_2 ($h_1 = 3.8 \text{ cm}$).

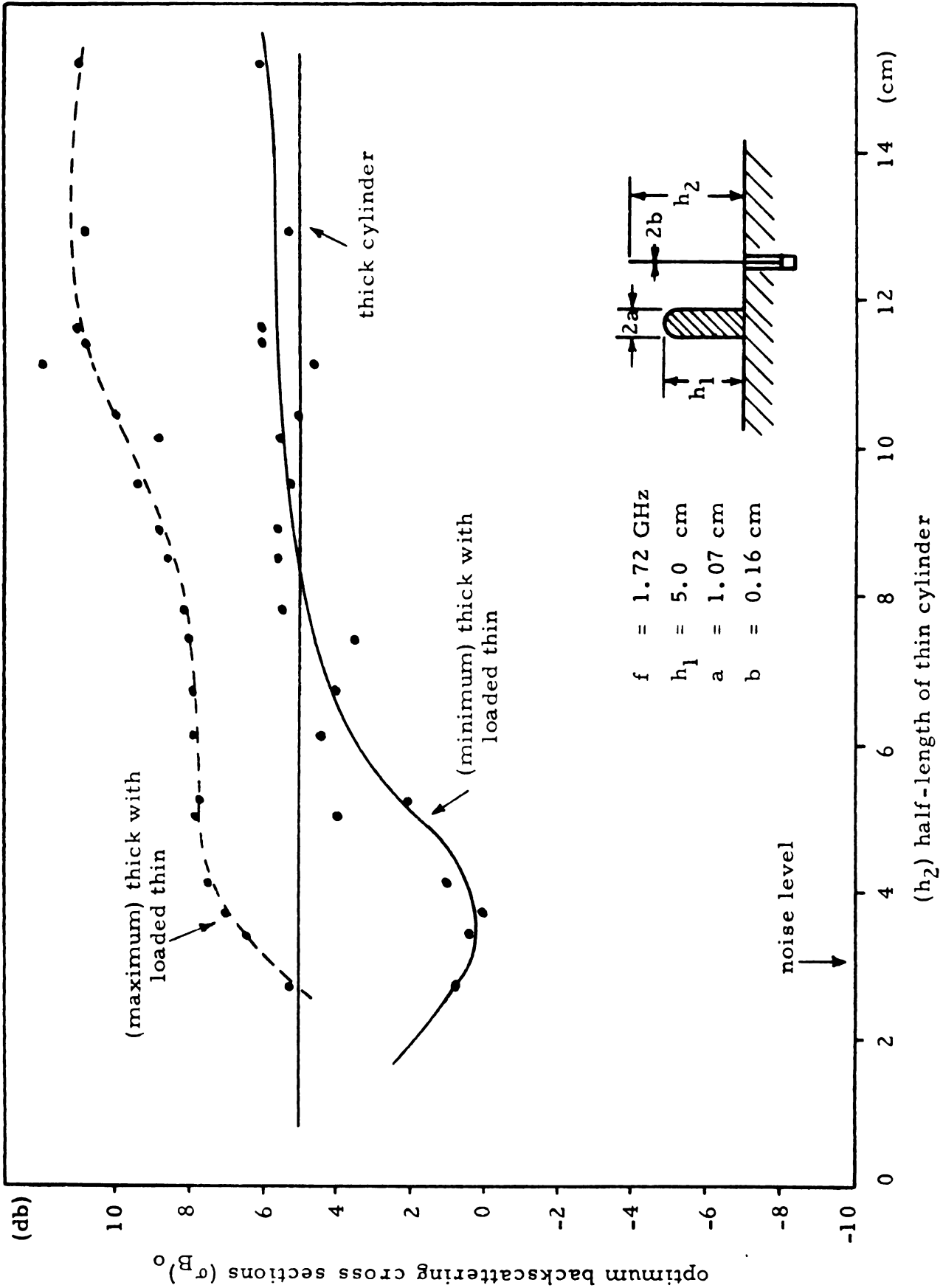


Figure 6.9. Maximum and minimum backscatters from a thick with a loaded thin cylinder as a function of thin cylinder half-length h_2 ($h_1 = 5.0 \text{ cm}$).

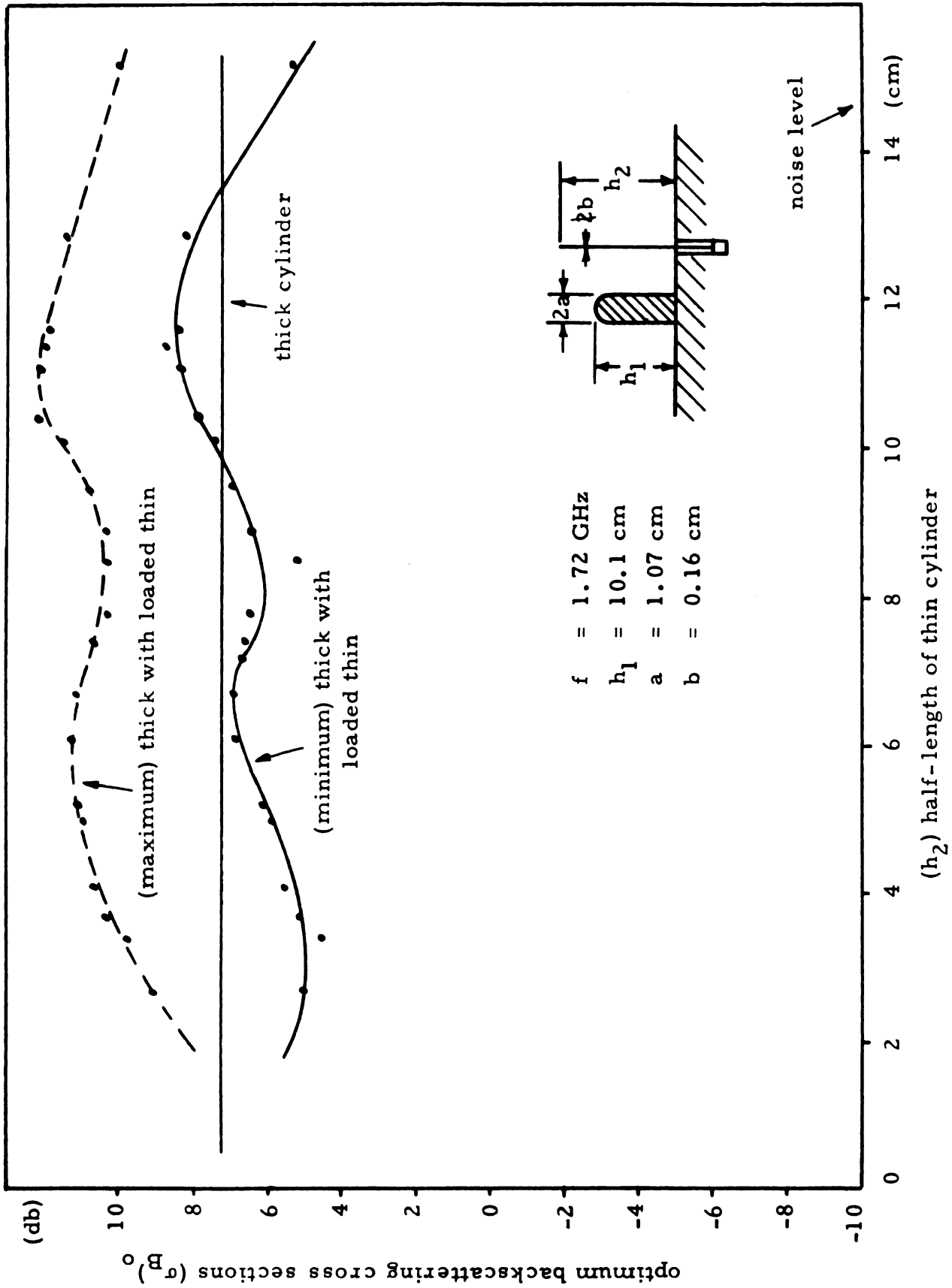


Figure 6.10. Maximum and minimum backscatters from a thick with a loaded thin cylinder as a function of thin cylinder half-length h_2 ($h_1 = 10.1 \text{ cm}$).

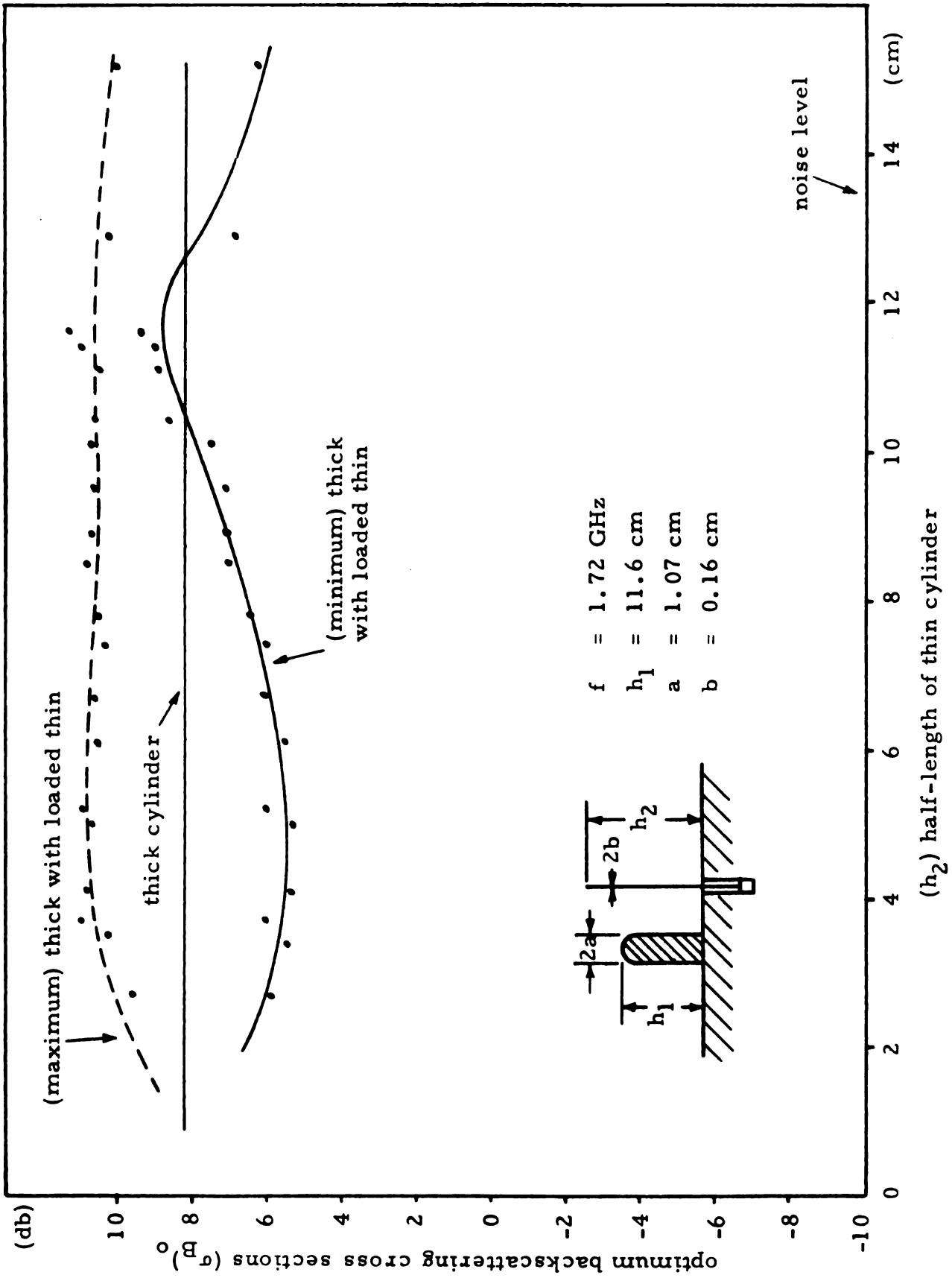


Figure 6.11. Maximum and minimum backscatters from a thick with a loaded thin cylinder as a function of thin cylinder half-length h_2 ($h_1 = 11.6$ cm).

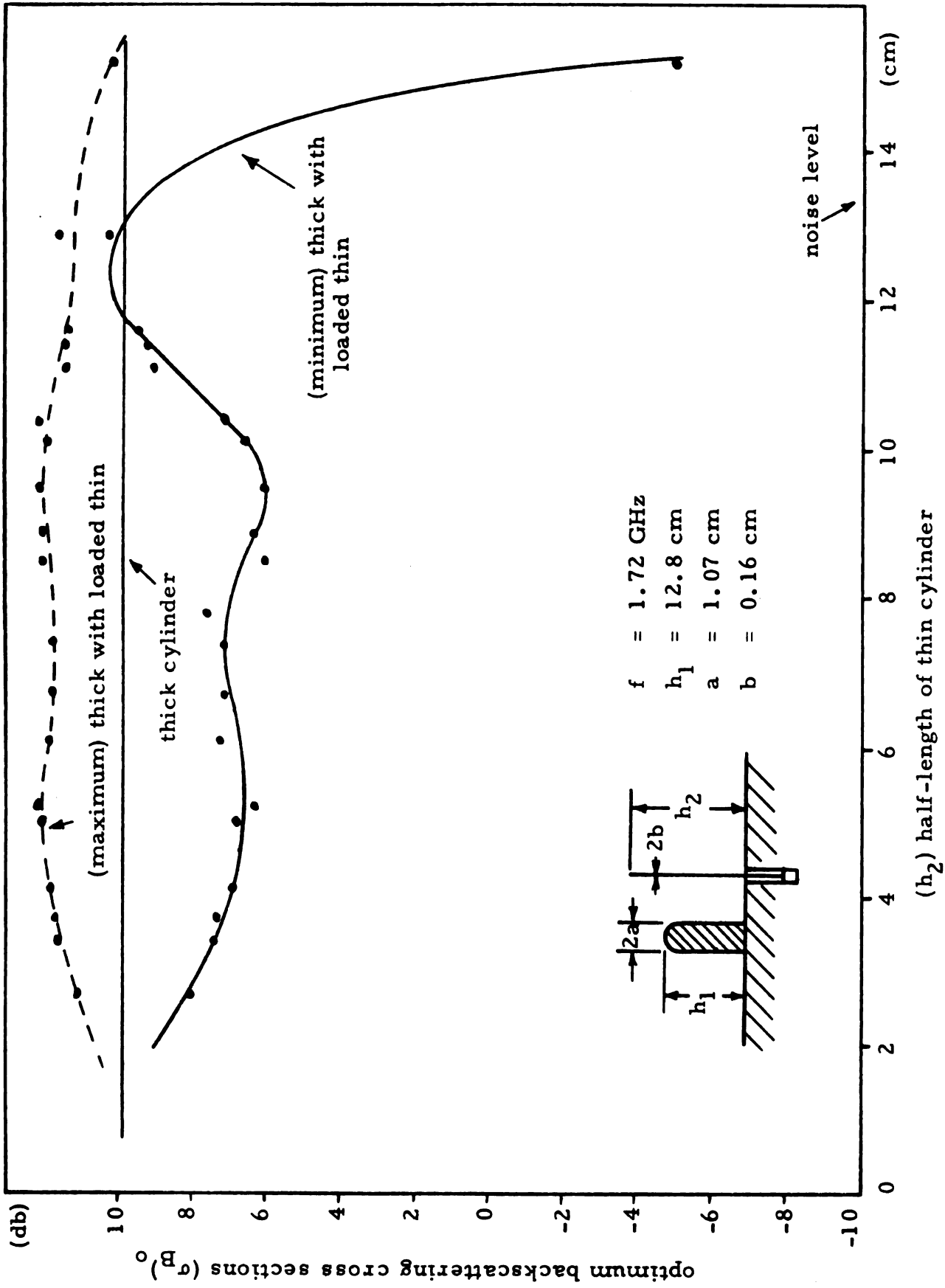


Figure 6.12. Maximum and minimum backscatters from a thick with a loaded thin cylinder as a function of thin cylinder half-length h_2 ($h_1 = 12.8 \text{ cm}$).

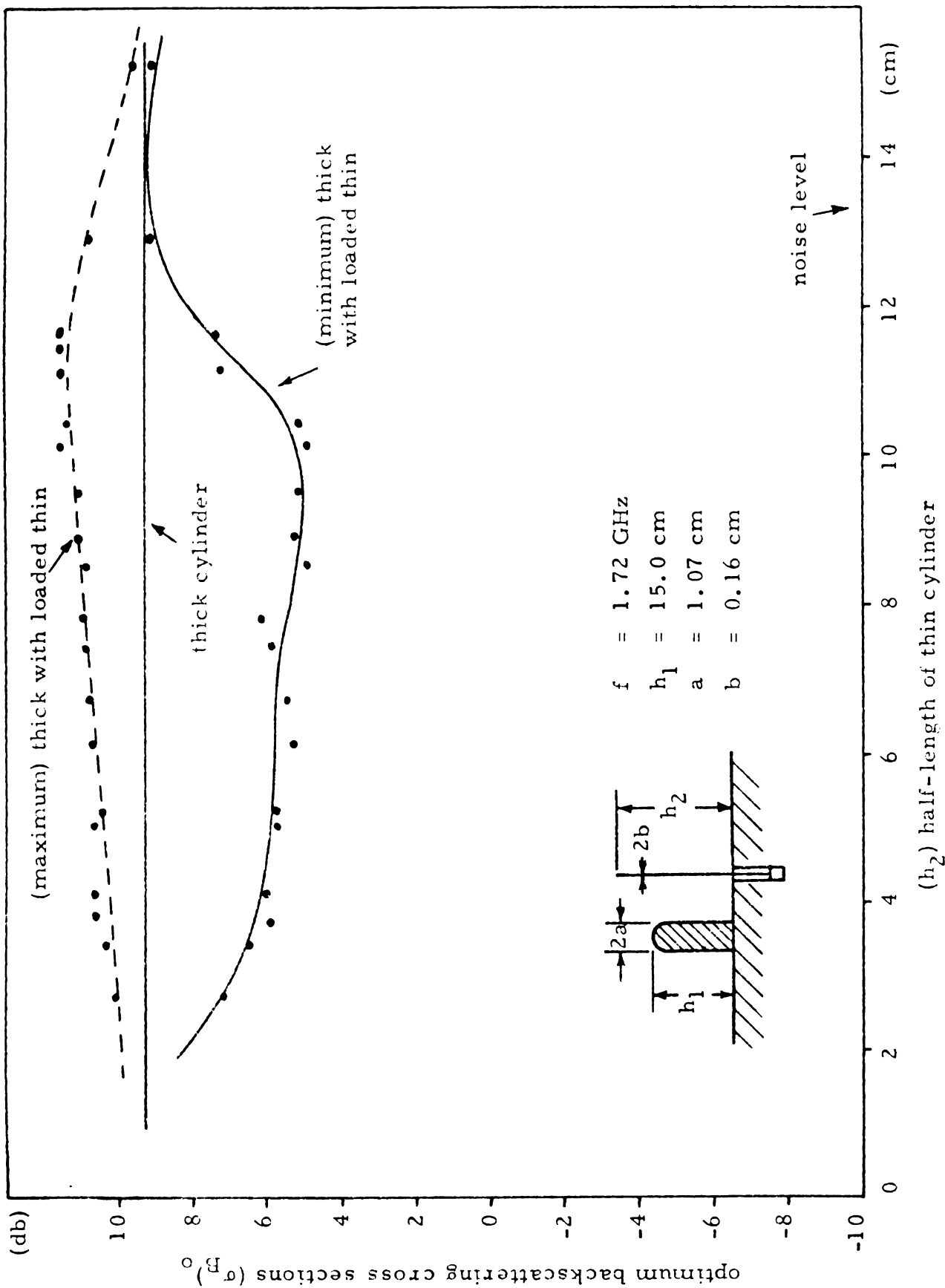


Figure 6.13. Maximum and minimum backscatters from a thick with a loaded thin cylinder as a function of thin cylinder half-length h_2 ($h_1 = 15.0$ cm).

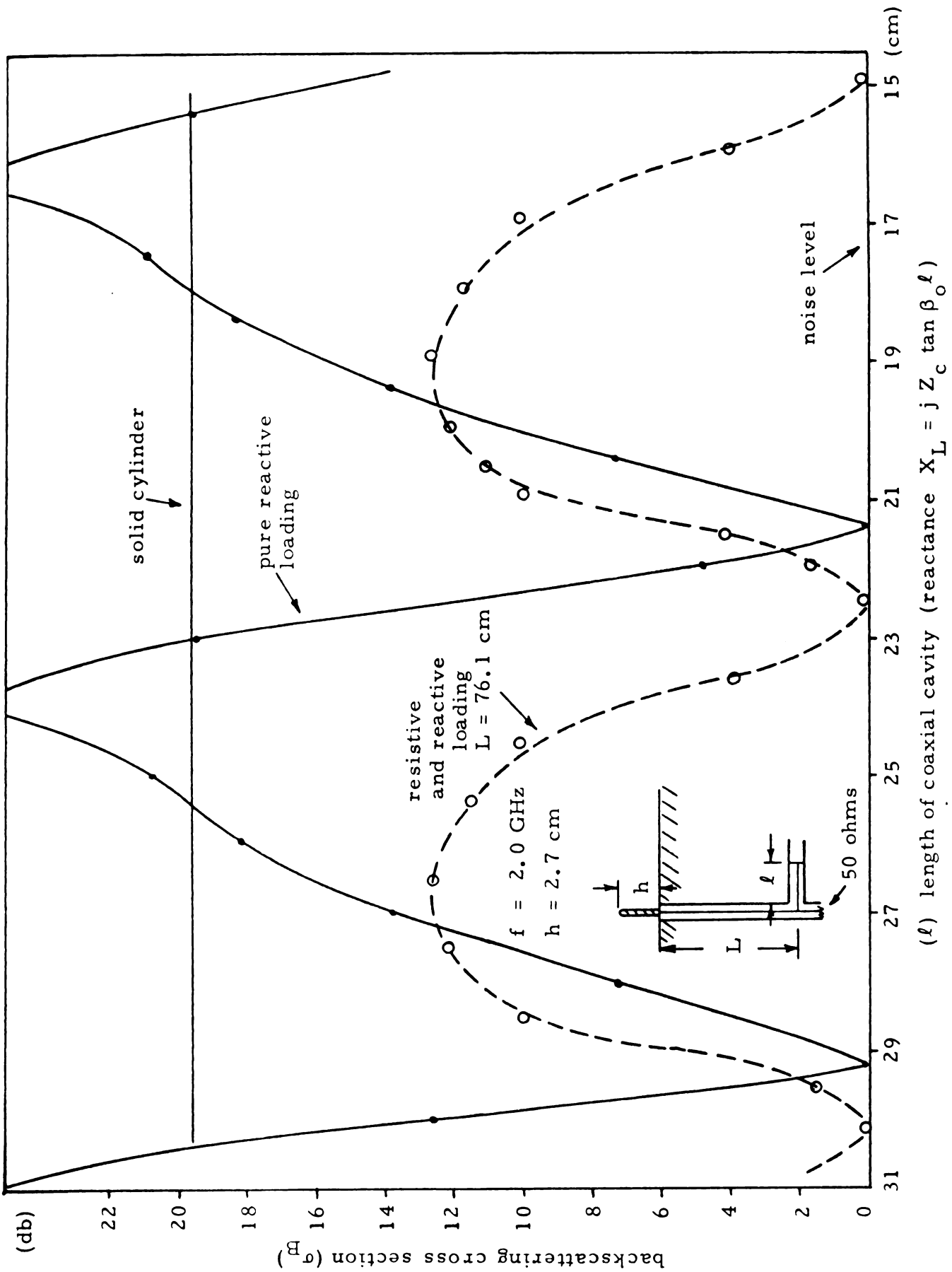
CHAPTER VII

TECHNIQUES FOR BANDWIDTH IMPROVEMENT

It is observed from the preceding chapters that there is, in connection with the compensation method, a need for bandwidth improvement. Such improvements would be desirable for these impedance loading techniques, as applied to metallic objects, to have extensive success in radar camouflage applications. The objective of this segment of the research is to improve the bandwidth of these impedance loading techniques, which are utilized to modify the backscattering cross sections of various shapes of conducting bodies. Two approaches, (1) resistive loading and (2) reactive loading using a coaxial cavity of high characteristic impedance, have been evaluated with some success.

7.1. Resistive Loading

The introduction of a resistive component in the loading impedance tends to somewhat improve the bandwidth. It is very difficult at the frequencies utilized in this study to obtain a lumped impedance with the correct frequency characteristics and physical dimensions small enough to be placed on the models under study. Consequently, high frequency devices, such as coaxial cavities, are sought. A 50 ohm termination (GR 874-50 Ω) is placed in parallel with an adjustable shorted coaxial line section to produce a loading with both reactive and resistive impedance components. In Figure 7.1, the backscattering cross section of a cylinder



(l) length of coaxial cavity (reactance $X_L = j Z_c \tan \beta_0 l$)

Figure 7.1. Backscattering cross section of a cylinder loaded with reactive and resistive elements as a function of reactive loading impedance ($h = 2.7$ cm).

($h = 2.7$ cm) loaded with such an impedance element is plotted as a function of the coaxial cavity length. The backscatter of a solid cylinder is indicated by a solid straight line and that of a cylinder with a purely reactive loading by a solid curve. A dashed line curve represents the backscatter from a cylinder loaded with an element having both reactive and resistive impedance components.

Comparison of the backscatters from the cylinder with the two different loading impedances indicates that the resistive component increases the bandwidth of minimization somewhat, since the minimum peak is not as sharp when the resistive component is present and the backscatter is over 7 dB lower than the solid cylinders for all values of reactance. The latter observation suggests that the resistive element dissipates a fraction of power incident upon the cylinder which might otherwise be scattered at resonance, thus reducing the backscattered field.

For a more pertinent comparison of the two loading devices, actual bandwidth measurements are obtained as shown in Figure 7.2. The backscatter from the resonant cylinder ($h = 3.5$ cm) with pure reactive loading is represented by a broken solid curve and that from the cylinder with reactive and resistive loading by a solid curve. A dashed line curve represents the backscattering cross section of the solid cylinder ($h = 3.5$ cm). All are plotted as a function of frequency. Direct observation indicates that the introduction of a resistive component does improve the bandwidth slightly. Even better results can be obtained if a coaxial line with a higher characteristic impedance is employed.

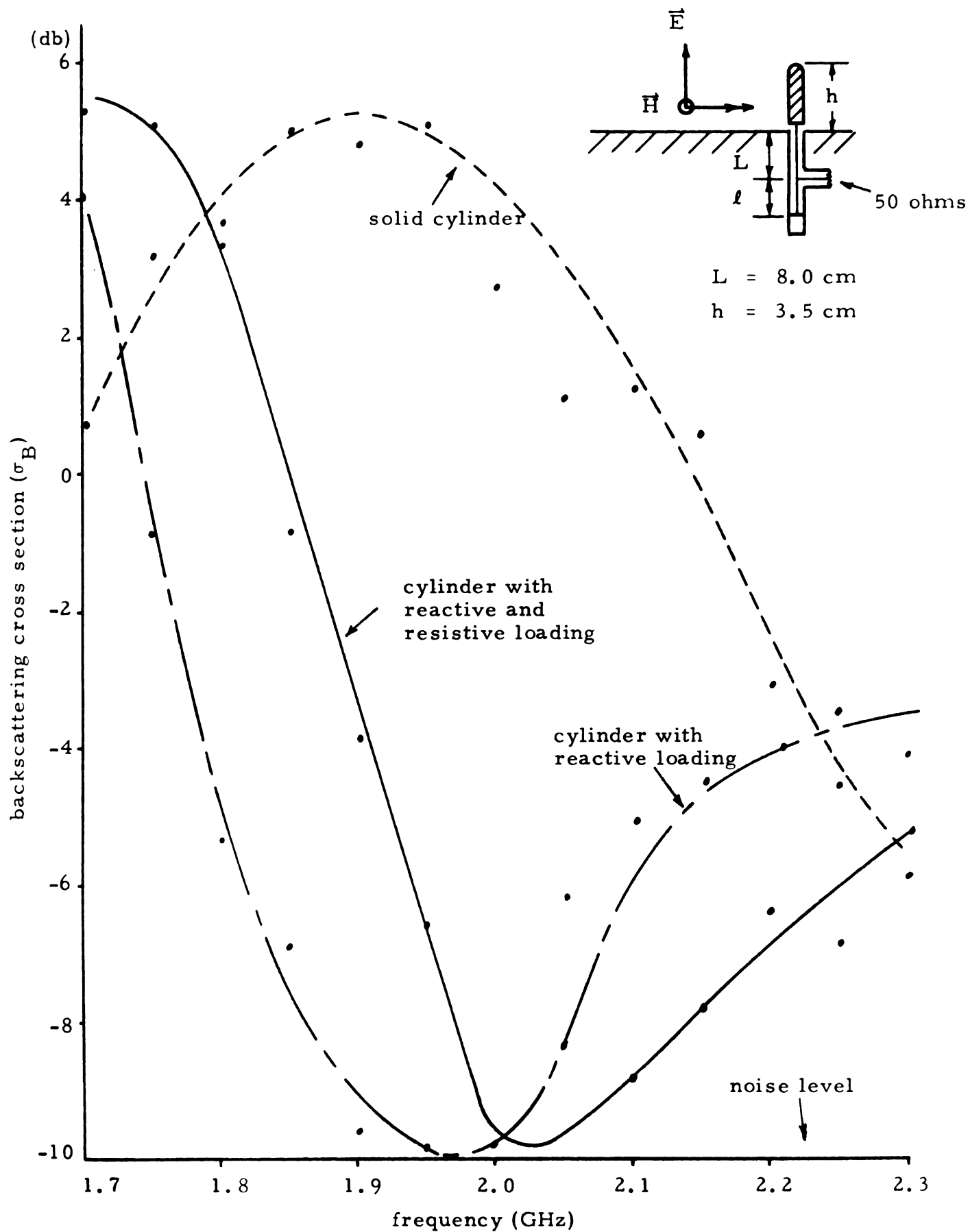


Figure 7.2. Backscattering cross sections of solid and loaded cylinders as a function of frequency ($h = 3.5$ cm).

7.2. Reactive Loading Using a Coaxial Cavity with High Characteristic Impedance

As suggested in the last section, a far better bandwidth improvement result is obtained by loading the metallic object by a coaxial line (or cavity) with 240 ohm characteristic impedance. With this coaxial cavity loading, the backscatter of the cylinder is minimized over quite a broad range of frequencies (1.7 to 2.3 GHz). With a conventional 50 ohm coaxial cavity, the minimization of scattering can be achieved only over a much narrower frequency range (1.9 to 2.1 GHz). The experimental measurements on the backscatters from a solid cylinder, a cylinder loaded with a 50 ohm coaxial cavity, and a cylinder loaded with a 240 ohm coaxial cavity are presented in Figure 7.3 as a function of frequency. The backscattering cross sections of the 50 ohm loaded and 240 ohm loaded cylinders ($h = 3.5$ cm) are represented by thin and thick solid curves, respectively, and that of the solid cylinder ($h = 3.5$ cm) by a dashed line curve. This bandwidth improvement by the technique of employing a high characteristic impedance coaxial line can easily be explained, since this coaxial line can provide a high impedance without operating about its antiresonant length, where a slight change in frequency can cause a large change in reactance.

The 240 ohm characteristic impedance coaxial line is also applied as the loading impedance for the sphere with loaded wires, as described in section 3.2. As in the case of the cylinder, this technique for bandwidth improvement is quite successful for the sphere ($a = 5.71$ cm). In Figure 7.4, the backscatters of the solid sphere (dotted line), sphere with solid wires (dashed line), sphere

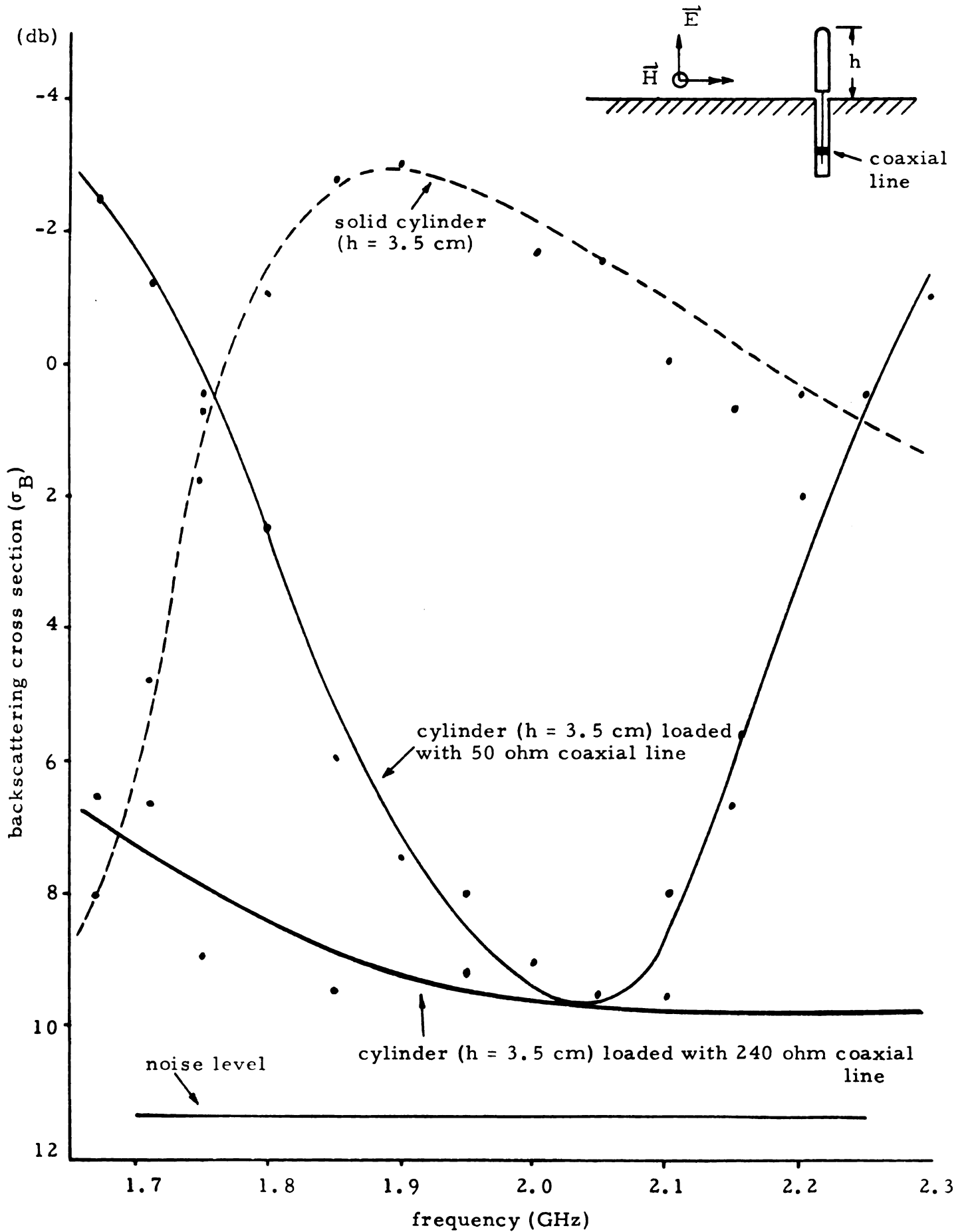


Figure 7.3. Backscattering cross sections of solid and loaded cylinders as a function of frequency ($h = 3.5$ cm).

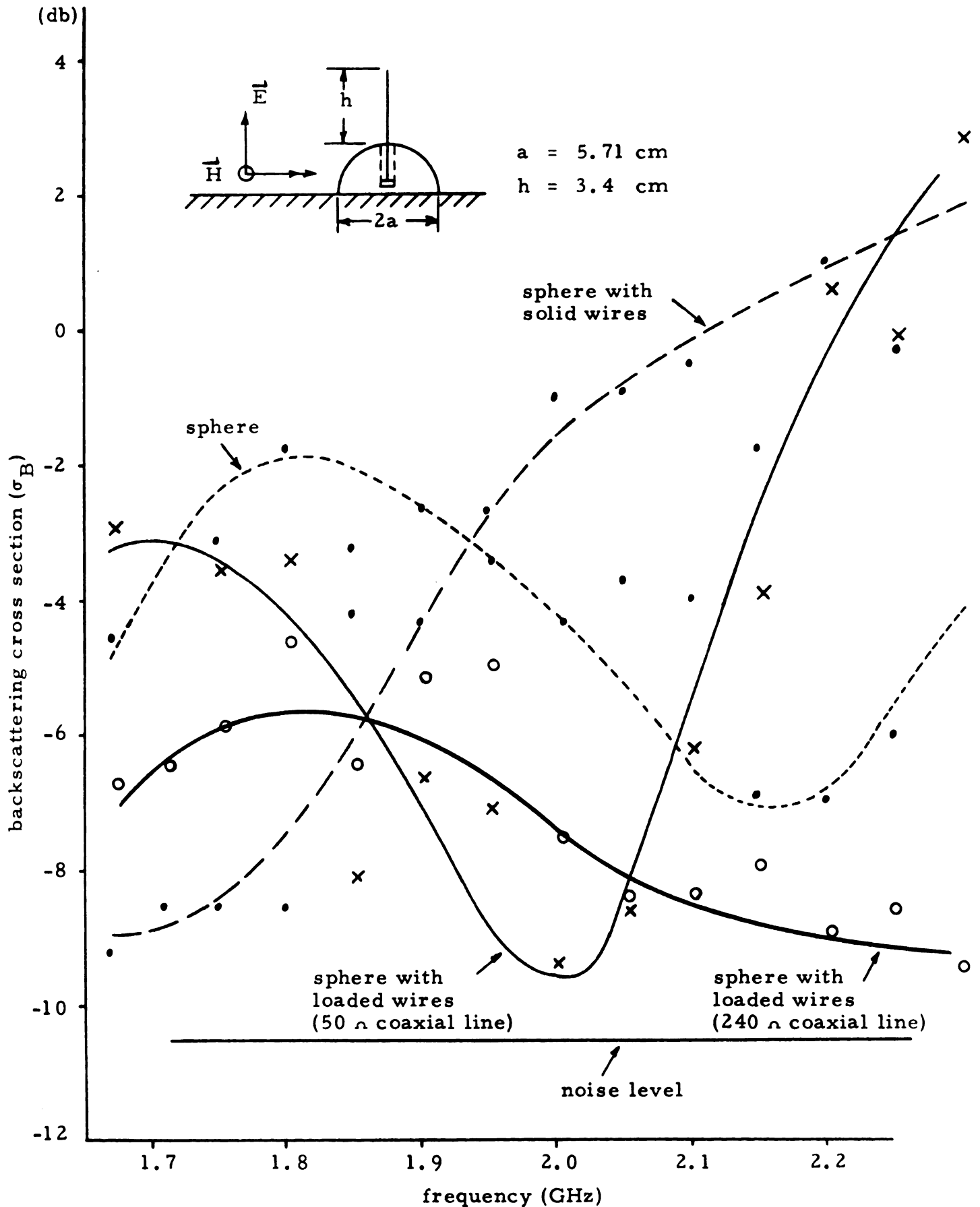


Figure 7.4. Backscattering cross sections of sphere and sphere with loaded wires as a function of frequency ($a = 5.71$ cm, $h = 3.4$ cm).

with loaded wires (thin solid line) using coaxial line with 50 ohm characteristic impedance, and the sphere with loaded wires using coaxial cavity of 240 ohm characteristic impedance (thick solid line) are plotted as a function of frequency. There are two interlocking reasons for the bandwidth improvement using this technique. The first is that the coaxial cavity can provide high impedances without operating about its antiresonant length, as explained above, and the second is that for this size sphere ($a = 5.71$ cm) length of wires ($h = 3.5$ cm), and center frequency (2.0 GHz), the required impedance for minimum backscatter is very small, which makes the use of a coaxial line very effective.

Bandwidth improvement in the backscattering enhancement of metallic objects can be achieved by similar techniques. In particular, the maximization of the backscatter from a sphere can be made quite broadband by the use of longer wires. It is observed in section 3.2, Figure 3.10, that the scattering from a sphere ($a = 5.71$ cm) with loaded wires ($h = 12.9$) is nearly independent of loading impedance and maintained a level about 5 dB above the cross section of the sphere.

REFERENCES

1. King, R. W. P., and T. T. Wu, The Scattering and Diffraction of Waves, Harvard University Press, Cambridge, Mass. (1959).
2. Blacksmith, P., Jr., R. E. Hiatt, and R. B. Mack, "Introduction to Radar Cross-Section Measurements," Proceedings of the IEEE, vol. 53, pp. 901-919, August 1965.
3. Chen, K. M., and V. Liepa, "Minimization of the Back Scattering of a Cylinder by a Central Loading," IEEE Trans. on Antennas and Propagation, vol. AP-12, pp. 576-582, September 1964.
4. Chen, K. M., "Minimization of Backscattering of a Cylinder by Double Loading," IEEE Trans. on Antennas and Propagation, vol. AP-13, pp. 262-270, March 1965.
5. Chen, K. M., "Reactive Loading of Arbitrarily Illuminated Cylinders to Minimize Microwave Backscatter," J. Res. Nat'l. Bur. Std., vol. 690, p. 1481, 1965.
6. Liepa, V. V., and T. B. A. Senior, "Modification to the Scattering Behavior of a Sphere by Reactive Loading," Proceedings of the IEEE, vol. 53, pp. 1004-1011, August 1965.
7. Green, R. B., "The Echo Area of Small Rectangular Plates With Linear Slots," IEEE Trans. on Antennas and Propagation, vol. AP-12, pp. 101-104, January 1964.
8. Lin, Juang-Lu, and Kun-Mu Chen, "Modification of Backscattering of a Loop by Impedance Loading," Division of Engineering Research, Michigan State University, East Lansing, Mich., Scientific Rept. 3, prepared under Contract AF 19(628)-5732, Air Force Cambridge Research Laboratories, L. G. Hanscom Field, Bedford, Mass., May 20, 1967.
9. Sletten, C. J., "Electromagnetic Scattering From Wedges and Cones," Air Force Cambridge Research Center, L. G. Hanscom Field, Bedford, Mass., Rept. E5090, July 1952.
10. Bechtal, Marley H., "Scattering Coefficients For the Backscattering of Electromagnetic Waves from Perfectly Conducting Spheres," Cornell Aeronautical Laboratory, Buffalo, N. Y., Rept. AP/Ris-1, December, 1962.
11. Chen, K. M., and M. Vincent, "A New Method of Minimizing the Radar Cross Section of a Sphere," Proceedings of the IEEE, vol. 54, pp. 1629-1630, November 1966.

12. Lin, J. L., and K. M. Chen, "Resonances of Loops," IEEE Trans. on Antennas and Propagation, vol. AP-15, pp. 477-478, May 1967.
13. Chen, K. M., J. L. Lin, and M. Vincent, "Minimization of Backscattering of a Metallic Loop by Impedance Loading," IEEE Trans. on Antennas and Propagation, vol. AP-15, pp. 492-494, May 1967.
14. Vincent, M. C., and K. M. Chen, "A New Method of Minimizing the Backscatter of a Conducting Plate," Proceedings of the IEEE, vol. 55, pp. 1109-1111, June 1967.
15. Chen, K. M., "Minimization of Radar Cross Sections of Cylinders by Compensation Method," Division of Engineering Research, Michigan State University, East Lansing, Mich., Scientific Rept. 1, prepared under Contract AF 19(628)-5732, Air Force Cambridge Research Laboratories, L. G. Hanscom Field, Bedford, Mass., February 25, 1967.
16. King, R. W. P., Theory of Linear Antennas, Harvard University Press, Cambridge, Mass. (1956).

MICHIGAN STATE UNIVERSITY LIBRARIES



3 1293 03177 7299